

AD-A277 911



NAVAL POSTGRADUATE SCHOOL
Monterey, California



DTIC
ELECTE
APR 12 1994
S G D

THESIS

**A COMPARISON OF MODELED AND OBSERVED OCEAN
MIXED LAYER BEHAVIOR
IN A SEA BREEZE INFLUENCED COASTAL REGION**

by

Patrick S. Cross

December, 1993

Thesis Advisor:
Co-Advisor:

Leslie K. Rosenfeld
Carlyle H. Wash

Approved for public release; distribution is unlimited.

DTIC QUALITY INSPECTED 3

12580 94-10953

94 4 11 069

REPORT DOCUMENTATION PAGE			Form Approved OMB No. 0704	
Public reporting burden for this collection of information is estimated to average 1 hour per response, including the time for reviewing instruction, searching existing data sources, gathering and maintaining the data needed, and completing and reviewing the collection of information. Send comments regarding this burden estimate or any other aspect of this collection of information, including suggestions for reducing this burden, to Washington Headquarters Services, Directorate for Information Operations and Reports, 1215 Jefferson Davis Highway, Suite 1204, Arlington, VA 22202-4302, and to the Office of Management and Budget, Paperwork Reduction Project (0704-0188) Washington DC 20503.				
1. AGENCY USE ONLY (Leave blank)		2. REPORT DATE 21 December 1993.		3. REPORT TYPE AND DATES COVERED Master's Thesis
4. TITLE AND SUBTITLE A COMPARISON OF MODELED AND OBSERVED OCEAN MIXED LAYER BEHAVIOR IN A SEA BREEZE INFLUENCED COASTAL REGION			5. FUNDING NUMBERS	
6. AUTHOR(S) Patrick S. Cross				
7. PERFORMING ORGANIZATION NAME(S) AND ADDRESS(ES) Naval Postgraduate School Monterey CA 93943-5000			8. PERFORMING ORGANIZATION REPORT NUMBER	
9. SPONSORING/MONITORING AGENCY NAME(S) AND ADDRESS(ES)			10. SPONSORING/MONITORING AGENCY REPORT NUMBER	
11. SUPPLEMENTARY NOTES The views expressed in this thesis are those of the author and do not reflect the official policy or position of the Department of Defense or the U.S. Government.				
12a. DISTRIBUTION/AVAILABILITY STATEMENT Approved for public release; distribution is unlimited.			12b. DISTRIBUTION CODE A	
13. ABSTRACT (maximum 200 words) A high temporal resolution data set from a mooring in Monterey Bay, California was analyzed and used to calculate heat and momentum fluxes for the purpose of forcing two ocean mixed layer models. The time frame for the study was September, 1992, a period representative of the sea breeze circulation frequently affecting this and other coastal regions. The models used were that of Price, Weller & Pinkel (1986), a Richardson number based mixing model, and Garwood (1977), a model based on the turbulent kinetic energy budget within the mixed layer. Both models were analyzed with respect to their ability to reproduce the observed diurnal variation of the temperature and depth of the mixed layer. Although the model predictions agree reasonably well with observations in regards to the phase of the diurnal temperature cycle, they were seen to underpredict its magnitude, particularly the nocturnal cooling. This lack of cooling in the models relative to the ocean could be due to penetrative convection, non-steady state turbulence, and/or diurnal advection present in the ocean but not in one or both models. Additionally, the models exhibited an upward temperature trend relative to the data which caused progressively increasing stratification. This trend was used to approximate the magnitude of vertical advective effects.				
14. SUBJECT TERMS Monterey, Mixed Layer, Air/Sea, Surface Flux, Diurnal, Sea Breeze, Heat Flux, Wind Stress, Coastal, California, Modeling			15. NUMBER OF PAGES 126	
			16. PRICE CODE	
17. SECURITY CLASSIFICATION OF REPORT Unclassified	18. SECURITY CLASSIFICATION OF THIS PAGE Unclassified	19. SECURITY CLASSIFICATION OF ABSTRACT Unclassified	20. LIMITATION OF ABSTRACT UL	

NSN 7540-01-280-5500

Standard Form 298 (Rev. 2-89)

Prescribed by ANSI Std. Z39-18

FORM QUALITY IMPROVED 3

Approved for public release: distribution is unlimited.

A Comparison of Modeled and Observed Ocean Mixed Layer
Behavior in a Sea Breeze Influenced Coastal Region

by

Patrick S. Cross
Lieutenant, United States Navy
B.S., New Mexico Institute of Mining and Technology, 1982

Submitted in partial fulfillment
of the requirements for the degrees of

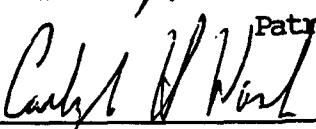
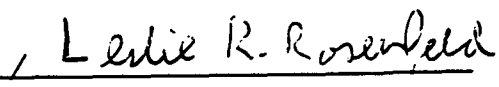
MASTER OF SCIENCE IN PHYSICAL OCEANOGRAPHY
AND MASTER OF SCIENCE IN METEOROLOGY

from the
NAVAL POSTGRADUATE SCHOOL
December 1993

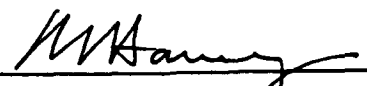
Author:



Patrick S. Cross

Approved by:

 , 
Carlyle H. Wash, Leslie K. Rosenfeld, Thesis Advisors


Roland W. Garwood, Second Reader


Robert L. Harney, Chairman
Department of Meteorology


Curtis A. Collins, Chairman
Department of Oceanography

ABSTRACT

A high temporal resolution data set from a mooring in Monterey Bay, California was analyzed and used to calculate heat and momentum fluxes for the purpose of forcing two ocean mixed layer models. The time frame for the study was September, 1992, a period representative of the sea breeze circulation frequently affecting this and other coastal regions.

The models used were that of Price, Weller & Pinkel (1986), a Richardson number based mixing model, and Garwood (1977), a model based on the turbulent kinetic energy budget within the mixed layer. Both models were analyzed with respect to their ability to reproduce the observed diurnal variation of the temperature and depth of the mixed layer. Although the model predictions agree reasonably well with observations in regards to the phase of the diurnal temperature cycle, they were seen to underpredict its magnitude, particularly the nocturnal cooling. This lack of cooling in the models relative to the ocean could be due to penetrative convection, non-steady state turbulence, and/or diurnal advection present in the ocean but not in one or both models. Additionally, the models exhibited an upward temperature trend relative to the data which caused progressively increasing stratification. This trend was used to approximate the magnitude of vertical advective effects.

Accession For	
NTIS	CRA&I <input checked="" type="checkbox"/>
DTIC	TAB <input checked="" type="checkbox"/>
Unannounced <input type="checkbox"/>	
Justification	
By	
Distribution /	
Availability Codes	
Dist	Avail and/or Special
A-1	

TABLE OF CONTENTS

I. INTRODUCTION	1
II. BACKGROUND	8
A. MIXED LAYER BASICS	8
B. MIXED LAYER MODELING	10
C. MIXED LAYER BEHAVIOR IN COASTAL REGIONS	12
III. MODEL DESCRIPTIONS	15
A. THE GARWOOD (1977) MODEL	16
B. THE PRICE, WELLER & PINKEL (1986) MODEL	22
IV. DATA	25
A. SOURCES	25
1. OASIS MOORING	25
2. NPS Profiler Site	27
B. DESCRIPTION OF ATMOSPHERIC AND OCEANIC DATA AND DERIVED QUANTITIES	27
1. Synoptic Weather Description	27
2. Hourly Data	29
a. Winds	29
b. Air Temperature	31
c. Humidity/Dew Point	31

d. Sea Surface Temperature	32
e. Temperatures at 10, 20, and 40 Meters	33
C. MIXED LAYER CHARACTERISTICS AT M1	33
D. SURFACE FLUXES	35
1. Cloud Cover Estimation	35
2. Model Forcing	36
V. MODEL RESULTS	60
A. MODEL SENSITIVITIES	60
1. Initial Conditions	60
2. Friction (PWP)	61
3. Time Step	62
4. Cloudiness	64
5. Absorption Coefficients	65
B. FINAL MODEL RUNS	66
1. Garwood	66
2. PWP	68
VI. DISCUSSION	85
A. RELATING MODEL TRENDS TO ADVECTION	85
B. DIURNAL CYCLE	86
1. Constant Wind Forcing	87
2. Constant Heat Flux	89
C. POSSIBLE REASONS FOR MODELS' UNDERESTIMATES OF NOCTURNAL COOLING	90
1. Penetrative Convection	90

2. Steady State TKE Assumption	91
3. Model Stratification	92
4. Diurnal Advection	92
VII. CONCLUSIONS AND RECOMMENDATIONS	103
A. MIXED LAYER BEHAVIOR IN MONTEREY BAY	103
B. ONE-DIMENSIONAL MIXED LAYER MODELS IN SEA BREEZE REGIONS	104
C. RECOMMENDATIONS	105
LIST OF REFERENCES	108
INITIAL DISTRIBUTION LIST	112

LIST OF FIGURES

Figure 1. Monterey Bay, California and the Salinas Valley. Mooring (M1) and Profiler (PRO) Locations are Shown. Also Shown for Reference are Monterey (MBA) and Santa Cruz (UCSC). Contour Interval is 200 Meters.	7
Figure 2. Bulk Mixed Layer Diagram.	8
Figure 3a. Schematic Diagram of OASIS Mooring Configuration: Courtesy of Francisco Chavez, MBARI.	39
Figure 3b. Schematic Diagram of the ATLAS Buoy: Courtesy of Francisco Chavez, MBARI.	40
Figure 4. Surface Pressure Chart From 4 September, 1992. Monterey Bay is Designated With a *. Solid Lines are Surface Pressures in Millibars and Dashed Lines Indicate 1000 to 500 mb Thickness.	41
Figure 5. Surface Pressure Chart From 10 September, 1992. Same Line Convention as in Figure 4.	42
Figure 6a. Full Resolution U and V Wind Components Measured at M1. The V Component is Dashed. This and All Subsequent Data and Model Plots are in Greenwich Mean Time. Local Time May be Obtained by Subtracting 7 Hours.	43
Figure 6b. Wind Speed at M1.	44

Figure 6c.	True Wind Direction at M1. Values Indicate the Direction the Wind Vector was Pointing. Periods of Large Variation Occur During Light Winds. . . .	45
Figure 6d.	Feather Plot of Hourly Wind Vectors Recorded at M1.	46
Figure 7.	Air Temperature (Solid) and Dew Point (Dashed) at M1. Dew Points Were Converted From Relative Humidities Measured by the Buoy.	47
Figure 8.	Relative Humidity at M1.	48
Figure 9.	Sea Surface Temperature at M1.	49
Figure 10.	Ocean Temperatures at the Surface, 10, 20, and 40 Meters Beneath M1.	50
Figure 11a.	Shortwave and Longwave Irradiance Recorded at the NPS Profiler Site. The Day of September is Designated on the Time Scale of Each Plot.	51
Figure 11a.	(Continued)	52
Figure 11a.	(Continued)	53
Figure 11a.	(Continued)	54
Figure 11b.	Photosynthetically Active Radiation at M1. Note Degree of Cloudiness on the 9th.	55
Figure 12a.	Total Wind Stress Computed in Accordance With Large and Pond (1981).	56
Figure 12b.	Solar Insolation Computed from Forcing Routine, Accounting for Estimated Cloud Cover. . .	57
Figure 12c.	Computed Heat Loss Terms. Sensible (Dotted), Latent (Lower Solid), Net Infrared (Dashed), and Net	

Heat Loss (Upper Solid - the Other 3 Summed) are Plotted, with Positive Values Indicating Heat Lost From the Ocean.	58
Figure 12d. Computed Net Surface Heat Flux. Sign Convention as in Figure 12c. This Represents the Solar Insolation Minus the Net Heat Loss From Figure 12c.	59
Figure 13a. CTD Temperature Profiles From 9 September at Various Points Within Monterey Bay. Profile #2 was used for model runs, as discussed in text.	71
Figure 13b. Initial Temperature Profile Used by the Models.	72
Figure 14. PWP Mixed Layer Temperatures With Varying Friction.	73
Figure 15. Step Wind Function (Top) Applied to Garwood Unsteady Model and Resulting Total TKE (Bottom) Versus Time.	74
Figure 16a. Garwood Mixed Layer Temperatures Computed Using Zero Cloud Cover Assumption and Using Estimated Cloud Cover.	75
Figure 16b. PWP Mixed Layer Temperatures With and Without Clouds.	76
Figure 17. Total Absorption Profiles Computed by Both Models. Garwood Absorption is Dashed and PWP is Solid. Note that PWP Breaks the Absorption into Red	

and Blue Profiles in the Ratio 0.6 Red and 0.4 Blue.	77
Figure 18a. Final Garwood Mixed Layer Temperatures Versus Observed Sea Surface Temperatures.	78
Figure 18b. Garwood Mixed Layer Depths.	79
Figure 19. Observed Sea Surface Temperatures Minus 10 Meter Temperatures. Values Near Zero Indicate Periods of Deepening to Greater than 10 Meters.	80
Figure 20. Sequence of Temperature Profiles From the Garwood Model. Time Since Model Initialization is Indicated at the Top of Each Profile.	81
Figure 21a. Final PWP Mixed Layer Temperatures Versus Observed Sea Surface Temperatures.	82
Figure 21b. PWP Mixed Layer Depths. Note That Depths are in Whole Numbers, Since They are Inferred from a Density Profile Which is Subject to the Model's Vertical Bin Spacing.	83
Figure 22. Sequence of Temperature Profiles from the PWP Model.	84
Figure 23a. Least Squares Fit to Garwood Temperatures.	94
Figure 23b. Least Squares Fit to PWP Temperatures.	95
Figure 24. Least Squares Fits to Observed Temperatures.	96
Figure 25a. Detrended Garwood Mixed Layer Temperatures (Solid) Versus Observed Sea Surface Temperature. Note Different Temperature Scale from Previous Plots.	97

Figure 25b. Detrended PWP Mixed Layer Temperatures Versus Observed Sea Surface Temperatures.	98
Figure 26a. Mixed Layer Temperatures with Constant Wind, Varying Heat Flux.	99
Figure 26b. Mixed Layer Depth with Constant Wind, Varying Heat Flux.	100
Figure 27a. Mixed Layer Temperatures with Constant Heat Flux, Varying Wind. Note Similarity of Garwood Pattern to Previous Result.	101
Figure 27b. Mixed Layer Depths with Constant Heat Flux, Varying Wind.	102

I. INTRODUCTION

The uppermost layer of the ocean is commonly referred to as the surface mixed layer, due to its relatively uniform velocity structure and isothermal, isohaline characteristics. The depth of the mixed layer is primarily determined by the balance between turbulence generated at the surface by the wind, and buoyant fluxes caused by surface heating and cooling. The wind acts to generate turbulence, eventually resulting in entrainment of water from below the mixed layer and a corresponding cooling and deepening of the layer. Conversely, when the buoyant flux is positive downward, as is the case on a sunny summer afternoon in the mid-latitudes, the mixed layer will shallow and warm. This occurs due to increased stratification of the uppermost portion of the water column, unless the wind mixing is strong enough to overcome this effect. Thus, in the one-dimensional case, the balance of these forces, shear instability due to wind, and buoyant forces due to surface heat flux, is the principal factor in determining the depth and temperature of the ocean mixed layer in a given region. Other factors affecting mixed layer depth and temperature are the input of fresh water from river runoff, precipitation, evaporation, and shear stress at the base of the mixed layer due to the presence of internal waves.

Of course, advection of heat, salt, and momentum add further complexity to this one-dimensional view.

Studies of mixed layer dynamics have generally involved long time scale forcing in open ocean regions. That is, they have been concerned with synoptic scale or larger weather patterns and monthly or seasonal insolation patterns. This study uses much of the knowledge of mixed layer dynamics and air/sea fluxes gained in these open water efforts and extends it to a coastal region. Specifically, the area of interest in this paper is Monterey Bay, off central California. The observed diurnal cycle in the radiation here is similar to previous studies, but the wind stresses also undergo a strongly diurnal variation, peaking each afternoon in what is commonly referred to as a land/sea breeze circulation. During much of the primary period of study, in fact, the area weather is under the influence of a quasi-stationary high pressure system, which greatly reduces wind variations on a synoptic scale. This leaves the local land/sea breeze influences and daily heating as the primary controllers of mixed layer variability, with the advection of cooler water into the study area playing a role as well in this upwelling favorable eastern boundary current regime. Rainfall is rare during the summer months in the study area (none fell during the period of interest) and river runoff is very slight, allowing fresh water input to be neglected in the modeling process. Also not considered in the models are the shear stresses at the base of

the mixed layer, since these were considered to be small in comparison to heat flux and surface shear.

This project was undertaken in an effort to broaden knowledge of coastal ocean dynamics as part of the Naval Meteorology and Oceanography Command's recent shifting of emphasis from the deep ocean to nearshore, in accordance with the CNO doctrine set forth in From the Sea. In particular, this study will give insights into mixed layer behavior in a region in which diurnal wind variability is a dominant feature of the overall wind stress pattern. In addition to its contribution to the science of coastal ocean dynamics and mixed layer processes, this effort will have applications to naval operations, including coastal ASW, mining, diving, and amphibious operations, particularly in areas with significant sea breeze signatures, which includes the coasts of most of the low and mid latitudes. The area of study was selected because of the availability of a unique data set with high temporal resolution, combined with a wealth of local area knowledge and supplementary data.

Few studies have examined the shallow ocean response to diurnal wind forcing. Rosenfeld (1988) presents results from the Coastal Ocean Dynamics Experiments (CODE) I and II, which indicate that off Point Arena in northern California there is a significant diurnal variation to the wind induced currents. The CODE region is also characterized by a predominantly diurnal wind variation during summer months, but the wind

accelerates along the coast to the south during the day in response to large scale heating in the central valley of California (Beardsley et al., 1987). In contrast, the present study area undergoes more of a classical onshore/offshore wind variation due to more local heating in the Salinas Valley and the winds are directionally controlled by the northwest to southeast orientation of that valley (Figure 1). While the coastal mountains in the CODE area are basically continuous, a significant break occurs in the Salinas/Monterey area, allowing the diurnal cross-shore flow to develop through much of the year. Other unique aspects of the area are the presence of strong upwelling centers to the north and south of Monterey Bay and the Monterey Submarine Canyon, which cuts through the center of the bay. The upwelling that occurs in the area to the north of our study area and is advected southward (Rosenfeld et al., 1993) and the possible upwelling at the study site add to the complexity of this coastal region by potentially introducing significant horizontal and vertical advection to the mixed layer problem.

The mixed layer of Monterey Bay will be investigated through a careful analysis of the available data during 1 through 11 September 1992 and a comparison of these data to results produced by two one-dimensional mixed layer models, those of Garwood (1977) and Price, Weller & Pinkel (1986). These two models represent two very different approaches to mixed layer physics. The heat and momentum fluxes that drive

the models are computed from the measured data. The models' ability to reproduce the observed diurnal cycle of mixed layer temperature and depth will be of primary interest, with a secondary goal of determining how well they reproduce the trend over an eleven day period. This latter effort is made in an attempt to quantify the advection necessary to maintain the cool temperatures of the bay in the presence of large downward heat fluxes.

Data used in this study are largely from mooring M1 (in the center of the bay as seen in Figure 1), owned and operated by the Monterey Bay Aquarium Research Institute (MBARI). This mooring collects a suite of meteorological and ocean temperature data at ten minute intervals. These data were provided courtesy of Francisco Chavez of MBARI. Ocean velocities measured by a downward looking Acoustic Data Current Profiler (ADCP) at fifteen minute intervals was provided by Leslie Rosenfeld of MBARI and the Naval Postgraduate School (NPS). These instruments will be described in greater detail in the next section. Some meteorological data were also obtained from the NPS meteorological station at Fritzche Field on Fort Ord (Figure 1).

Some basic concepts of ocean mixed layer physics will be presented in the next chapter, followed by a brief account of previous one-dimensional modeling efforts and coastal mixed layer studies. Chapter III is a presentation of the key

features of the two models used in this study. A description of the data sources and the data itself is contained in Chapter IV, including a presentation of computed fluxes, while Chapter V is a description of the model sensitivities along with the results of the model runs. Chapter VI is the discussion portion of the thesis, with detailed analysis of the performance of the models compared with the observations. Finally, conclusions and recommendations for further research and model improvement will be presented in Chapter VII.

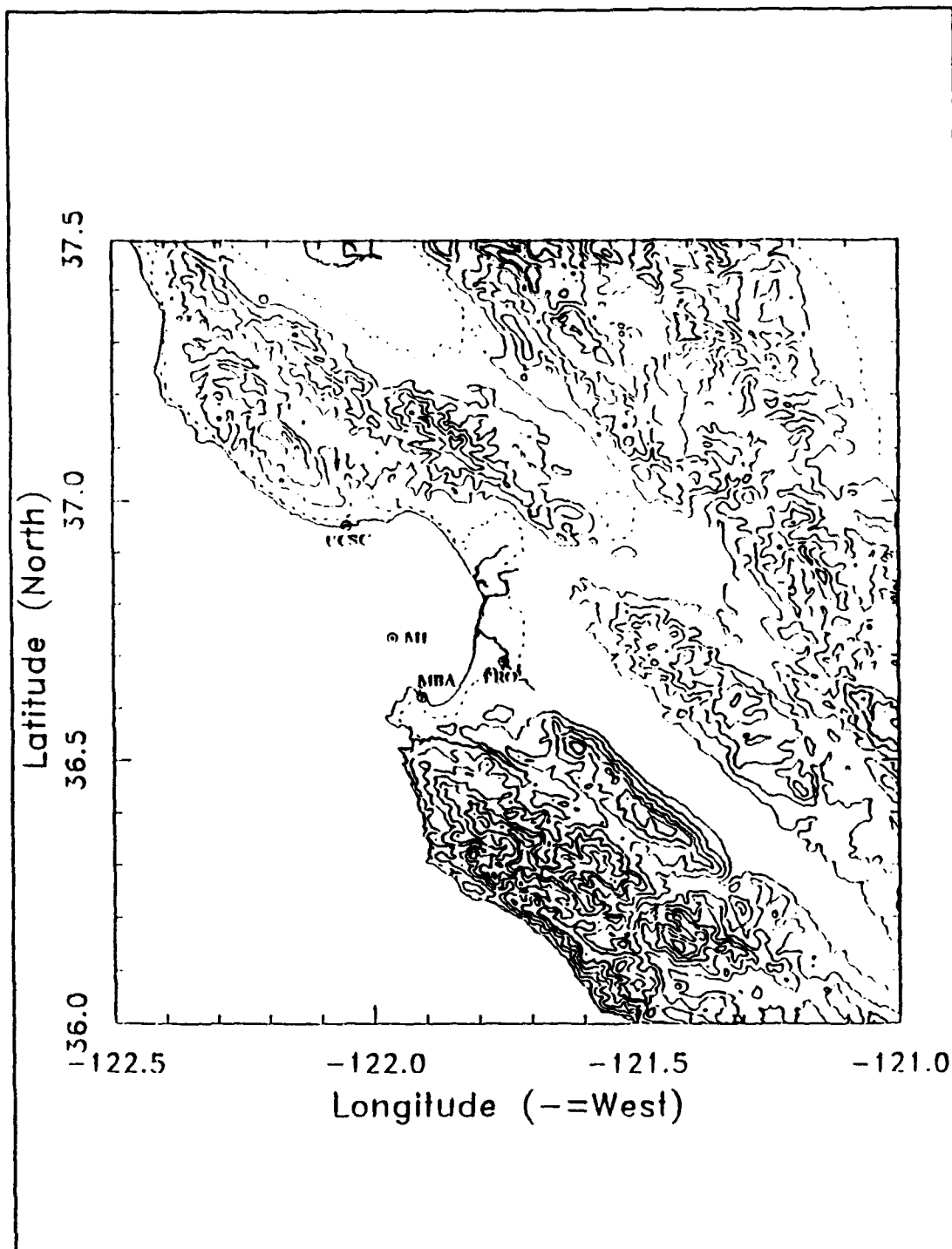


Figure 1. Monterey Bay, California and the Salinas Valley. Mooring (M1) and Profiler (PRO) Locations are Shown. Also Shown for Reference are Monterey (MBA) and Santa Cruz (UCSC). Contour Interval is 200 Meters.

II. BACKGROUND

A. MIXED LAYER BASICS

It is now widely accepted that in all areas of the world's oceans, there exists a layer of varying depth near the surface which may be considered as a nearly isothermal, isohaline and isovelocity slab. This allows temperature, salinity and velocity within the mixed layer to be approximated as bulk quantities, greatly simplifying the governing equations. A simple mixed layer diagram which reflects this bulk picture is presented in Figure

2. The depth at which the sharp gradients of these variables begins is referred to as the mixed layer depth, termed h . The thin layer below this depth is called the entrainment zone, with thickness δ . This is the region in which cold,

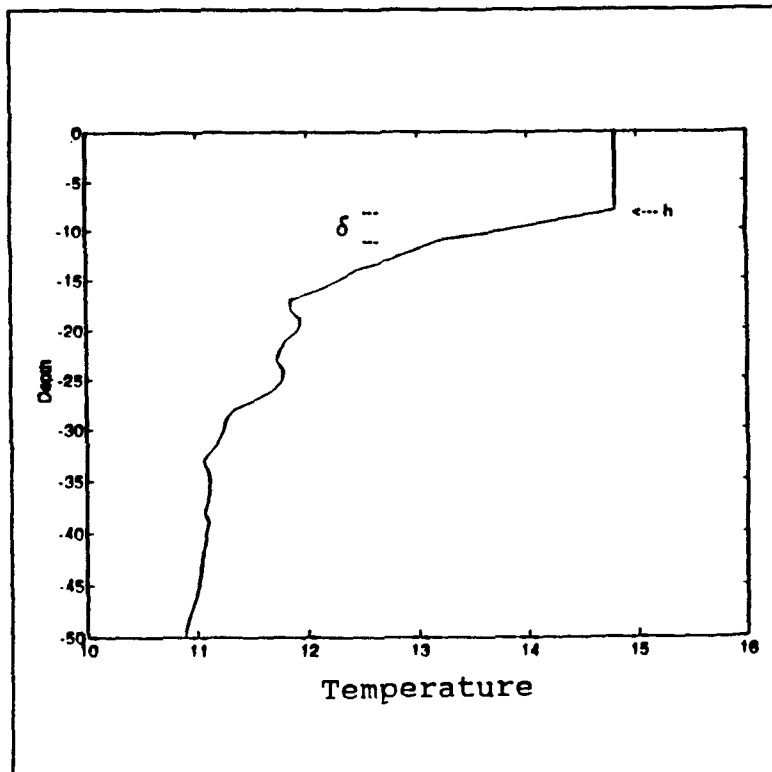


Figure 2. Bulk Mixed Layer Diagram.

dense water from below is entrained into the mixed layer, lowering the mixed layer temperature.

The mixed layer depth, and thus its temperature, is determined by the amount of turbulence available for mixing, as discussed in the introduction. Shear instability at both the top and bottom of the mixed layer contributes to this, although the surface forcing due to wind stress appears to be of much greater significance. As the wind stress acting on the ocean surface increases, turbulence generation due to shear also increases. Heat flux at the surface is the other key factor. When the total flux, a combination of heat gained from solar insolation, Q_s , and the heat lost from the surface due to latent, Q_e , sensible, Q_h , and net infrared radiation, Q_b is positive downward, as would generally be the case during the day in mid-latitude summer, mixed layer turbulence is damped as the stratification increases. Bulk theory assumes that the water below the entrainment zone remains completely non-turbulent. At night, the heat loss from the surface becomes dominant in the absence of downward heat flux (in general) and buoyant turbulence generation occurs, enhancing any wind mixing which may be present. This occurs through convective overturning of the water as its surface is cooled. In summary, wind shear at the surface always acts to generate turbulence which is available for mixed layer deepening, while buoyant fluxes may be either a source or a sink for the generation of turbulence.

B. MIXED LAYER MODELING

Treatment of the mixed layer with a one-dimensional model is a valid approach, in that vertical variations in water properties over about 100 meters typically far exceed any horizontal variations over 1000 km or more (Niiler and Kraus, 1977). This allows horizontal derivatives to be neglected, greatly simplifying the dynamics needed in the model. An early mixed layer model, Ball (1960), which was actually developed for the atmosphere, studied convective effects in the absence of horizontal motion over heated ground. This was extended to ocean mixed layer applications by the pioneering work of Kraus and Turner (1967), whose model became the basis for the group of so called integrated models, which are based on the bulk assumptions mentioned previously and which include both of the models used in this study.

There are basically three other categories of mixed layer models as described by McCormick and Meadows (1988). The first of these is the turbulence closure models, such as Mellor and Yamada (1974, 1982) and Kundu (1980), which solve for Reynolds stress terms in the turbulent energy equations through higher order terms. These models are relatively complex and require additional assumptions and empirically defined constants. Next are the deterministic solutions, such as Deardorff (1970). This model computes the Reynolds terms directly from variables which must be known with very fine spatial and temporal resolution and is extremely time

consuming. Finally, there are the eddy diffusion models, including Kent and Pritchard (1959), Pacanowski and Philander (1981), and McCormick and Scavia (1981). These are based on the thermal energy equation and the assumption that the Reynolds terms can be expressed according to a local relationship between mean scalar fields and eddy fluxes, as first done by Munk and Anderson (1948). Martin (1985) demonstrated, using a comparison of the Garwood (1977), Niiler (1975), and Mellor and Yamada (1974, 1982) models that, at ocean weather stations Papa and November in the Pacific, the complicated models of the turbulence closure type did not perform better in any significant way than the simpler integrated models. In fact, the Garwood model reproduced the temperature pattern at both stations better than the others. The deterministic models have proven too unworkable and the eddy diffusion type has received much criticism. Therefore, this study focused on two models of the integrated Kraus and Turner type, which will be discussed here in more detail.

The Kraus and Turner model was seen in several studies to have a problem with excessive wintertime erosion of the thermocline and it was widely considered that an improvement was necessary in the area of the parameterization of viscous dissipation (Martin, 1985). In other words, by neglecting the viscous dissipation, the model retained excessive turbulence and thus overdeepened the mixed layer. The models of Geisler and Kraus (1969), Miropol'skiy (1970), Denman (1973), and

Niiler (1975) were all variations of Kraus and Turner (1967) with dissipation included as a fixed fraction of wind stress production (Garwood, 1977). Resnyanskiy (1975), Kim (1976), and Elsberry et al. (1976) extended this by recognizing the need for additional dissipation during certain types of storm forcing. Finally, Pollard, Rhines and Thompson (1973) deviated from other Kraus and Turner based models by utilizing a total kinetic energy budget, rather than a turbulent kinetic energy budget. Whereas the original Kraus and Turner type determines entrainment by weighing the wind generated turbulence and buoyant forces at the base of the mixed layer, this second type, referred to as the dynamic instability type by Cushman-Roisin (1981), deepens the layer when the mean flow becomes unstable based on some criterion. The two models presented in this study represent these two branches of Kraus and Turner based integrated mixed layer models. Garwood's is of the turbulence budget type, while Price et al. (1986) is based on mean flow dynamic instability for its mixing.

C. MIXED LAYER BEHAVIOR IN COASTAL REGIONS

As mentioned in the introduction, most of the above models have been applied principally to mid-ocean, long time scale problems. There have been some studies, however, in which coastal influences and diurnal scale mixed layer behavior have been investigated. Price et al. (1986) looked at the diurnal cycle in the temperature and currents using high temporal

resolution data from R/P *Flip*. They defined a "trapping depth" as the mean depth value of a temperature anomaly profile, where the temperature anomaly is the difference between the temperature at a given depth and some reference temperature. They observed that the key to understanding the diurnal cycle of mixed layer heat content was to determine how this depth in responds to surface wind stress and stabilizing surface heat flux. Their mixed layer model will be presented in the next chapter.

The Coastal Upwelling Ecosystems Analysis (CUEA) program in the 1970's resulted in several studies in which a diurnally varying wind was observed. Like the winds of the northern California CODE region, the winds off Oregon and Peru were found by Halpern (1974), Burt et al. (1973, 1974), and Johnson (1975) to vary mainly in the along shelf direction, whereas the winds off Africa were more similar to the Monterey Bay region in that they exhibited more of a cross shore sea breeze type circulation (Halpern, 1977). All three regions exhibited a clockwise rotation of the diurnal winds (Rosenfeld, 1988). Off Africa, a diurnal cross-shelf wind magnitude of 3.5 m/s was observed out to 32 km from shore (Halpern, 1977). These studies also observed that the surface currents rotated clockwise, with the winds. Halpern (1977) concluded that these diurnal currents, since they were only in the upper water column, might be generated by the diurnal period wind, but no direct connection had been established (Rosenfeld,

1988). Rosenfeld (1988) studied the surface currents in the CODE area and modeled mixed layer behavior using the model of Price et al. (1986). She observed diurnal currents 2 to 3 times their average value during times of strong upwelling favorable winds. Again, they were found to be clockwise rotating and surface-intensified, with magnitudes up to 20 cm/s. A strong correlation with the diurnal winds was observed.

These previous studies have not thoroughly investigated the diurnal mixed layer thermal structure. The Rosenfeld (1988) work focused primarily on describing upper ocean currents at the diurnal period. Price et al. (1986) looked at the diurnal temperature cycle, but not in a region with diurnally varying winds. The present study is focused on this thermal structure in a sea breeze influenced region. Currents are not specifically analyzed in this study, as a one-dimensional model is not generally as useful for this purpose as it is for predicting temperature variations (Niiler and Kraus, 1977). Also, companion studies to this one (Foster, 1993 and Petruncio, 1993) investigate thoroughly the diurnal wind-driven and tidal currents, respectively, within Monterey Bay.

III. MODEL DESCRIPTIONS

Both the Garwood (1977) and the Price et al. (1986) models (hereinafter referred to as Garwood and PWP) are one-dimensional ocean mixed layer models. That is, they use only vertical heat and momentum fluxes at a given point to compute the deepening or shallowing of the mixed layer, without regard to horizontal or vertical advective effects. Vertical advection can be incorporated into a one-dimensional model, as done by Luan (1993) with PWP, and by Adamec et al. (1981) and Muller et al. (1984) with Garwood, but this modification was not made to either model used here due to the uncertainty involved in estimating its magnitude and variability. Advection, of course, is likely to be of significance in a coastal region such as this, where boundary currents and upwelling effects are present. These influences, as well as internal forces from below the mixed layer, were acknowledged to be a likely source of model error, but it was expected that they would be roughly quantifiable through comparison of the model temperature patterns with observations.

The same forcing was used to run each model. Computation of these air/sea fluxes is discussed in Chapter IV. Both use a vertical resolution of 1 meter and a time step of 1 hour, for reasons discussed in Chapter V. The following subsections will present the pertinent aspects of the two models,

demonstrating that, although both stem from the integrated model of Kraus and Turner (1967), they are fundamentally different in their approaches to mixing and entrainment of water from below the mixed layer. The Garwood model is based on the turbulent kinetic energy equation within the mixed layer, while PWP uses a Richardson number criterion to determine when mixing to another level should occur. The reader is referred to the original papers for details not contained in the following paragraphs, i.e., Garwood (1977) and Price et al. (1986).

A. THE GARWOOD (1977) MODEL

The basis for this model is the budget for turbulent kinetic energy (TKE) within the mixed layer. It has its roots in the basic Kraus & Turner model, but, like others developed since, includes a parameterization of viscous dissipation. Additionally, it is unique in its recognition of the non-isotropic nature of mixed layer turbulence, and accounts for this by breaking up the TKE equations into horizontal and vertical components (McCormick and Meadows, 1988). It was presented by Garwood (1977) as a model capable of simulating cyclical steady states by the mixed layer from diurnal to annual time scales.

Conservation of heat is generalized to an equation for conservation of buoyancy within the mixed layer, where buoyancy is defined as

$$\tilde{\rho} = \frac{g(\rho_0 - \tilde{\rho})}{\rho_0} \quad (1)$$

and

$$\tilde{\rho} = \rho_0 [1 - \alpha(\tilde{T} - T_0) + \beta(\tilde{s} - s_0)] \quad (2)$$

The tilde represents a total instantaneous value and the subscript 0 indicates an arbitrary representative value. T is temperature, s is salinity, ρ is density, and α and β are the thermal and haline expansion coefficients, respectively. Entrainment is derived from a solution of the total turbulent kinetic energy equation,

$$\frac{1}{2} \frac{\partial (\overline{u^2} + \overline{v^2} + \overline{w^2})}{\partial t} = - [\overline{uw} \frac{\partial U}{\partial z} + \overline{vw} \frac{\partial V}{\partial z}] + \overline{bw} - \frac{\partial}{\partial z} \left[w \left(\frac{\overline{u^2 + v^2 + w^2}}{2} + \frac{p}{\rho_0} \right) \right] - \epsilon \approx 0, \quad (3)$$

where upper case letters denote mean quantities and lower case represents fluctuating components. Overbars indicate instantaneous quantities that have been averaged over time. The letters u , v , and w represent eastward, northward, and upward velocities and ϵ is viscous dissipation. In this equation, the rate of entrainment depends on the rate of supply of energy from above the entrainment zone, which is the third term on the right hand side of equation (3), computed at depth h . The entrainment mechanism is theorized to be of Benjamin's (1963) class C, in which local Helmholtz instabilities act to advect packets of denser water up into the mixed layer. An entrainment time scale, τ_e , is defined as

the time needed to transport turbulent energy to the entrainment zone. This is given by

$$\tau_e = a_1 h \langle w^2 \rangle^{-1/2} \quad (4)$$

where a_1 is a constant of proportionality, $\langle w^2 \rangle^{1/2}$ is the rms vertical velocity scale, and the angle brackets represent vertical integration over the entrainment zone.

Assuming momentum and buoyancy transport below the entrainment zone are negligible, the mean buoyancy and momentum equations

$$\frac{\partial B}{\partial t} = -\frac{\partial \bar{b}w}{\partial z} + \frac{\alpha g}{\rho_0 c_p} Q \quad (5)$$

$$\frac{\partial U}{\partial t} = fV - \frac{\partial \bar{u}w}{\partial z} \quad (6)$$

$$\frac{\partial V}{\partial t} = -fU - \frac{\partial \bar{v}w}{\partial z} \quad (7)$$

can be integrated across the entrainment zone of thickness δ to yield the following so-called jump conditions

$$-\bar{b}w(-h) = \Delta B \frac{\partial h}{\partial t} \quad (8)$$

$$-\bar{u}w(-h) = \Delta U \frac{\partial h}{\partial t} \quad (9)$$

$$-\bar{v}w(-h) = \Delta V \frac{\partial h}{\partial t}, \quad (10)$$

where the Δ 's represent a jump from above to below the entrainment zone. Garwood postulates that the critical factor in determining the entrainment rate is the quantity

$$P = \frac{\overline{bw}}{\frac{\partial}{\partial z} \left[w \left(\frac{E}{2} + \frac{P}{\rho_0} \right) \right]}, \quad (11)$$

where E is the TKE ($u^2 + v^2 + w^2$) and the relationship represents the ratio of buoyancy flux to convergence of energy flux. This, together with equation (4) produces the Garwood entrainment equation

$$P(-h) = \frac{h \overline{bw}(-h)}{(\overline{w^2})^{1/2} \langle E \rangle} = m_4, \quad (12)$$

where m_4 becomes the first of five empirically derived dimensionless constants in the model. With the introduction of two new unknowns, $\langle E \rangle$ and $\langle w^2 \rangle$, the prediction of the upper ocean thermal profile requires closure through mean turbulent field modeling of the vertically integrated turbulent kinetic energy component equations, plus the bulk equations for buoyancy and momentum (Garwood, 1977). Vertical integration of equations (5), (6), and (7) across the depth of the mixed layer, with assumptions of negligible vertical fluxes below the mixed layer and homogeneity within the layer, yields the bulk relationships for buoyancy and momentum in the model,

$$h \frac{\partial \langle B \rangle}{\partial t} + \Delta B \frac{\partial h}{\partial t} \Lambda = \frac{\alpha g Q_0}{\rho_0 c_p} - \overline{bw}(0) \quad (13)$$

$$h \frac{\partial \langle U \rangle}{\partial t} + \Delta U \frac{\partial h}{\partial t} \Lambda = f h \langle V \rangle - \overline{uw}(0) \quad (14)$$

$$h \frac{\partial \langle V \rangle}{\partial t} + \Delta V \frac{\partial h}{\partial t} \Lambda = -f h \langle U \rangle - \overline{vw}(0). \quad (15)$$

The Heaviside step function Λ is zero in the case where the mixed layer is shallowing, and 1 otherwise. Again, horizontal advection of buoyancy and momentum are neglected.

Garwood defines a convective turbulent eddy time scale, τ_1 , proportional to mixed layer depth divided by rms turbulent velocity, and a rotational time scale, τ_2 , equal to the inverse Coriolis parameter. These time scales are combined according to

$$\frac{1}{\tau_e} = \frac{1}{\tau_1} + \frac{1}{\tau_2} \quad (16)$$

to produce the Garwood version of the turbulent dissipation rate, or

$$D = m_1 \langle E \rangle^{3/2} (1 + R_0^{-1} \frac{m_5}{m_1} \frac{u_*}{\langle E \rangle^{1/2}}), \quad (17)$$

where $R_0 = u_*/hf$ is a Rossby number for the mixed layer and m_1 and m_5 are two new empirically derived constants.

The bulk equation for pressure redistribution R used in the model is

$$R = m_2 \langle \bar{E} \rangle^{3/2} - 3m_2 \langle \bar{E} \rangle^{1/2} \langle \bar{w}^2 \rangle. \quad (18)$$

With an assumption that the mean layer velocity is proportional to u_* , the surface friction velocity, the final term of the model may be generated. This is the net wind generated shear production rate, or

$$G = - \int_{-h}^0 \left[\bar{u} \bar{w} \frac{\partial U}{\partial z} + \bar{v} \bar{w} \frac{\partial V}{\partial z} + \frac{\partial}{\partial z} \left(\frac{\bar{w} \bar{p}}{\rho_0} + \frac{\bar{w} \bar{E}}{2} \right) \right] dz = m_3 u_*^3 + \frac{(\Delta U)^2 + (\Delta V)^2}{2} \frac{\partial h}{\partial t}. \quad (19)$$

The preceding development results in the final equations which represent the Garwood (1977) model. These are

$$-\bar{bw}(-h) = \frac{m_4 \langle \bar{w}^2 \rangle^{1/2} \langle \bar{E} \rangle}{h} \quad (20)$$

$$\begin{aligned} \frac{1}{2} \frac{\partial}{\partial t} (h \langle \bar{u}^2 + \bar{v}^2 \rangle) = & m_3 u_*^3 - \frac{bw(-h) |\Delta C|^2}{2\Delta B} - m_2 \langle \bar{E} \rangle^{3/2} + 3m_2 \langle \bar{E} \rangle^{1/2} \langle \bar{w}^2 \rangle \\ & - \frac{2}{3} (m_1 \langle \bar{E} \rangle^{3/2} - m_5 f h \langle \bar{E} \rangle) \end{aligned} \quad (21)$$

$$\begin{aligned} \frac{1}{2} \frac{\partial}{\partial t} (h \langle \bar{w}^2 \rangle) = & \frac{h}{2} [bw(-h) - u_* b_*] + m_2 (\langle \bar{E} \rangle^{3/2} - 3 \langle \bar{E} \rangle^{1/2} \langle \bar{w}^2 \rangle) \\ & - \frac{1}{3} (m_1 \langle \bar{E} \rangle^{1/2} + m_5 f h) \langle \bar{E} \rangle. \end{aligned} \quad (22)$$

where $C = U + iV$, m_1 through m_5 are empirical constants, and the other quantities are as previously defined. Equation (20) represents the entrainment buoyancy flux, while equations (21) and (22) are the horizontal and vertical components of turbulent kinetic energy within the mixed layer, respectively.

B. THE PRICE, WELLER & PINKEL (1986) MODEL

This model also benefits from the assumption of thermal, haline and velocity uniformity within the mixed layer. Its fundamental difference, following from Pollard et al. (1973), is the way in which it determines when mixing to another vertical level should occur.

The PWP model begins with the one-dimensional heat and momentum equations, as follows

$$\frac{\partial T}{\partial t} = -\frac{1}{\rho_0 c_p} \frac{\partial Q}{\partial z} \quad (23)$$

$$\frac{\partial u}{\partial t} = f v - \frac{1}{\rho_0} \frac{\partial G_x}{\partial z} \quad (24)$$

$$\frac{\partial v}{\partial t} = -f u - \frac{1}{\rho_0} \frac{\partial G_y}{\partial z}, \quad (25)$$

where the G_x and G_y represent the components of the shear stress in the water column, which at the surface equals the wind stress. Equations (24) and (25) are modified in the version of the PWP model used here to include a frictional term, as done in Rosenfeld (1988). The value assigned to the friction parameter is discussed in Chapter V.

As in Garwood (1977), density is calculated using a linearized equation of state, similar to equation (2). Absorption of solar insolation is handled in much the same way as it is in the Garwood model. Both absorb about half of the incoming irradiance in the upper meter of water, with an

exponential decay below that. PWP additionally breaks the solar energy into long and shortwave components and absorbs them according to different vertical decay scales. A brief discussion of water type assumptions made to determine the absorption coefficients is contained in the model sensitivities section of Chapter V.

Mixing is modeled as in the dynamic instability model of Price et al. (1978). It takes place in such a way as to satisfy conditions for static, mixed layer and shear flow stability, which are represented by equations (26), (27), and (28), respectively.

$$\frac{\partial \rho}{\partial z} \geq 0 \quad (26)$$

$$R_b = \frac{g \Delta \rho h}{\rho_0 (\Delta V)^2} \geq 0.65 \quad (27)$$

$$R_g = \frac{g \frac{\partial \rho}{\partial z}}{\rho_0 \left(\frac{\partial V}{\partial z} \right)^2} \geq 0.25 \quad (28)$$

Here, R_b is a bulk Richardson number and R_g a gradient Richardson number. As the surface fluxes are input to the model at each time step, vertical mixing occurs until all three of these conditions are met throughout the profile. PWP state that the latter two conditions are the predominant mixing processes and that they are entirely wind driven.

As the model runs, solar radiation is absorbed as described above, and surface heat loss is removed from the

uppermost meter of the water column at each time step. Densities are then computed and mixed to achieve static stability. Next, wind stress is absorbed and a value of R_b is computed and compared to the critical value of 0.65. Entrainment of denser water from below the mixed layer takes place as necessary to achieve condition (26). Price et al. (1986) also include the shear flow stability requirement to account for the fact that their observations indicate a smooth transition layer below the mixed layer, as opposed to the sharp jump assumed by other models, and because shear instability is likely at levels of strong stratification. R_g is calculated only within this transition layer and mixing takes place until it is above the critical value of 0.25 throughout this region. This has the effect of smoothing out the transition from mixed layer to the region below.

IV. DATA

A. SOURCES

1. OASIS MOORING

A modified ATLAS (Automated Temperature Line Acquisition System) mooring (Milburn and McClain, 1986), located at 36°45'N, 122°01'W (see Figure 1), was the primary source of meteorological and oceanographic data used in this study. The modification, done at MBARI, includes a controller known as OASIS, Ocean Acquisition System for Interdisciplinary Science (Chavez et al., 1991). The mooring, designated as M1, is owned and maintained by MBARI, with Dr. Francisco Chavez acting as supervising scientist. It is schematically depicted in Figure 3a, with the details of the buoy itself shown in Figure 3b. Above the waterline, it is equipped with sensors for air temperature, humidity, wind speed and direction and photosynthetically active radiation (PAR). Below the surface is a thermistor chain with sensors at 10, 20, 40, 60, 80, 100, 150, 200, 250, and 300 meters. CTD sensors are located at the surface, 10, and 20 meters. Other sensors include a fluorometer and a transmissometer, although these were not specifically used in this study. All of these data are collected at a 10 minute interval and transmitted to MBARI via packet radio telemetry. Winds are measured 3.8 meters above

the sea surface at a frequency of 2 Hz and averaged over one minute. The mooring is also equipped with an acoustic Doppler current profiler (ADCP), which samples at a 15 minute interval. Data quality for all parameters of interest to this study was excellent throughout the period with no gaps or systematic errors, with the exception of the sea surface temperature sensor on the ATLAS mooring, which read consistently high by a few degrees. Sea surface temperatures used were therefore obtained from the CTD sensor mounted on the mooring at the surface. The time response of this sensor is on the order of seconds, whereas the time response for the subsurface sensors is on the order of minutes.

A possible error in the data was in the measurement of wind direction. This is determined on board the buoy by combining a compass measurement of the buoy orientation with an anemometer vane measurement of the wind direction relative to the buoy. Later in the mooring deployment, the compass failed. While examination of the data used here show no conclusive evidence of a problem with wind direction, comparisons with data from other nearby land stations suggest that wind direction could be off by up to 30°. Since it is only the strength and rotation rate of the wind that is important in a one-dimensional analysis, this possible error should not present a problem for this study. Specifications and details of operation for the OASIS mooring are contained

in the Pacific Marine Environmental Laboratory reference manual (1992).

2. NPS Profiler Site

Shortwave and longwave irradiance data used in this study were collected at the Naval Postgraduate School's (NPS) meteorological station located on Fort Ord as shown in Figure 1. This site, located 23 kilometers east-southeast of the mooring, is equipped to measure a variety of meteorological parameters at 2 minute resolution. However, only the irradiance data was of practical use due to distance from M1 and availability of other necessary data from the mooring itself. Shortwave irradiance is measured with an Eppley Precision Pyranometer (Model PSP) and longwave irradiance is measured with an Eppley Precision Infrared Radiometer (Model PIR). Specifications for both are contained in the Eppley Laboratory reference manual (Eppley Laboratory, 1971).

B. DESCRIPTION OF ATMOSPHERIC AND OCEANIC DATA AND DERIVED QUANTITIES

1. Synoptic Weather Description

During most of the period of study, Monterey Bay was under the influence of the typical summer high pressure system over the eastern North Pacific Ocean. A 1030 mb high centered near 45°N, 160°W can be seen in Figure 4, which indicates the surface pressure pattern at 1200Z on 3 September, and which is representative of the period 1 to 8 September. Generally

clear skies inland with some low-level stratus offshore can be seen in the imagery from this time period. The result of this pattern, which persists for long intervals in this region, is light and variable synoptic scale winds, with subsidence associated with the eastern portion of this system creating the usual low-level marine inversion over the cool upwelled waters of the coastal region. This marine layer is the source of the frequent night and morning fog, which occurs to varying degree on each of the days of the study period.

The clear inland weather associated with this fair weather system, combined with the weak large scale forcing, allowed for extensive heating in the Salinas Valley. High temperatures in King City, near the head of the valley, reached to near 100°C during most of the period. This heat, in the presence of the light synoptic scale winds, allowed for near classical development of sea breeze conditions in the Monterey Bay.

During the 9th and 10th of September, the high pressure weakened to 1023 mb and gave way along the coast to low pressure centered off northern California. This produced significant cloudiness in the study area. The surface pressures from 10 September are shown in Figure 5. Synoptic scale flow remained weak during this time, but the cloudiness greatly reduced the heating onshore and thus the sea breeze signature, as will be seen in the following sections.

2. Hourly Data

The following subsections present the raw wind, sea surface temperature, air temperature, humidity, and 10, 20 and 40 meter sea temperatures collected at mooring M1. Radiation data will be presented in the next section, along with a discussion of its use. Corresponding figures are located at the end of this chapter. The data are shown with the full temporal resolution of 10 minutes. However, it is noted here that hourly averages of wind components, surface and air temperatures, and humidity were computed and used to generate the model forcing for reasons discussed in Chapter V. A comparison of raw and hourly averaged data indicated that all of the key features were maintained in this process, particularly the timing and duration of each diurnal event.

a. Winds

U and V wind components are shown in Figure 6a, while total wind speed is shown in Figure 6b. The east/west component dominates the signal on most days. Readily apparent is the strongly diurnal variation in the magnitude of the winds. Wind magnitude tends to be quite light at night and into early morning, averaging about 2 m/s over the 11 day period. At an average time of 1737Z (1037 PDT), the sea breeze front reaches the mooring location and winds accelerate rapidly, reaching a peak of 6 to 12 m/s by the mean time of 0029Z (1729 PDT), averaged over all 11 days of the period.

The peak wind of the period occurred at 0116Z on the 6th, which corresponds to 1816 PDT on the 5th, when the wind exceeded 12 m/s. A plot of true wind direction (Figure 6c) shows that the rapid increase in wind speed associated with the onset of the sea breeze corresponds to the abrupt shifting of the direction toward the southeast, or about 130 degrees true, as would be expected by the orientation of the Salinas Valley. In general, the winds taper off more gradually in the late afternoon and are replaced with the light, variable winds, with little or no tendency to favor an offshore land breeze toward the west. This offshore wind is better developed at the profiler site. Another view of the winds is shown in Figure 6d, a feather plot of hourly averaged wind vectors, which shows that the wind is generally blowing toward the southeast, but intensifies most afternoons from a mean direction of 310°T.

It should be noted that the strongest sea breeze days were 6, 7, and 8 September, when the inland and coastal weather was the clearest and maximum heating occurred in the valley. Correspondingly, the wind magnitudes observed at the mooring were extremely light on 9 through 11 September, when extensive cloudiness was present both in the bay and at the profiler site, as well as further inland. The winds on these days only reached maxima of 5 to 6 m/s.

The winds can clearly be characterized as being overwhelmingly dominated by variations in the diurnal

frequency band, although to a reduced degree during this latter period. Therefore, the momentum fluxes computed from these winds will be strongly diurnal. The phase relationship of this diurnal wind stress pattern to the diurnal heating will be discussed later in this chapter.

b. Air Temperature

As would be true in most areas, air temperatures also exhibit a strongly diurnal variation, although the magnitude of the day/night swing is small compared to the nearby land data. Temperatures observed at M1 in early September are seen in Figure 7. The mean air temperature over the period was 14.41°C , with a standard deviation of 0.83. The average high temperature was 15.22°C , and the low averaged 13.50°C . An average diurnal temperature swing of 1.71°C occurs over the period, although of note is the 3.25°C range seen from maximum to minimum on the 6th. Mean time of warmest temperatures for the day is 0115Z (1815 PDT), with a range of 2226Z to 0353Z. Daily lows occur between 1206Z and 1928Z, with an average of 1658Z (0958 PDT).

c. Humidity/Dew Point

As mentioned previously, the ATLAS mooring measures relative humidity. These data are shown in Figure 8. For the purposes of computing fluxes, as will be discussed in the next section, a conversion to dew point temperatures was made. These are plotted along with the air temperatures in

Figure 7. As would be expected, the air was quite moist throughout the period, with the exception of the late afternoon of the 5th (about 0000Z on the 6th), when the relative humidity dipped briefly to 76% with a strong, relatively dry sea breeze due to the presence of drier air offshore. Otherwise, the humidity is consistently above 90% with the air at or near saturation on several evenings and mornings, as well as most of the 9th through the 11th, related to fog and/or low clouds.

d. Sea Surface Temperature

Ocean surface temperatures as measured by the surface CTD on the OASIS mooring are presented in Figure 9. The diurnal cycle is again the dominant feature of this pattern. Over the 11 day period, the sea surface temperature averages 14.64°C , with a standard deviation of 0.51. Daily maxima occur between 2027Z and 0223Z, with an average time of 2303Z (1603 PDT), and have a mean value of 15.30°C . The minimum temperature averages 14.26°C and occurs at 1334Z (0634 PDT) in the mean. Thus, the surface temperature minima and maxima lead those of the air temperature by 3:24 and 2:12 h, respectively. The magnitude of the diurnal variation in sea surface temperature data will be of importance in later model result discussions. This day to night swing ranges from 0.57°C to 1.55°C and averages 0.96°C .

e. *Temperatures at 10, 20, and 40 Meters*

Ocean temperatures from the surface, 10, 20 and 40 meter thermistors are shown in Figure 10. At 10 meters, the diurnal pattern is still quite apparent and dominates the temperature signal. Occasions on which the mixed layer deepens to or below this depth are seen here as convergences of the surface and 10 meter traces. It is clear that this occurs on several nighttime cooling cycles, but not at all during the latter portion of the period when winds were light. Direct measurements of mixed layer depth were not available during the study period (with the exception of a series of CTD casts made on 9 September on a MBARI cruise). The 20 meter temperatures show a signal dominated by much higher frequency variation than diurnal, driven by internal waves rather than surface forcing. During September 4th, it appears that the mixed layer actually deepened briefly to this depth. At 40 meters, a similarly high frequency temperature pattern is seen, although quite damped relative to 20m. Of note is a slight downward trend in the 10 and 20 meter data over the period. This will be discussed more quantitatively with respect to advective effects in Chapter VI.

C. MIXED LAYER CHARACTERISTICS AT M1

The data described above depict an ocean mixed layer that, like in other areas, undergoes a strongly diurnal variation in thermal structure. The mostly clear weather permits

significant heating and resultant stratification during the day, with relatively calm conditions and convective cooling at night. The mixed layer depth is generally less than 20 meters and often shoals to less than 10 meters, particularly when the winds are light and the insolation is strong. The wind pattern described is also varying diurnally, with near calm conditions being rapidly replaced with winds of 8 to 12 m/s. The peaks of wind stress occur in the late afternoon to early evening each day, approximately coincident with the peak in air temperature but well after that of solar insolation. Thus, the afternoons are characterized by the strongest turbulence generation due to the wind, but also fairly strong buoyant damping from the continuing downward heat flux. The winds die down fairly rapidly as darkness sets in, reducing the shear generation of turbulence, but at the same time, convective cooling is creating buoyant turbulence. By early morning, buoyant damping caused by the rising sun can quickly shallow the mixed layer, since the winds are typically at their weakest at that time. The next chapter will present a discussion of model sensitivities, followed by the model results themselves. A discussion of their ability to handle mixed layer behavior in this relatively complex environment will follow in Chapter VI.

D. SURFACE FLUXES

1. Cloud Cover Estimation

No direct measurements of cloud cover were made during the study period. In order to provide reasonable cloud cover information for the purpose of generating valid surface fluxes, it was necessary to estimate cloud cover from available indirect methods. To achieve this, insolation and longwave downward irradiance data from the nearby NPS profiler site and photosynthetically active radiation (PAR) data from the mooring were integrated to create the best possible estimation of percent cloud cover.

These data are shown in Figures 11a and b. Insolation data was compared with that observed on 7 September (an extremely clear day) and 10 September (a completely cloud covered day) to obtain an approximation of cloud cover in eighths for the daytime periods. The presence of fog or low clouds is evident in the data during the intervals when the value of longwave irradiance jumps to about 400 W/m^2 , such as 1000 through 1900 GMT on the 1st, and remains fairly steady at that level. This was very useful for confirming and adjusting the cloud cover during the daylight hours, but also served to provide a means for rather accurate assessment of clouds at night. A steady 400 W/m^2 is consistently indicative of complete low-level stratus or fog. These downward irradiance data demonstrate that the cloud cover is frequently either

100% or 0%, as there are only relatively brief occasions when an intermediate value is measured.

The combination of the downward irradiance and incoming shortwave radiation produced an estimate of cloud cover at the profiler site. The PAR data were then used to assess the validity of this cloud pattern at the mooring. In general, the PAR sensor confirmed the mainly sunny pattern, with some clouds at the end of the period, seen at the profiler. On the 9th (peak centered prior to 10/00Z in Figure 11b), however, it was clear that a much cloudier day occurred at M1 than at the profiler. This information was then used to increase the estimate of cloud cover at the buoy on that day.

2. Model Forcing

As mentioned previously, the same program was used to generate the heat and momentum fluxes for both models. Hourly averages of U and V wind components, air temperature and dew point, sea surface temperature, and cloud cover were computed from the data, and used as the input for the flux generation. Latent and sensible heat fluxes, as well as wind stresses, were computed in accordance with the methods of Large and Pond (1981). Net longwave irradiance and incoming shortwave irradiance were computed using the formulations of Husby and Seckel (1975). These calculations were combined into a forcing program by R.W. Garwood of NPS. Adjustments were made for latitude and longitude and the code was altered to allow

hourly, vice three-hourly, inputs of the meteorological values in order to better reflect the diurnal time scale mixed layer evolution. Sensible, latent, and infrared heat fluxes were combined into a net heat loss value. This, together with the solar insolation values and wind stresses, was passed to the models for forcing, with adjustments made for different format and unit requirements in each model. Plots of all the forcing values computed and passed to the models are contained in Figures 12a, b, c, and d.

The first of these is computed wind stress, using the relationship

$$\tau = \rho_a C_D U_*^2, \quad (29)$$

where C_D is the drag coefficient from Large and Pond (1981) and ρ_a is the density of air (1.23 kg/m^3). Figure 12b shows the solar insolation pattern, adjusted from the ideal, cloudless sine wave pattern to reflect the cloud cover influences estimated as described in the last subsection. Figure 12c presents the individual heat loss terms, with positive values indicating heat lost from the ocean to the atmosphere, along with the total hourly heat loss passed to the models for forcing. From this last figure, it is clear that the largest term in the net loss is the infrared radiation, Q_b . This reaches a minimum of about 30 W/m^2 during cloudy periods and a maximum of about 75 W/m^2 on clear days. The sensible heat flux can be seen to generally be near 0,

reaching a maximum loss of 7 W/m^2 late on the 7th and a minimum of -25 W/m^2 early on the sixth (negative values indicate a gain of heat by the ocean), when a brief surge of relatively dry, warm air passed through the mooring area. The latent heat flux is obviously closely tied to the wind stress pattern shown in Figure 12a. Finally, a summary plot (Figure 12d) shows the net heat flux computed by the forcing routine, demonstrating the dominance of the short wave solar heating.

A statistical summary of the wind stress and net heat flux is offered here for later use in the discussion of the model results. Wind stress averaged 0.340 dynes/cm^2 over the period, with a standard deviation of 0.407 . The average minimum of 0.044 occurred at 1730Z (1030 PDT) in the mean. The maximum averaged 0.942 dynes/cm^2 and occurred typically at 0029Z (1729 PDT), although on the stronger wind days in the middle of the period, this peak occurred closer to 1840 PDT. The maximum downward heat flux each day had a mean value of 650 Watts/m^2 . The timing of this peak was very regular at 2011Z (1311 PDT).

Black body irradiance from the sea surface was combined with measured longwave down data as a check on the validity of the computed net infrared heat loss, the largest term in the total heat loss. Values were in good agreement (within a maximum error of 20 W/m^2). Varying heat loss within the range of reasonable values showed the insensitivity of the models to this parameter, relative to wind and insolation.

A hand-drawn sketch of a vertical assembly, possibly a probe or a well. The sketch is oriented vertically with the top at the top. At the very top, there is a small, narrow, conical structure. Below this, the main body is a long, vertical tube. Various components and labels are indicated along the tube:

- At the top, below the conical structure, is the label "CAGE RING".
- Below the cage ring, there are three small circles, each with a label: "1" SAS", "3/4" SAS", and "BASTY BRACKET".
- Below these circles is the label "3/4" SAS".
- Further down is the label "12 M CHAIN".
- Below the chain is the label "3/4" SAS".
- Below that is the label "3/8" WIRE ROPE IN THIS TUB".
- Below the wire rope is the label "TEMP CABLE 3/16 M".
- Below the cable is a small circle with the label "6" 9 SAS".
- Below the circle is the label "6" 1/2" SAS".
- Below the circle is the label "5/8" SAS".
- Below the circle is the label "1/2" CIV IN".
- Below the circle is the label "6" 8 SAS (WITH PLASTIC PIPING)".
- Below the circle is the label "FIRE PROTECTING TUBING".
- Below the tubing is the label "3/4" INCH 5/16 M".
- At the bottom of the tube, there is a small circle with the label "3" 1/2" INCH".

39

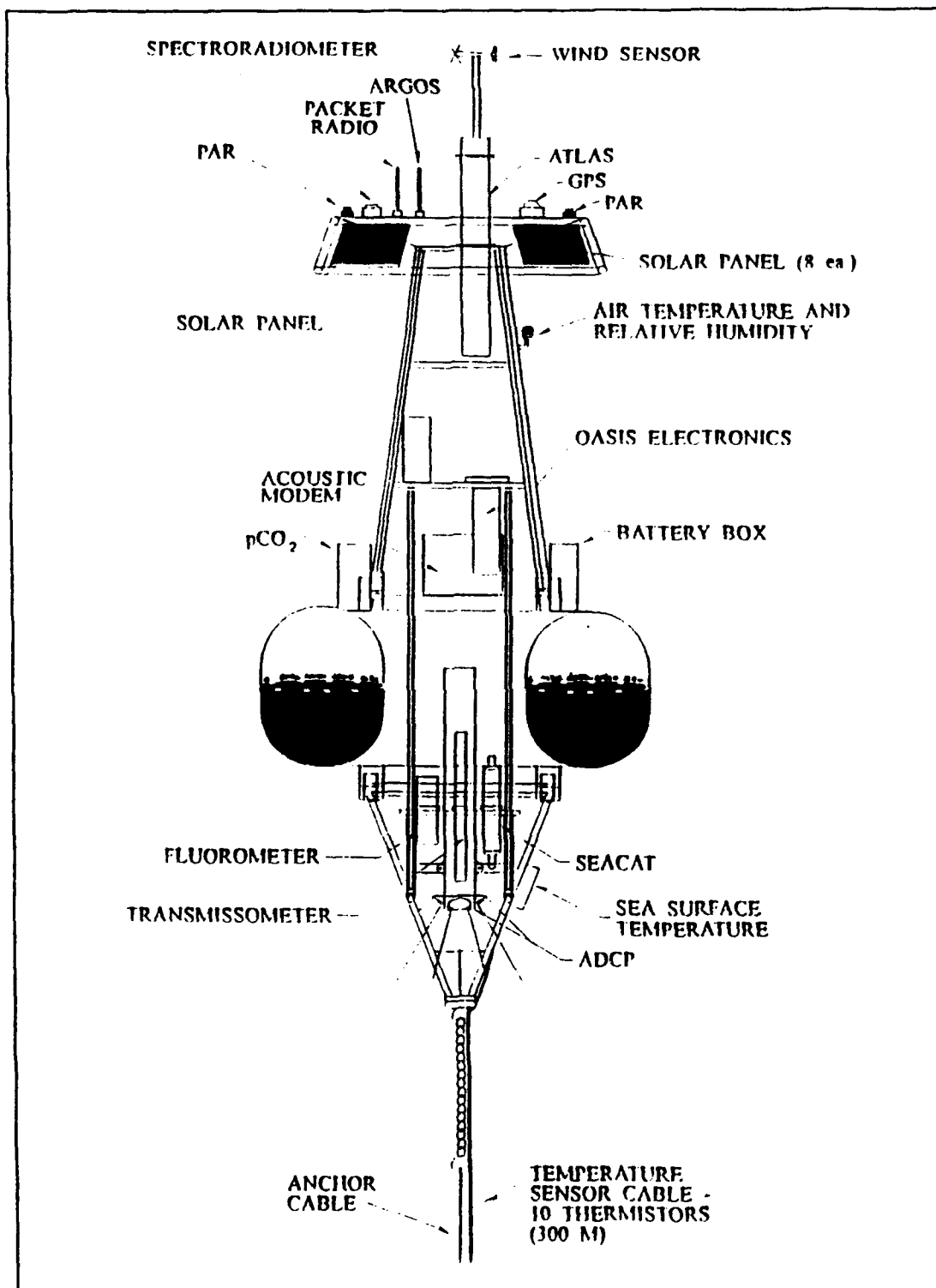


Figure 3b. Schematic Diagram of the ATLAS Buoy: Courtesy of Francisco Chavez, MBARI.

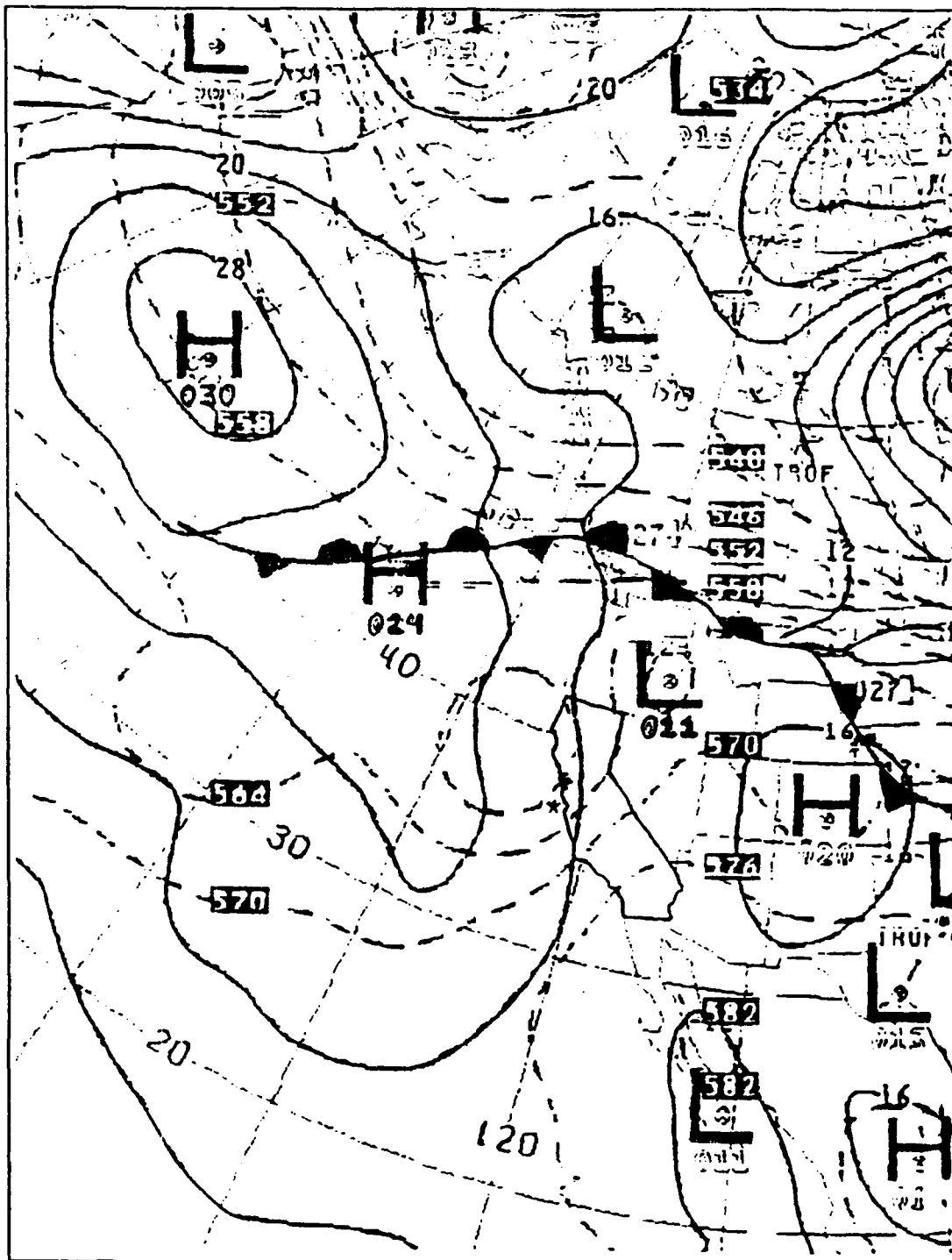


Figure 4. Surface Pressure Chart From 4 September, 1992. Monterey Bay is Designated With a *. Solid Lines are Surface Pressures in Millibars and Dashed Lines Indicate 1000 to 500 mb Thickness.

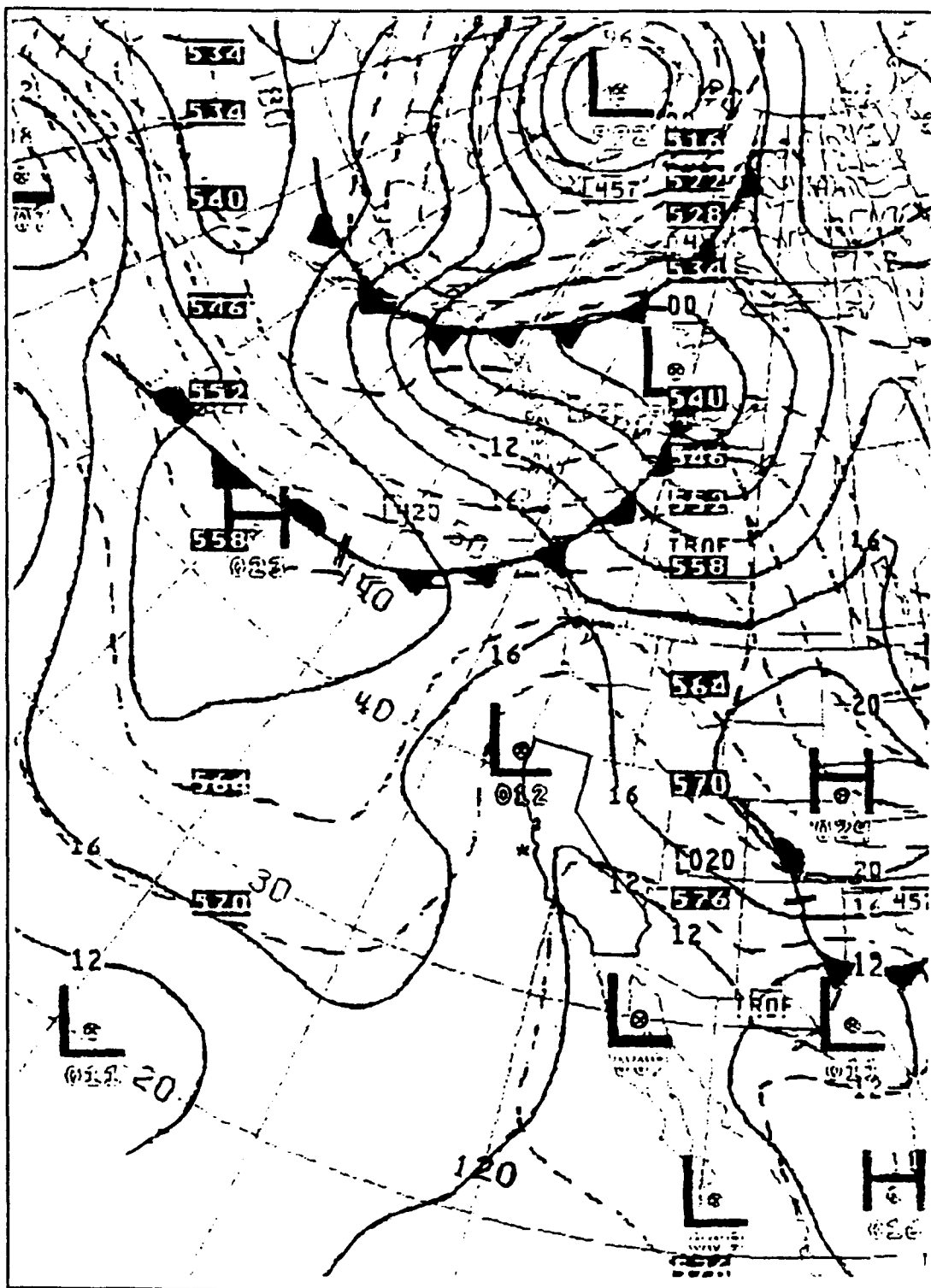


Figure 5. Surface Pressure Chart From 10 September, 1992. Same Line Convention as in Figure 4.

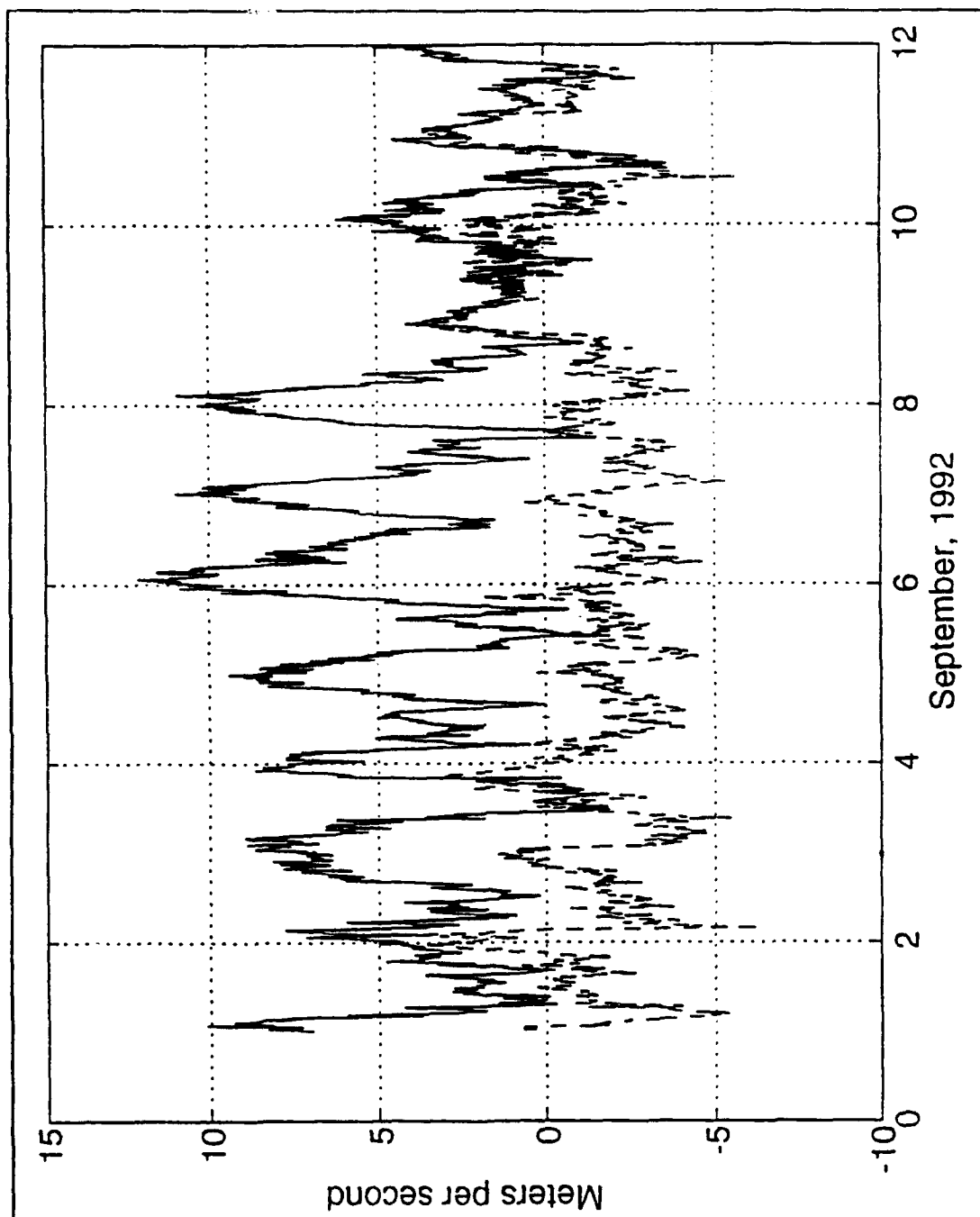


Figure 6a. Full Resolution U and V Wind Components Measured at M1. The V Component is Dashed. This and All Subsequent Data and Model Plots are in Greenwich Mean Time. Local Time May be Obtained by Subtracting 7 Hours.

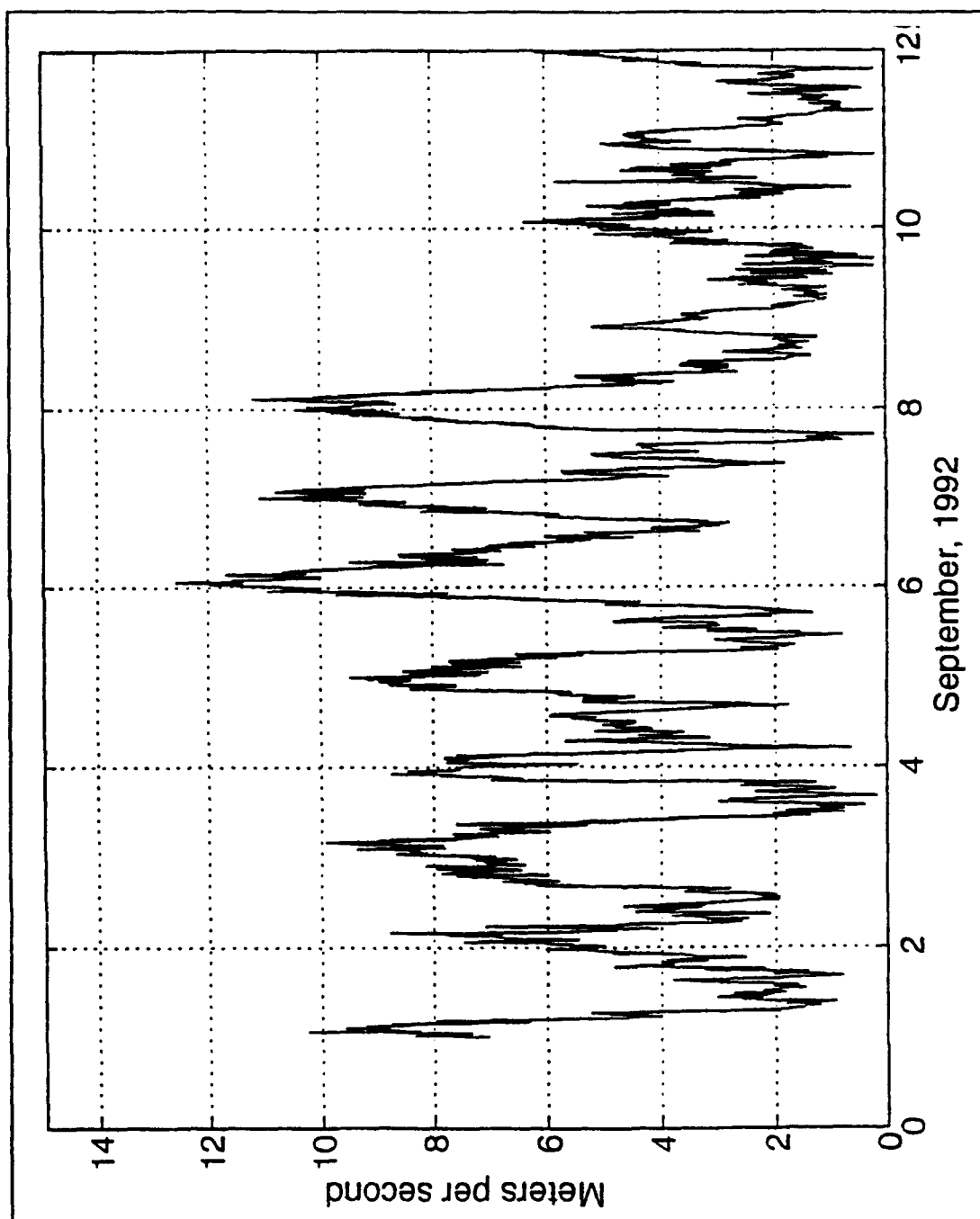


Figure 6b. Wind Speed at M1.

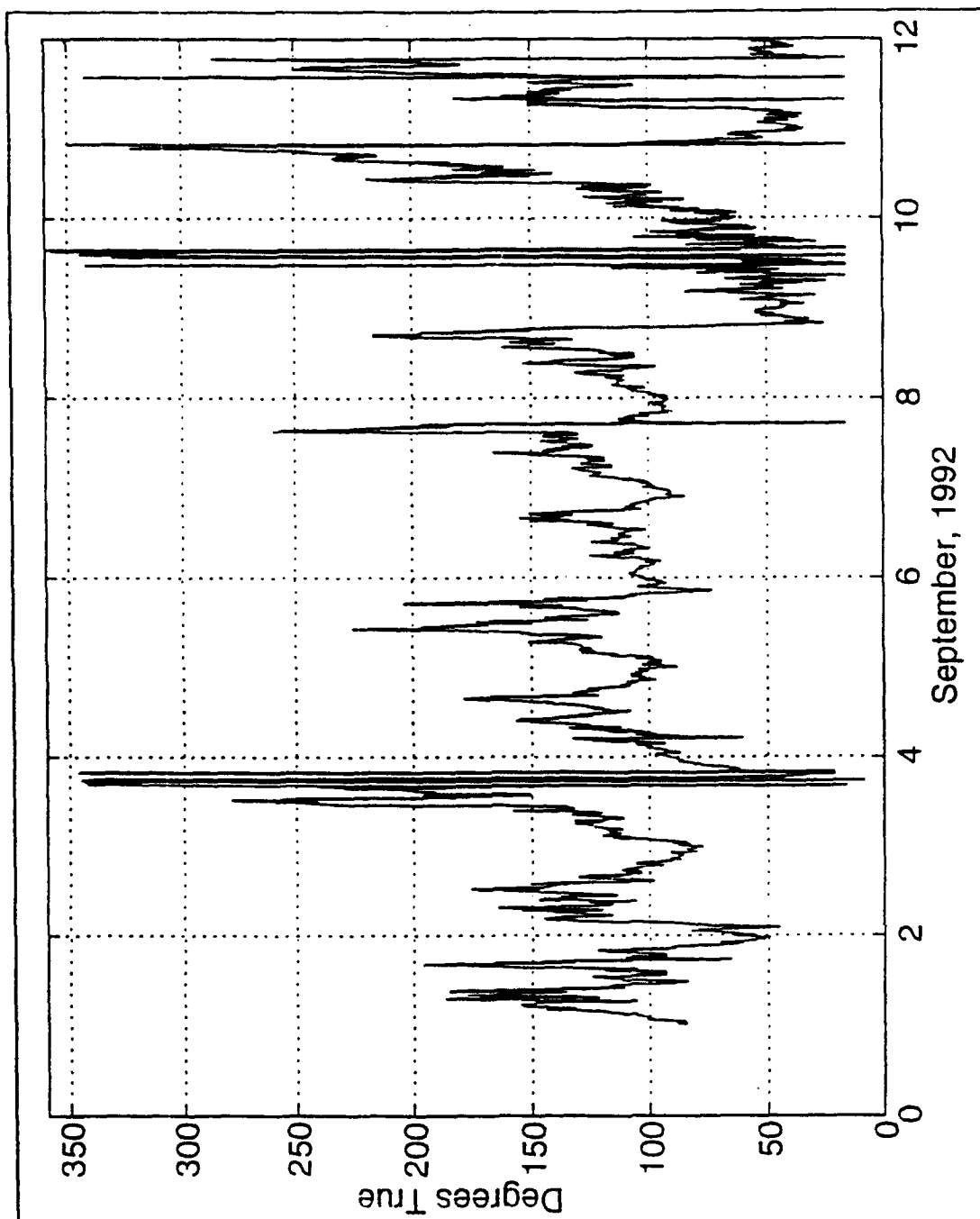


Figure 6c. True Wind Direction at M1. Values Indicate the Direction the Wind Vector was Pointing. Periods of Large Variation Occur During Light Winds.

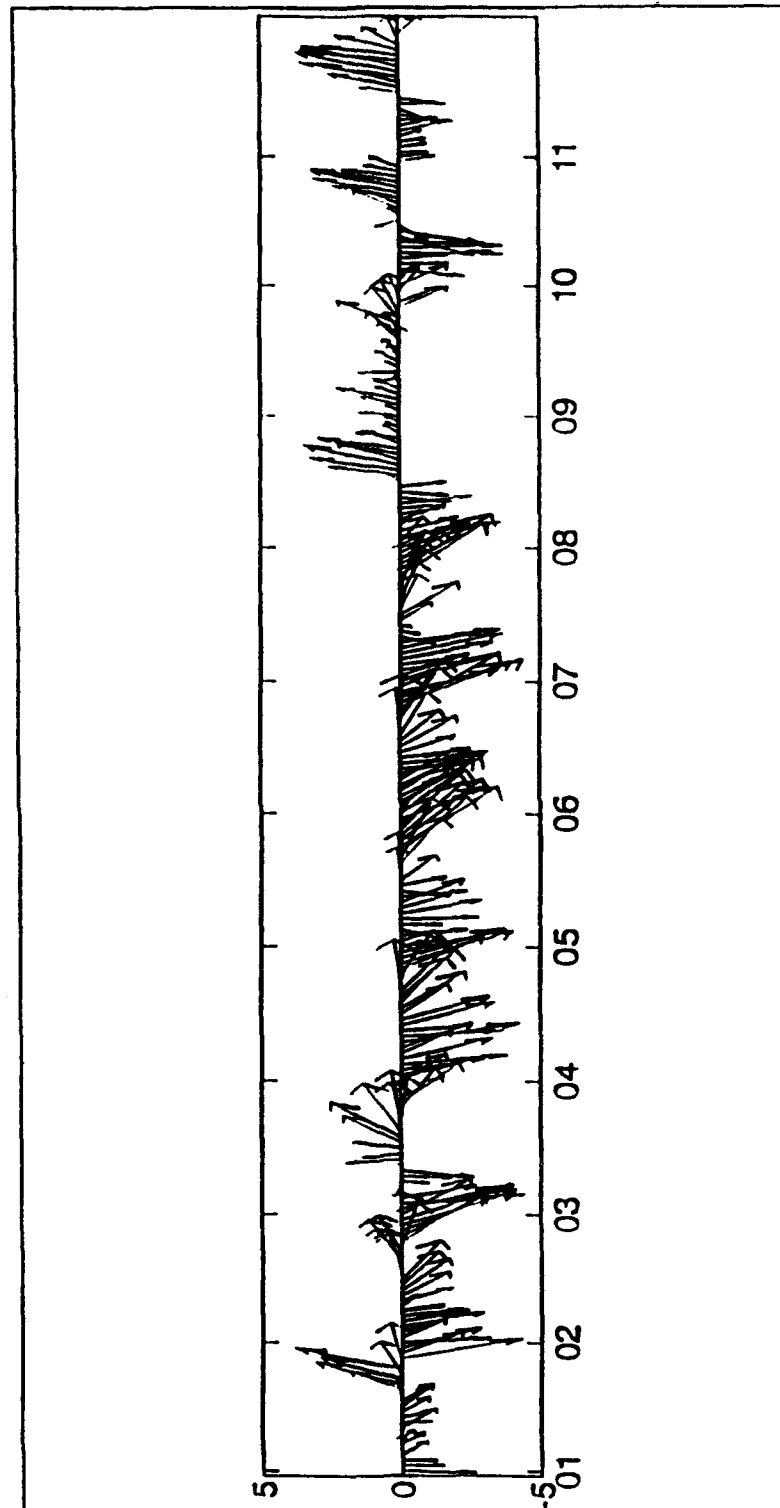


Figure 6d. Feather Plot of Hourly Wind Vectors Recorded at M1.

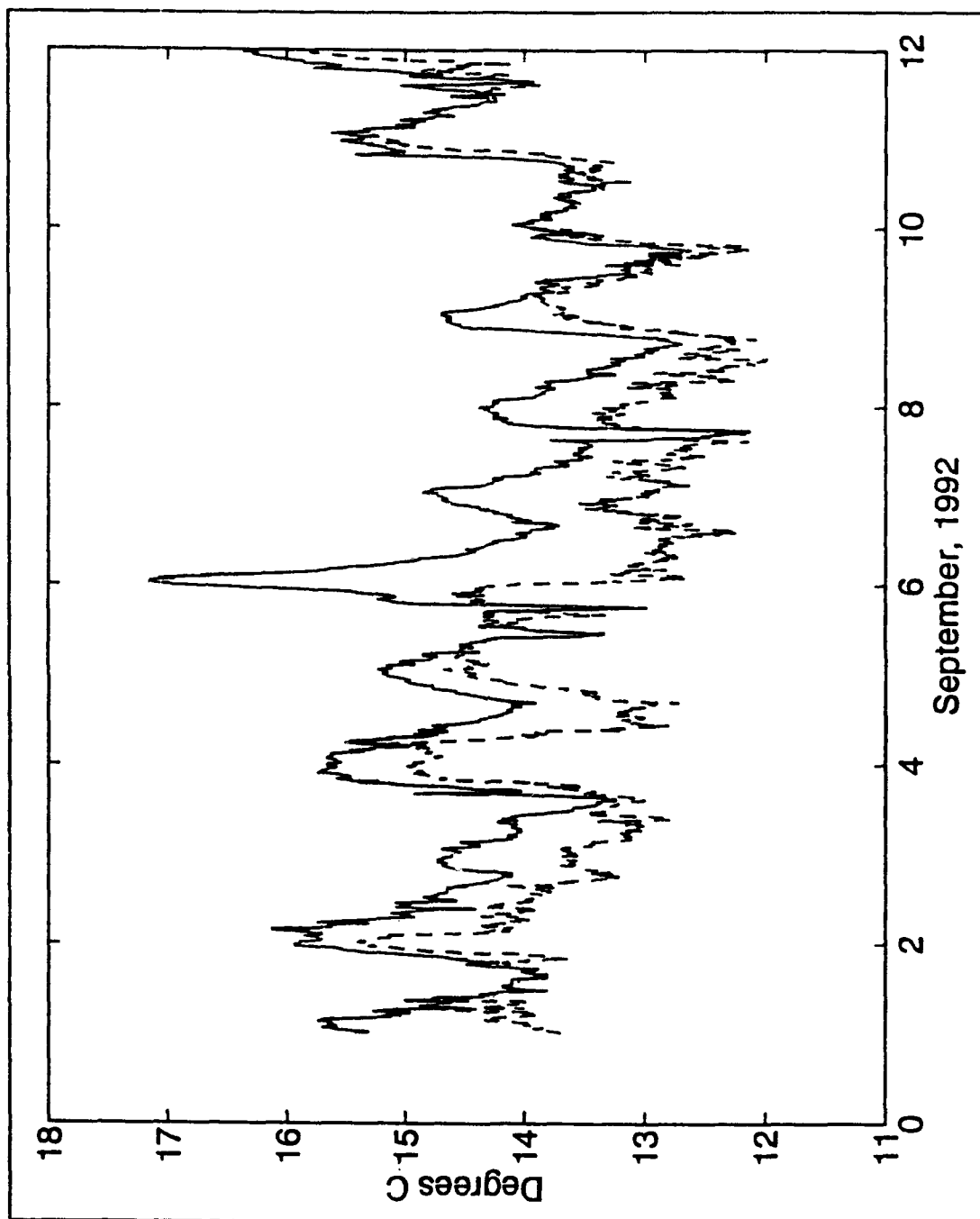


Figure 7. Air Temperature (Solid) and Dew Point (Dashed) at M1. Dew Points Were Converted From Relative Humidities Measured by the Buoy.

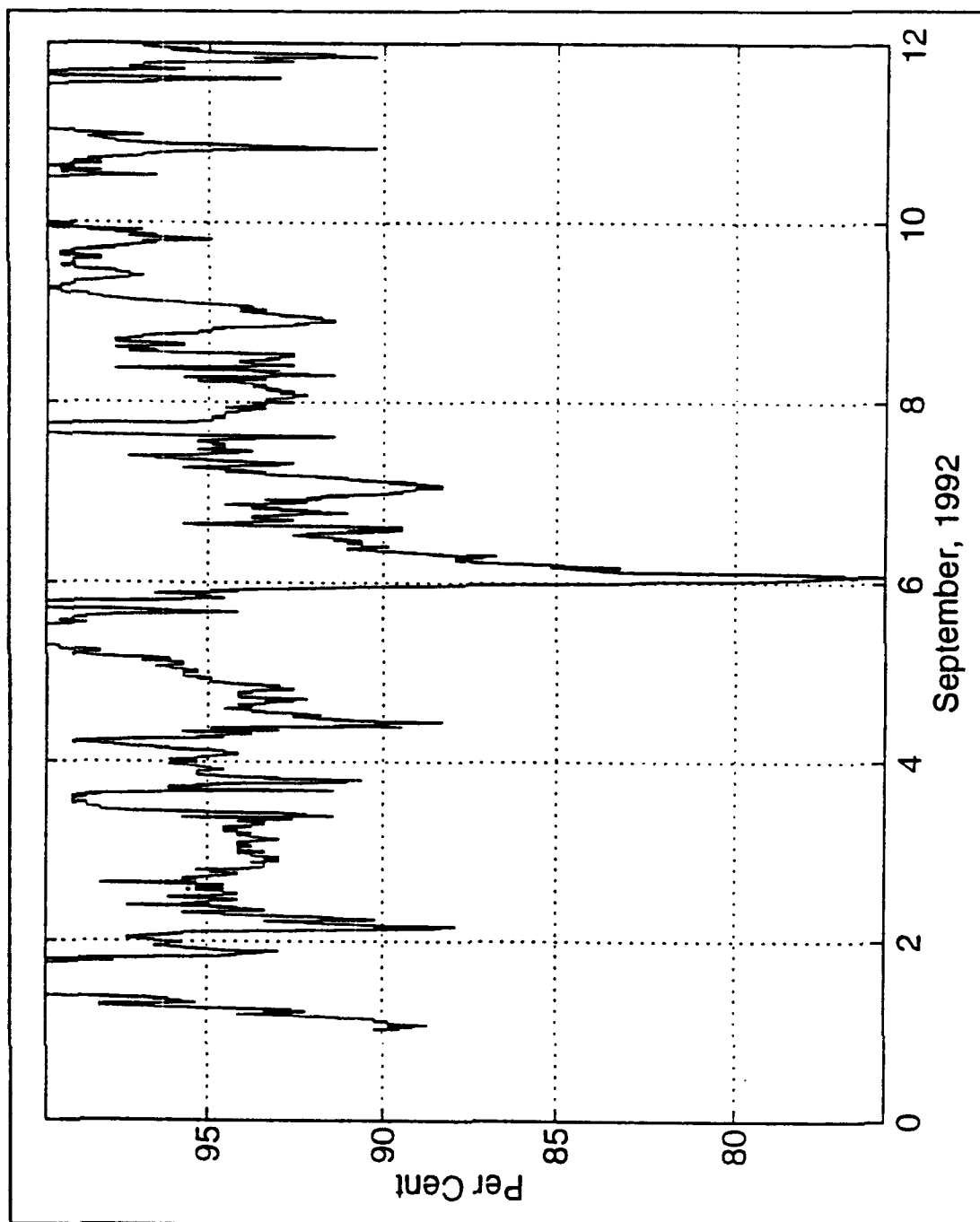


Figure 8. Relative Humidity at M1.

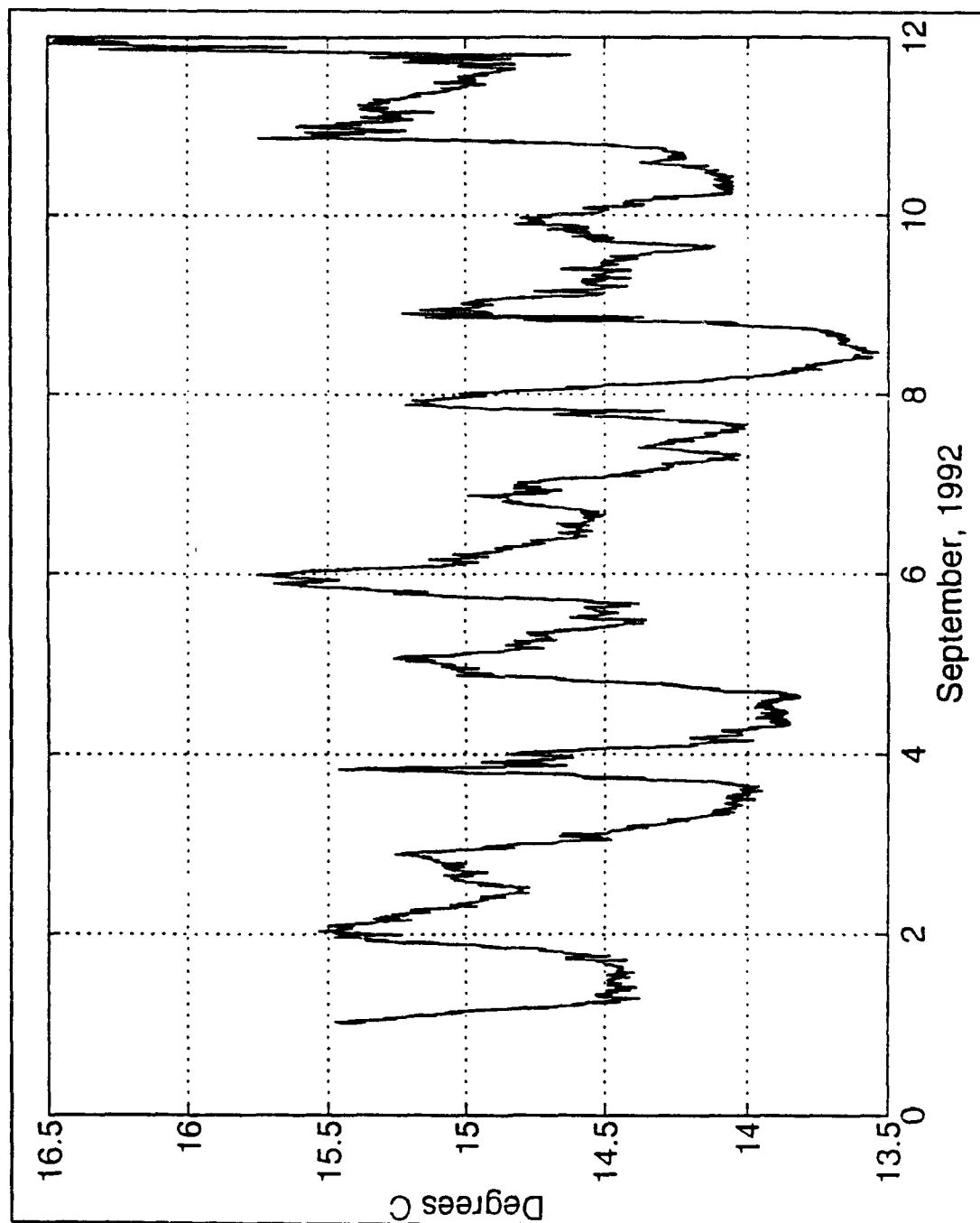


Figure 9. Sea Surface Temperature at M1.

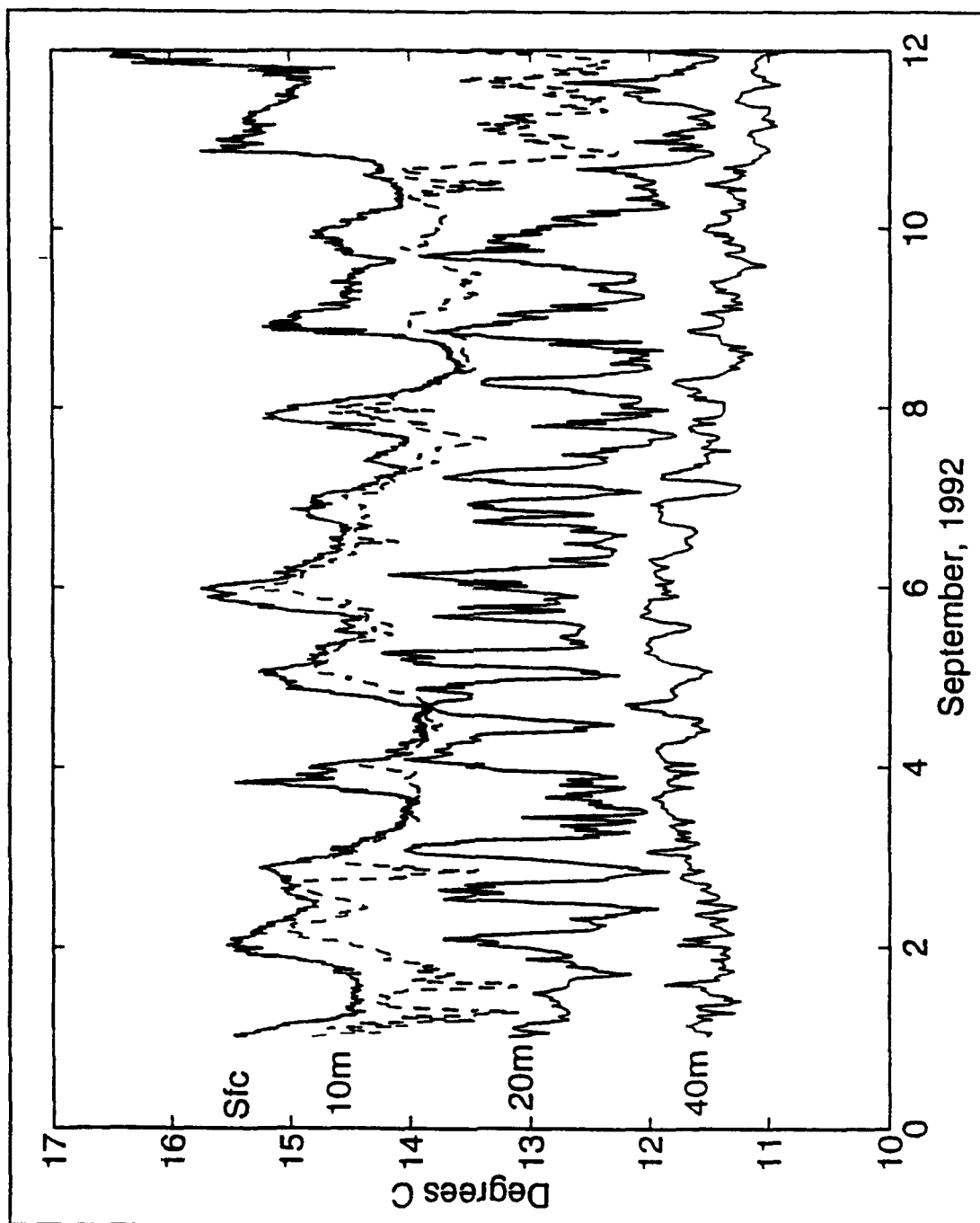


Figure 10. Ocean Temperatures at the Surface, 10, 20, and 40 Meters Beneath M1.

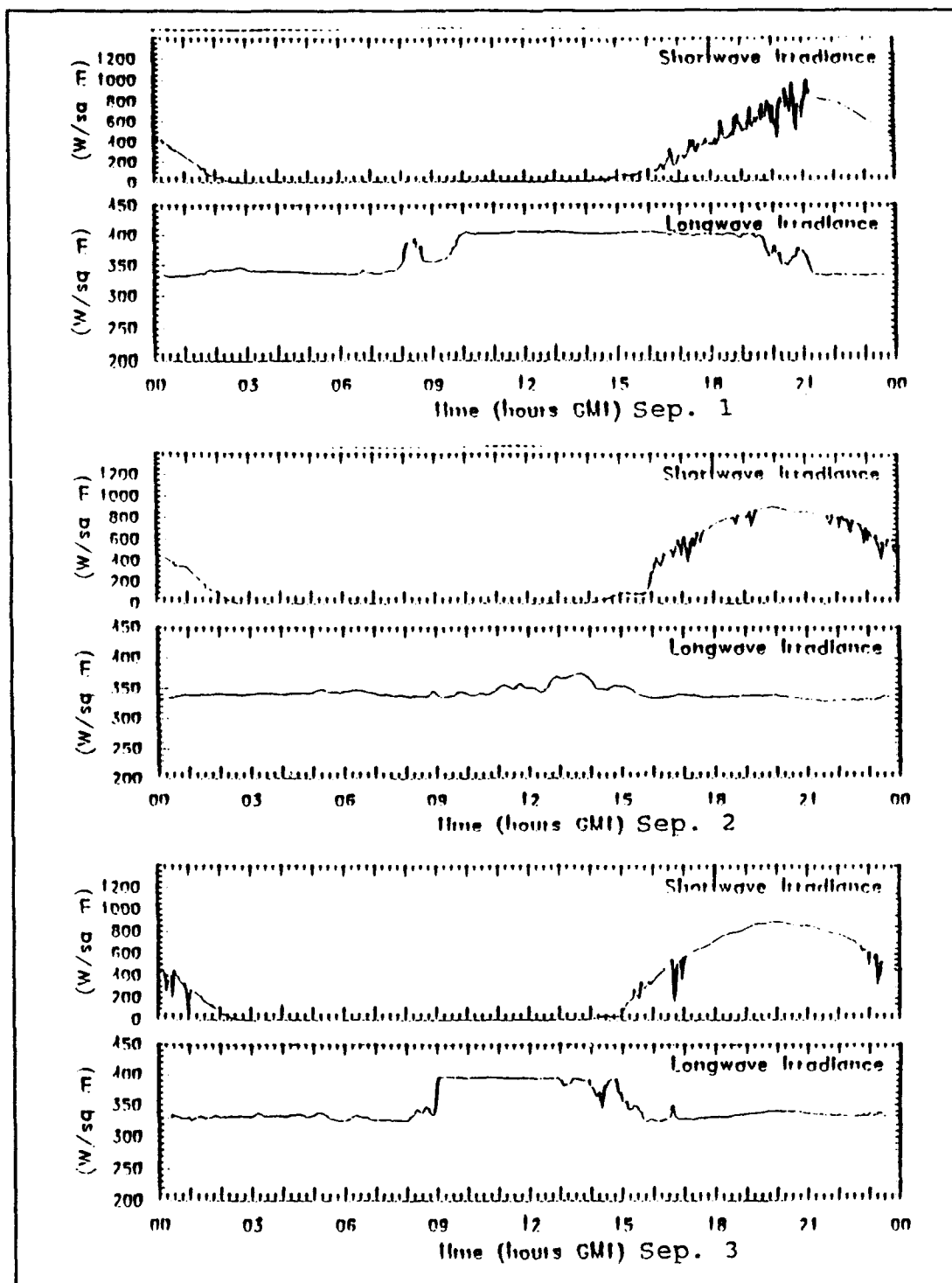


Figure 11a. Shortwave and Longwave Irradiance Recorded at the NPS Profiler Site. The Day of September is Designated on the Time Scale of Each Plot.

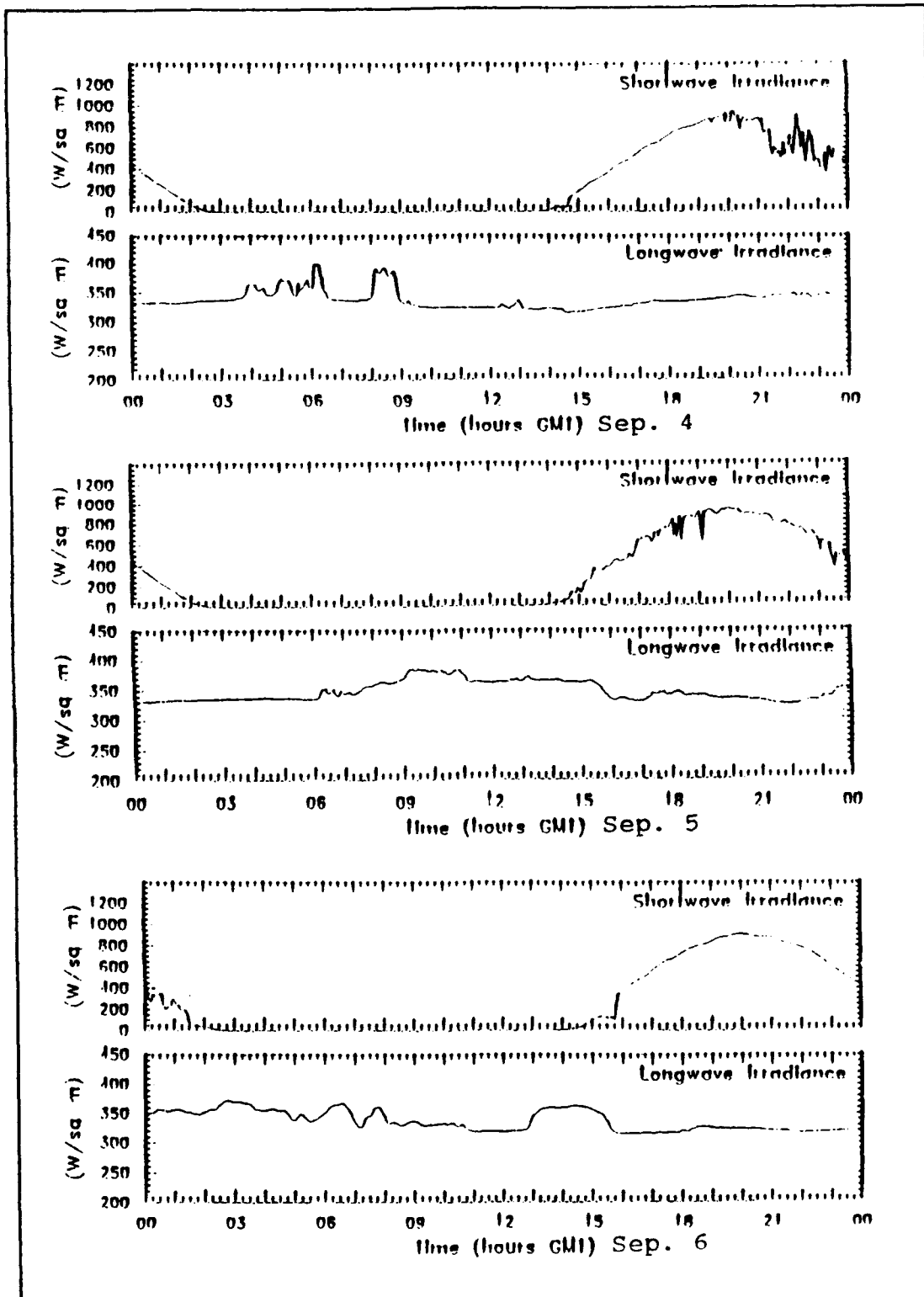


Figure 11a. (Continued)

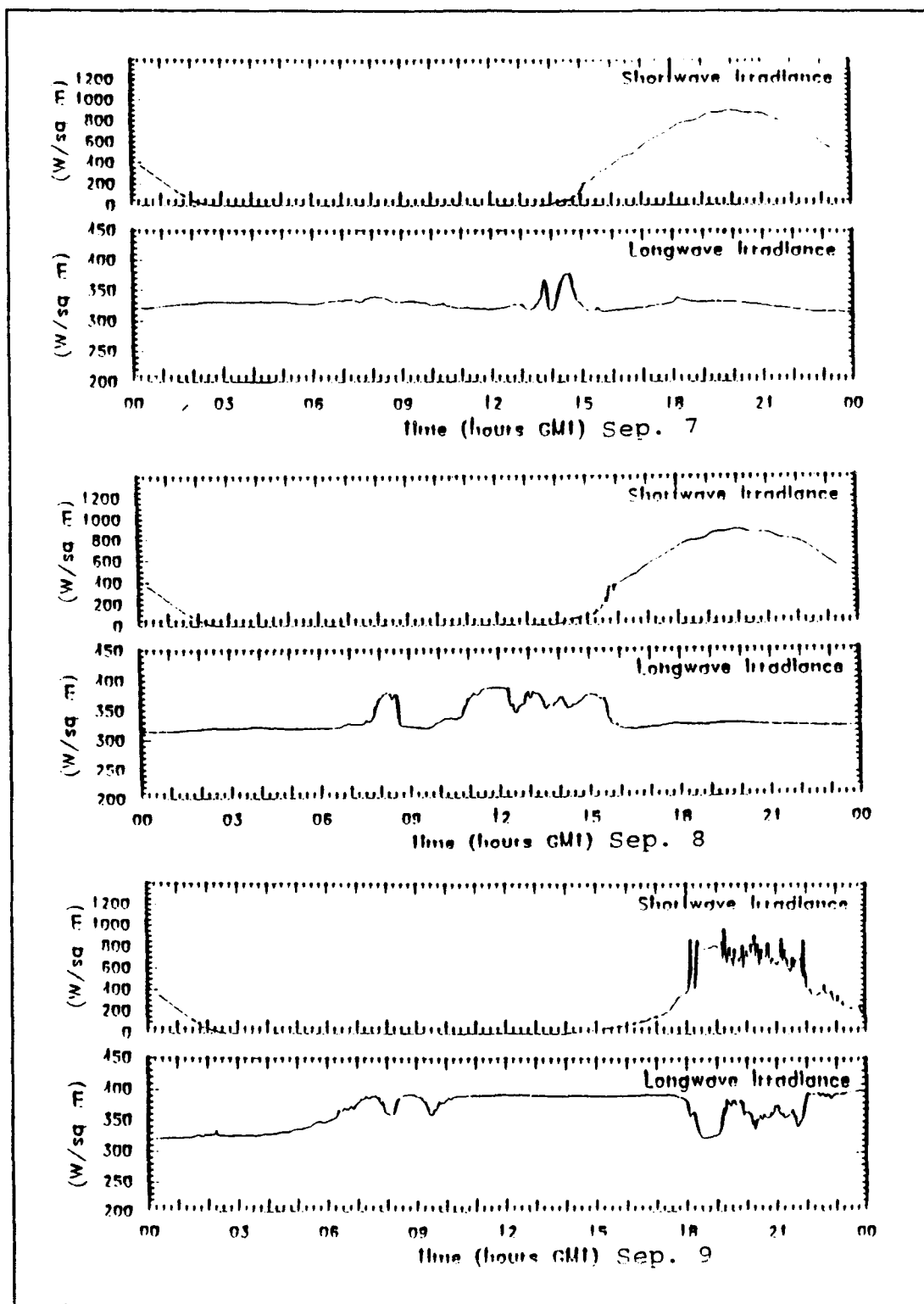


Figure 11a. (Continued)

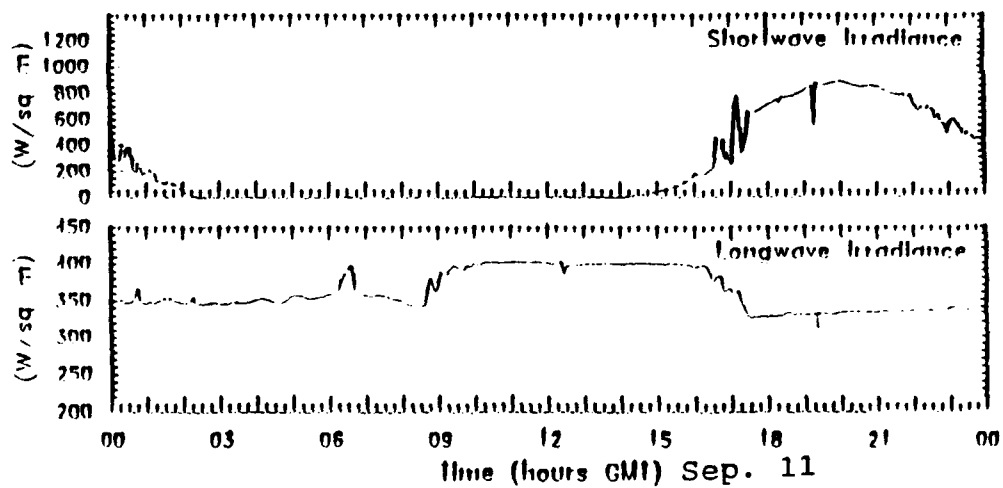
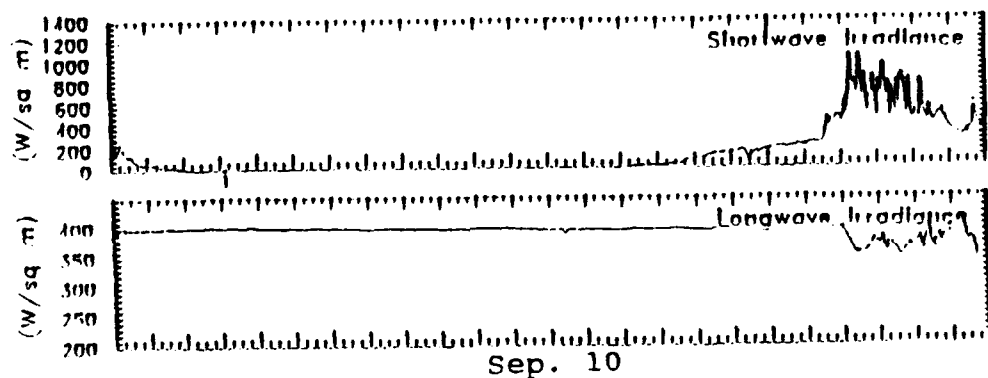


Figure 11a. (Continued)

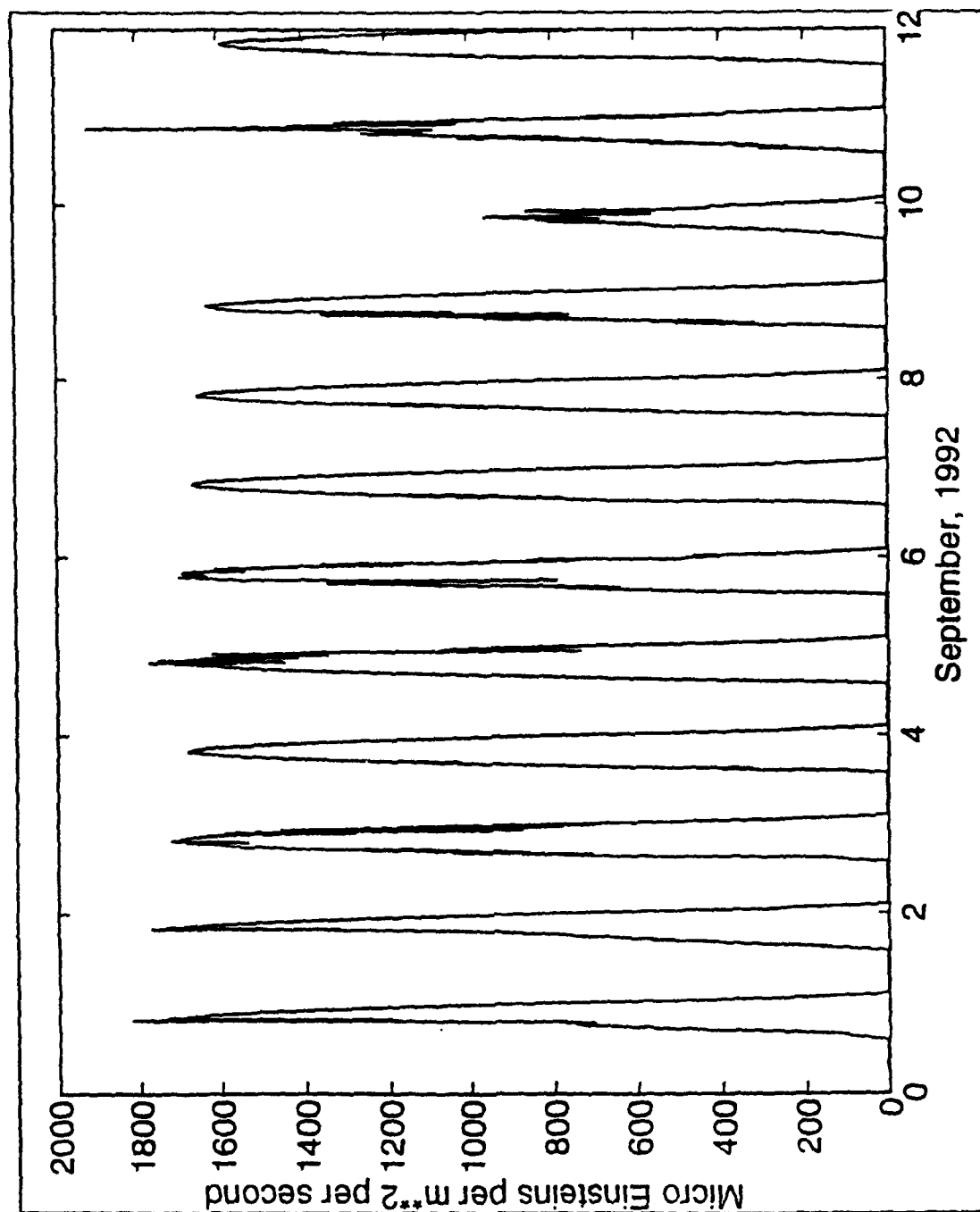


Figure 11b. Photosynthetically Active Radiation at M1.
Note Degree of Cloudiness on the 9th.

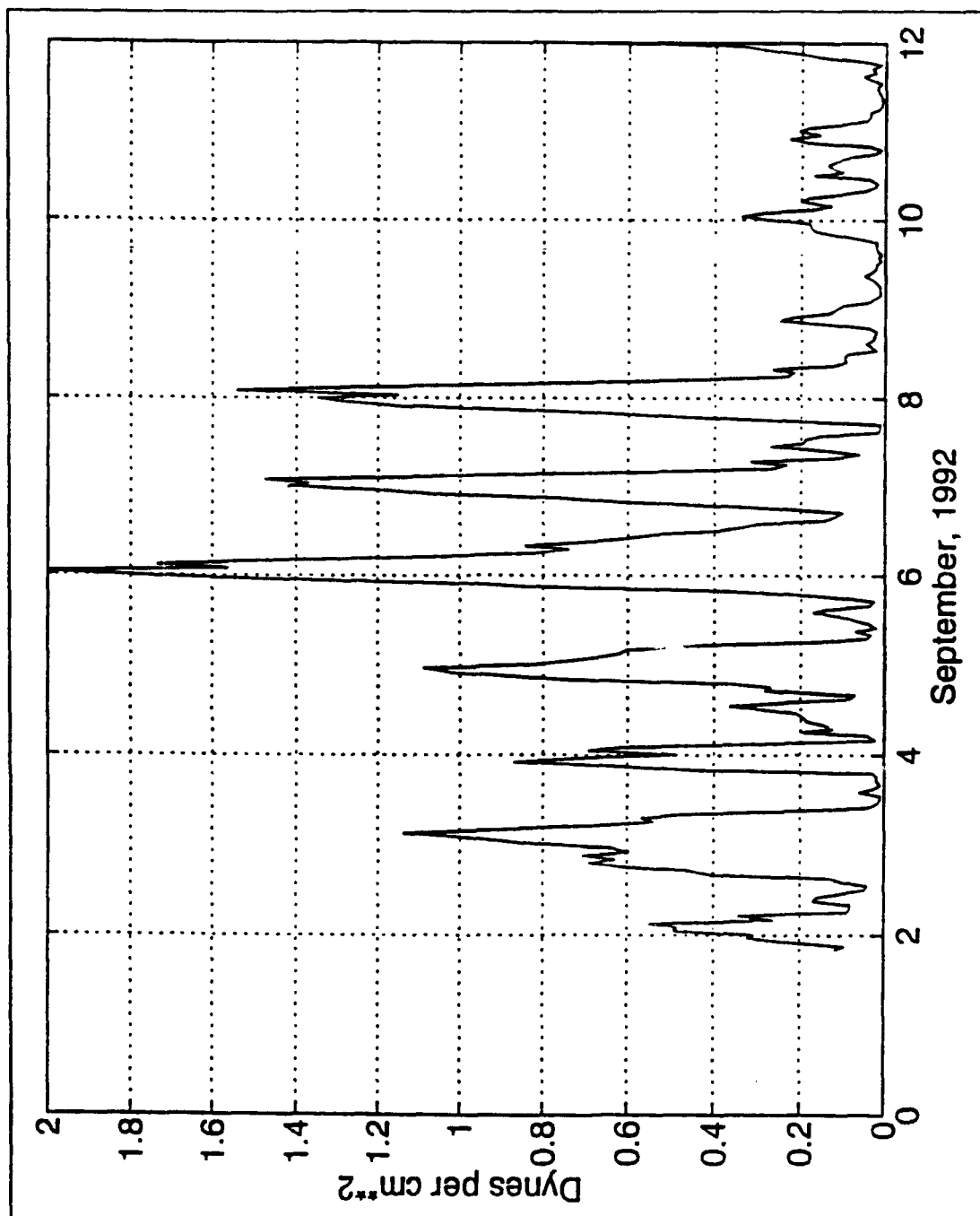


Figure 12a. Total Wind Stress Computed in Accordance With Large and Pond (1981).

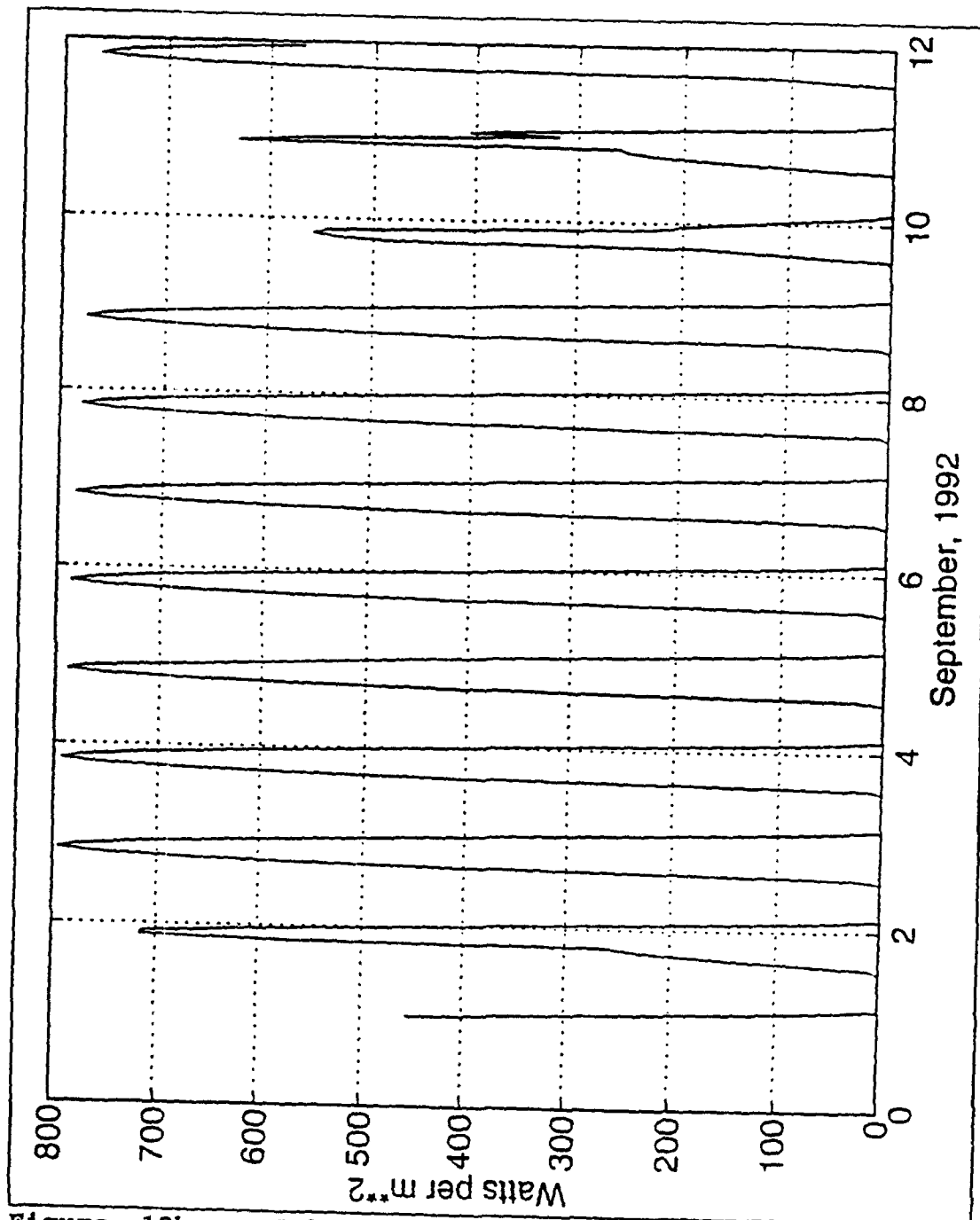


Figure 12b. Solar Insolation Computed from Forcing Routine, Accounting for Estimated Cloud Cover.

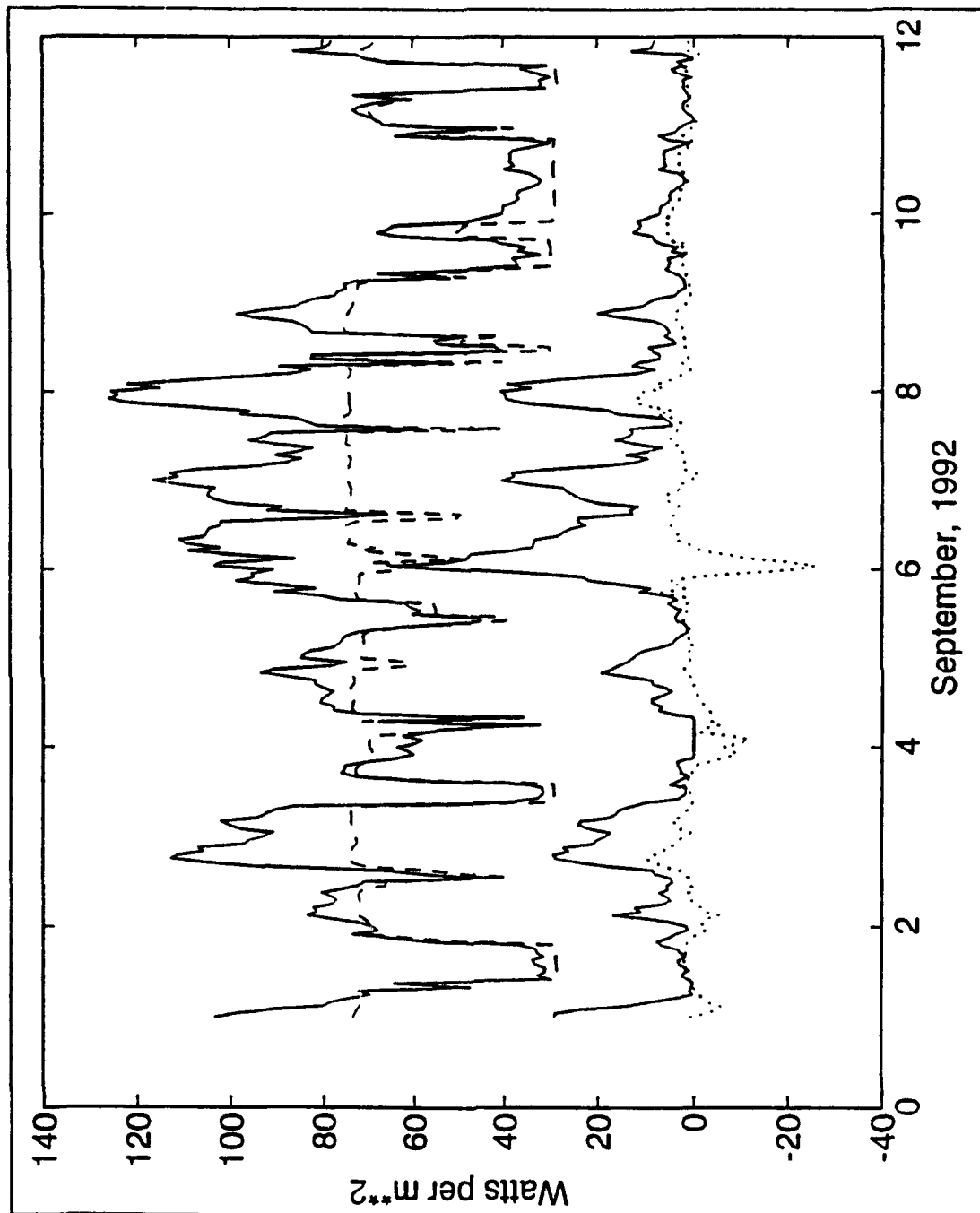


Figure 12c. Computed Heat Loss Terms. Sensible (Dotted), Latent (Lower Solid), Net Infrared (Dashed), and Net Heat Loss (Upper Solid - the Other 3 Summed) are Plotted, with Positive Values Indicating Heat Lost From the Ocean.

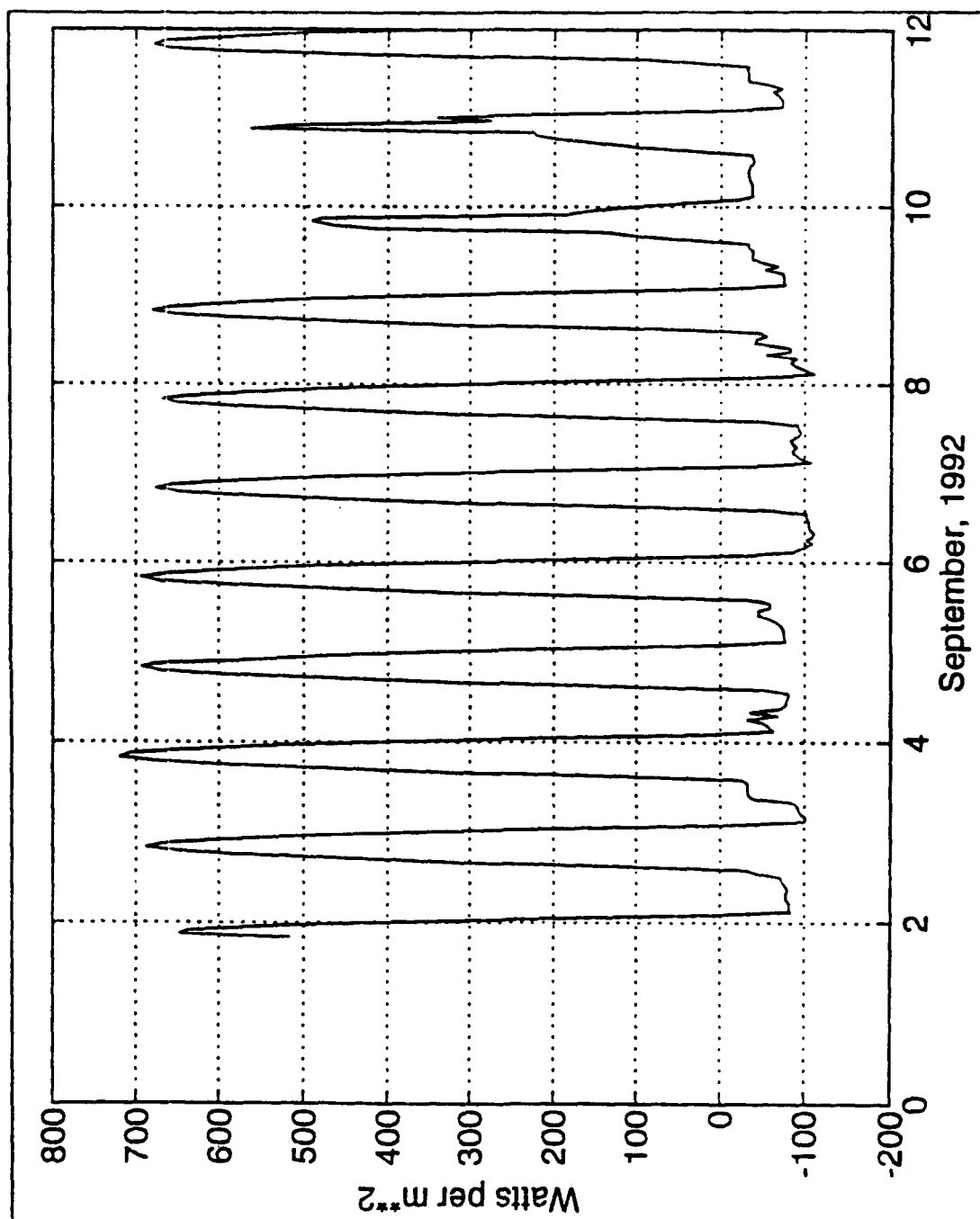


Figure 12d. Computed Net Surface Heat Flux. Sign Convention as in Figure 12c. This Represents the Solar Insolation Minus the Net Heat Loss From Figure 12c.

V. MODEL RESULTS

A. MODEL SENSITIVITIES

1. Initial Conditions

In order to run the two mixed layer models, an initial density profile was needed. A CTD or bathythermograph cast was not available for the beginning of the 1st of September, when the data collection began, but a MBARI cruise made on 9 September conducted nine CTD casts. All of the casts were made within the bay. The temperatures from the upper 50 meters of each cast are shown in Figure 13a. Initial runs of the models were made using the cast from this cruise which most nearly matched the surface temperature with that of the ATLAS buoy at 0000Z on 1 September 1992 (designated #1 in Figure 13a). Experimentation with a variety of other initial temperature profiles indicated that the early model heat content in the mixed layer was strongly dependent on the starting temperature profile. Since the initial profile in the early runs was nearly matched with the data in surface temperature and time of day, but was not located near the mooring (about 15.5 kilometers to the northeast), it was decided that a profile taken at the mooring site would be more representative of conditions at that site. Subsequent model runs were started at 2000Z on the 1st, since the CTD cast

located at the buoy (designated #2 in Figure 13a) was made at that time, although on a different date. A 0.325°C mismatch in surface temperature between the CTD cast from the 9th and the ATLAS data on the 1st was corrected by adding that amount to the CTD cast along the 51 meters of that cast used as an initial profile. In this way, the stratification of the water column was preserved, and the most representative initial temperature profile possible was attained. Final runs presented in the next section were initialized using this profile, which is shown separately in Figure 13b.

Experimentation with varying initial salinity profiles was also conducted. As designed, the Garwood model assumes a constant salinity with depth, while PWP allows the input of observed salinities. For comparison, a test PWP run was made, assuming a constant salinity. The difference in mixed layer depths and temperatures produced was indistinguishable. Therefore, no modification of the Garwood model to allow observed salinities to be used in the calculation of an initial density profile was deemed necessary.

2. Friction (PWP)

As mentioned in the model descriptions, the PWP model contains a parameterization of friction, which is treated in terms of a relaxation time of the surface currents. Initial runs of this model left this variable at its default value of 9999, which corresponds to no friction. It was decided that

a value of 5 days would be more correct. This value is in agreement with that used by Rosenfeld (1988) in the CODE region of northern California. In terms of the mixing and thermal structure of the upper ocean, this adjustment made little difference over the 11 day study interval, as can be seen in Figure 14, but was considered to be more accurate than using no frictional term at all.

3. Time Step

Another important model variable to be established was the degree to which it was reasonable to reduce the model time step in the interest of representing the short temporal scale mixed layer response to the sea breeze environment. It was considered that running the models at a 10 minute time step to correspond with the available data might be ideal. However, the Garwood model presumes that TKE reaches a steady state within the mixed layer at each time step. To test the validity of this assumption for short time scales, a second model written by R.W. Garwood of NPS, in which the complete unsteady physics of the turbulent kinetic energy equations is preserved, was used to test the time needed for TKE to reach steady state after a step wind function is applied to the problem. These equations are:

$$\frac{\partial h}{\partial t} = w_e - \bar{W}_{z=h} \quad (30)$$

$$\frac{\partial (h\bar{E})}{\partial t} = 2m_3 u_*^3 + (\bar{u}^2 + \bar{v}^2) w_e - (\alpha g h \Delta \bar{T}) w_e - \alpha g h \frac{Q_0}{\rho c_p} - D \quad (31)$$

$$\frac{\partial (h\bar{W}^2)}{\partial t} = -(\alpha g h \Delta \bar{T}) w_e - \alpha g h \frac{Q_0}{\rho c_p} + R - \frac{D}{3} \quad (32)$$

$$\frac{\partial \bar{T}}{\partial t} = \frac{Q_0}{\rho c_p h} - \Delta \bar{T} \frac{w_e}{h} \quad (33)$$

$$\frac{\partial (h\bar{u})}{\partial t} = f h \bar{v} + \frac{\tau_x}{\rho} \quad (34)$$

$$\frac{\partial (h\bar{v})}{\partial t} = -f h \bar{u} + \frac{\tau_y}{\rho}, \quad (35)$$

where h is mixed layer depth, T is mixed layer temperature, w_e is entrainment velocity, E is total TKE, W is the mean vertical velocity at the base of the mixed layer, u_* is the surface friction velocity, ΔT is the temperature change at the base of the mixed layer, $Q_0/(\rho c_p)$ is the net surface heat flux, R is a pressure redistribution term, D represents viscous dissipation, f is the Coriolis parameter, and τ is wind stress. Figure 15 shows the wind function, an idealized sea breeze, that was applied to this model and the resulting total TKE versus time. This step function is roughly equivalent to an increase of wind from 8 to 12 m/s. It can be seen that an hourly or greater time step is valid, since a

steady state can be reached within that time. However, a shorter interval between turbulent calculations, such as 10 minutes, does not allow this steady state to occur and thus prevents proper distribution of the energy. Therefore, it was determined that hourly fluxes should be computed from the hourly averaged ATLAS data. The PWP model was also run at a one hour time step for the purpose of uniformity between the two models, although it is noted here that it could be run with a shorter time step, as in Price et al. (1986), since the mixing is not based on a turbulence steady state. Since the hourly averaged data reflect the diurnal cycle well, no model runs at 10 minute time steps were deemed necessary.

4. Cloudiness

Another factor affecting the model results was the cloud cover. As discussed previously, a best estimate of this input value was made from the available irradiance data. Initial runs of the models, however, were made assuming no cloud cover. Figures 16a and b show the Garwood and PWP model mixed layer temperatures with and without cloud cover. It is apparent that this was not an especially important factor through most of the study period when the weather was primarily clear, except for periods of fog at night. However, there is a significant reduction in the warming trend of the models in the later period during which extensive cloudiness was present.

5. Absorption Coefficients

Two final tuneable parameters in the PWP model are the values for longwave and shortwave absorption coefficients. The net incoming solar radiation is absorbed in the ocean according to

$$I(z) = I(0) [I_l e^{-\frac{z}{\lambda_l}} + I_s e^{-\frac{z}{\lambda_s}}] \quad (36)$$

where l and s designate longwave and shortwave components of insolation (Rosenfeld, 1988). Values of $I_l = .6$ and $I_s = .4$ were used as in Price et al. (1986). Coastal type III (Jerlov, 1976) was assumed as in the CODE area, with values of $\lambda_l = 1.4 \text{ m}^{-1}$ and $\lambda_s = 7.9 \text{ m}^{-1}$.

Garwood absorption is treated similarly, with exponential decay of absorption with depth below 1 meter, but the incoming radiation is not broken into long and shortwave components. Figure 17 gives the absorption profiles with depth for the two models.

The following results describe the model performance with all of the preceding adjustable parameters set as described. They represent our best estimate of the actual absorption, cloudiness, friction, and initial conditions as discussed above and computed at a one hour time step at 1 meter vertical resolution.

B. FINAL MODEL RUNS

1. Garwood

Mixed layer temperatures and depths computed by the Garwood model, initialized at 2000Z on the 1st with the temperature profile shown in Figure 13b, (located at the mooring), are presented in Figures 18a and b. Also in Figure 18a are the observed surface temperatures as presented previously. Immediately apparent is an upward trend in the model temperatures relative to the data, resulting in large deviations from the observations by the 9th through the 11th of September. In fact, least squares fits of the data and the model output indicate only a slight upward trend in the data of 0.04°C over the 11 day period, but an upward trend of 2.93°C over the 10.17 days of model output. This corresponds to an average increase of 0.289°C per day. This trend will be discussed in the following chapter with respect to possible advective effects.

Also of note in Figure 18a is the fact that while the general temporal agreement between the model and observed temperature patterns is reasonably good, the diurnal cycle is under-represented by the Garwood model. Daily increases are sharp, as they are in the data, but in all cases except the 9th, exhibit a lower magnitude than those in the data. Of greater significance in the overall trend, the nocturnal cooling in the model is much less than observed, especially on

days 2, 3, and 7 when a large degree of actual cooling occurred. Also, the rate at which the cooling occurred in the model was greatly reduced relative to that seen in the observations. Mixed layer cooling on the 9th and 10th, the days with heavy cloud cover, was more in line with that seen in the data.

Specific characteristics of the model output for the purpose of comparison with surface temperature data are offered here. Due to the large trend in the data, only timing of the diurnal events and magnitude of the daily temperature cycles will be given. The Garwood model produced mixed layer temperature minima at a mean time of 1418Z (0718 PDT) and maxima at 2206Z (1506 PDT). Thus, the modeled temperature minima lag the data by an average of 44 minutes, while the peaks actually lead those in the data by an average of 57 minutes. The day to night temperature falls ranged from 0.14°C to 1.01°C, with an average drop of 0.42°C. This compares with an average drop of 0.96°C in the data. Thus, the Garwood model cooled the mixed layer by an average 0.54°C less than that seen in the surface temperature data.

Mixed layer depths show a pattern consistent with these thermal results. The mixed layer can be seen to deepen the most on the days when the cooling is the strongest. As previously mentioned, no direct measurements of mixed layer depths were available. However, Figure 19 shows the difference between the observed surface temperatures and those

at 10 meters. The mixed layer can be seen to extend to at least 10 meters depth (at least briefly, but for most of a day on more than one occasion) on the 2nd through the 8th, and again on the 10th. By contrast, Figure 18b indicates that the modeled mixed layer deepens below 10 meters only on the 3rd, 6th, 7th, and 8th. In general, then, it would appear, consistent with the lack of cooling indicated in the model temperatures, that this model also somewhat underestimates the depth to which the diurnal mixed layer deepening occurs.

Temperature profiles at the start of the model run and at specified times thereafter are presented in Figure 20. From this progression, it can be seen that the stratification in the water column is increasing with time, such that by 192 hours (the end of the eighth day of model time) significant warming has occurred through the upper 13 meters. These results are consistent with the warming trend seen in the model mixed layer temperature results.

2. PWP

The PWP model results, in response to the same forcing as used in the Garwood model, with friction and absorption as defined in the last section, are shown in Figures 21a and b. A surprisingly similar pattern of temperatures and mixed layer depths resulted. Again, there is an upward trend in the model temperatures relative to the data, although somewhat less than that seen in the Garwood model, of 2.00°C over the 10.17 day

period of study, or 0.196°C per day. The dampening of the diurnal temperature variation is even more extreme in this model, with very little cooling occurring on any nightly cycle, and with too little diurnal warming as well.

PWP produced minimum temperatures at a mean time of 1426Z (0726 PDT), quite consistent with Garwood. The maximum also agreed very closely with the Garwood results, occurring at an average 2206Z (1506 PDT). Thus, there is again a lag in the model temperature troughs of an average 52 minutes, while the daily maxima occur an average 60 minutes earlier in this model than they do in the data. The even more inadequate nocturnal cooling in this model is evidenced by the fact that the mean day to night mixed layer temperature fall was only 0.20°C . The range of temperature drops was from 0.118°C on the 5th to 0.313°C on the 6th, when strong winds allowed maximum shear production. Even on this day, however, the model fell far short of the 0.96°C average cooling in the data.

As would be expected with its cooler overall temperatures, the PWP model produced mixed layer depths that were slightly greater than those produced by Garwood. (Note that the PWP model outputs mixed layer depth in integer form in accordance with the vertical bin spacing of the model, while Garwood's model computes h precisely from the TKE relationships.) Following the strong wind day of the 6th, in fact, the layer deepened to 16 meters in this model. The

mixed layer depth reaches 10 meters or more on the 2nd, 4th, and the 6th through the 8th. This would seem to be slightly more in agreement with the observed occasions of deepening to 10 meters or more.

Again, a series of model generated temperature profiles is provided in Figure 22 to give a more complete view of the model's development of the mixed layer with time. As in the Garwood profiles, stratification can be seen to build with time such that by the end of the eighth day warming has occurred down to 16 meters. In PWP, however, the profiles are smoother and the stratification is concentrated between 15 and 18 meters. In Garwood, the profiles are characterized by significant stratification over more than one depth band, as can be seen in the last panel of Figure 20.

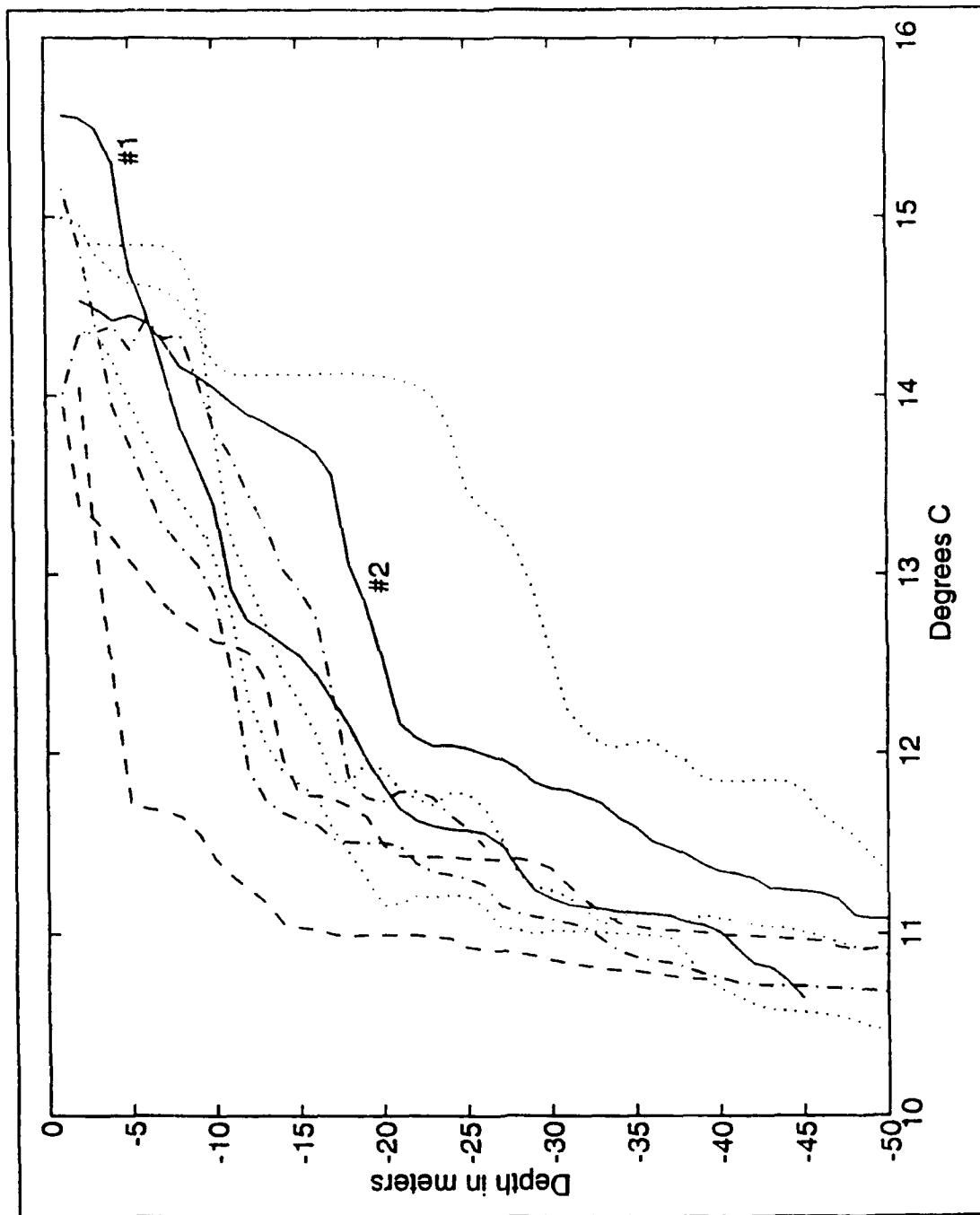


Figure 13a. CTD Temperature Profiles From 9 September at Various Points Within Monterey Bay. Profile #2 was used for model runs, as discussed in text.

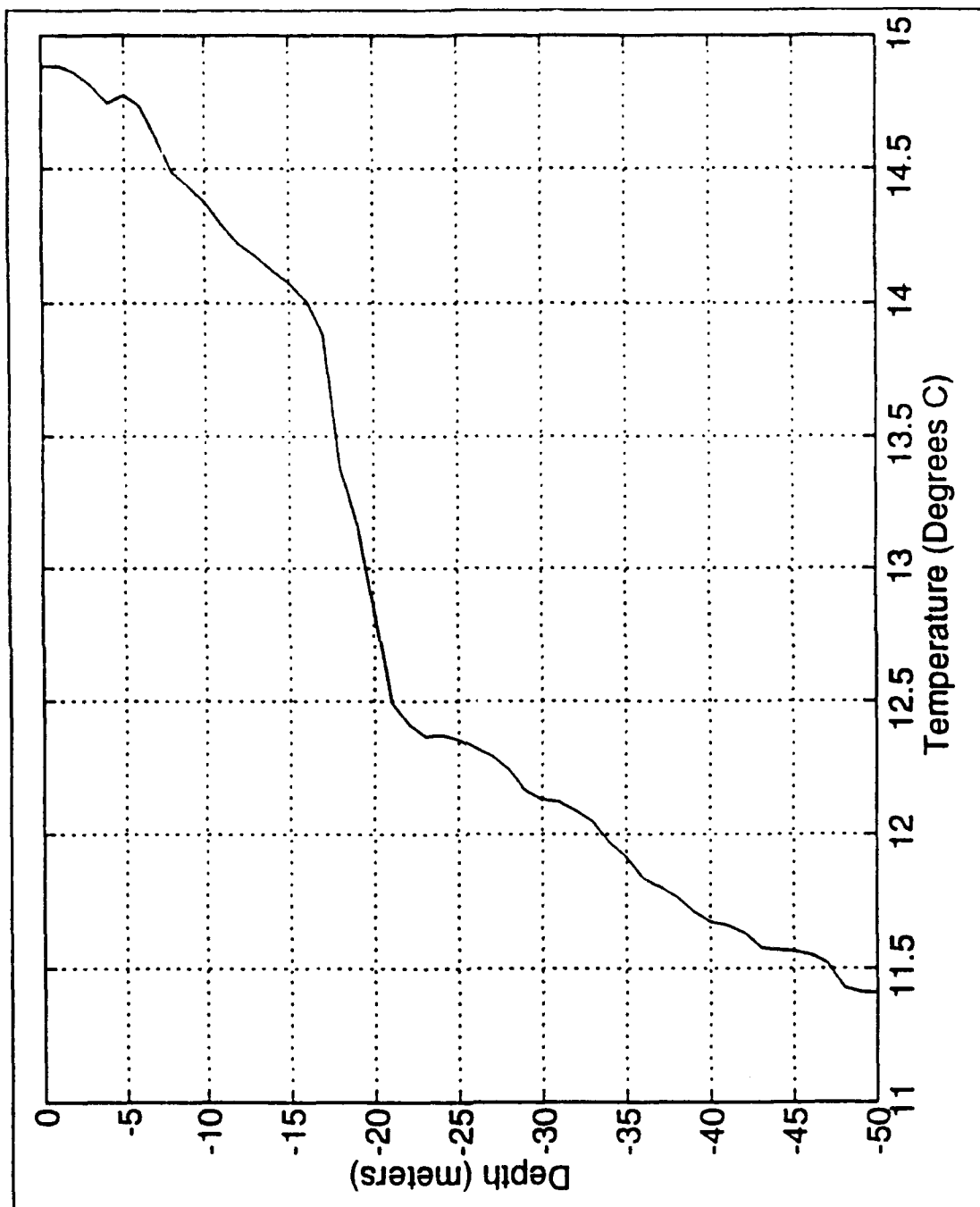


Figure 13b. Initial Temperature Profile Used by the Models.

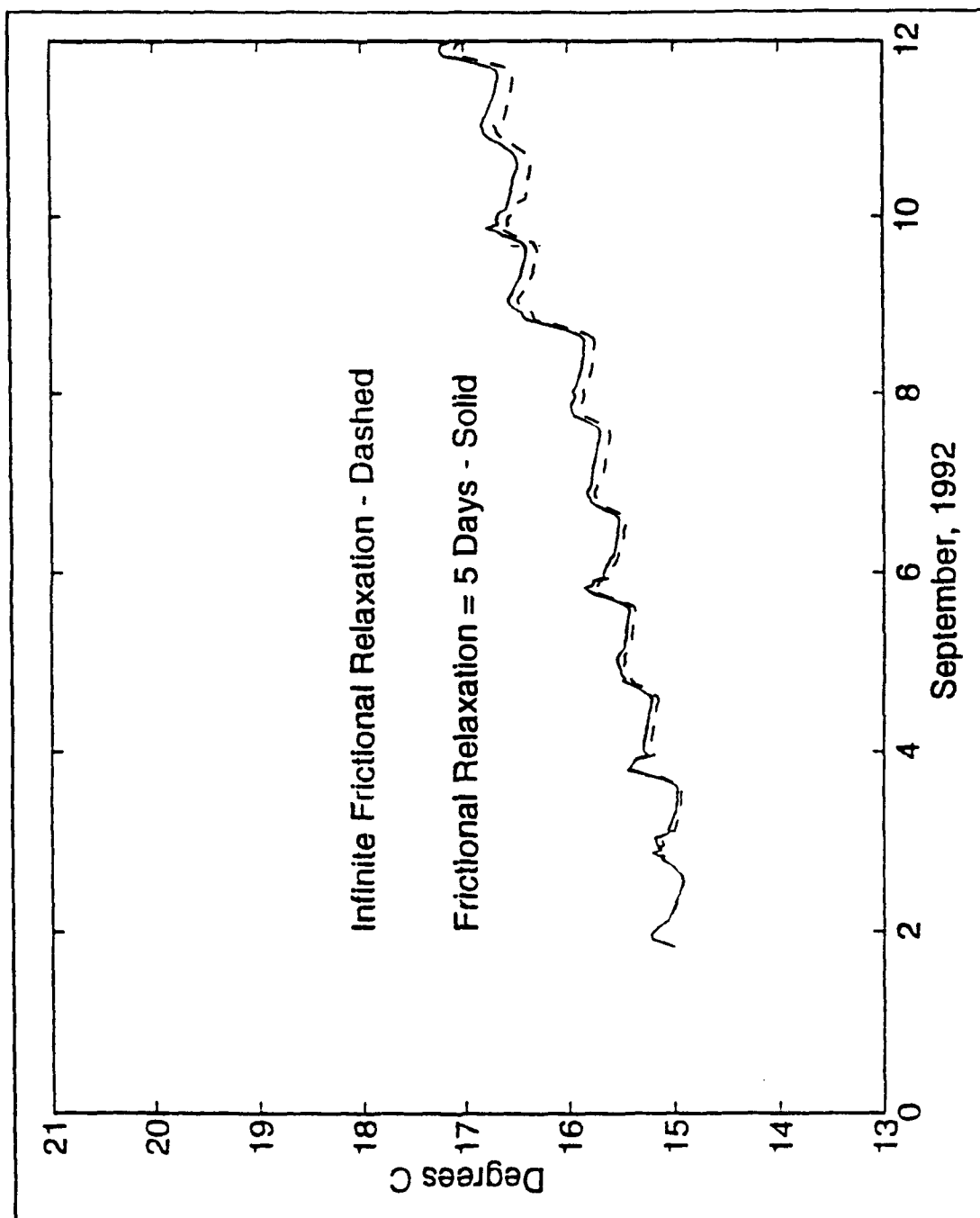


Figure 14. PWP Mixed Layer Temperatures With Varying Friction.

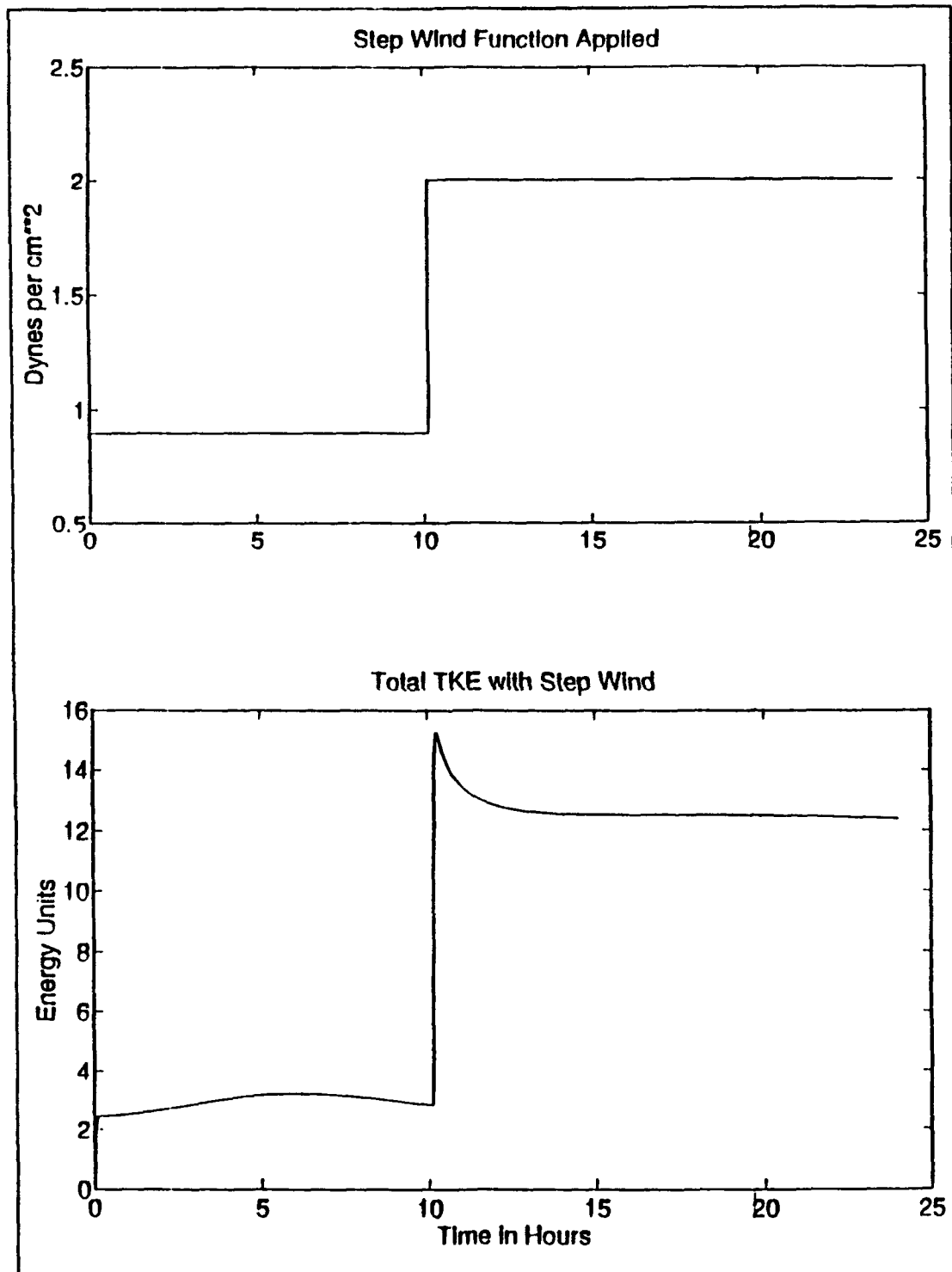


Figure 15. Step Wind Function (Top) Applied to Garwood Unsteady Model and Resulting Total TKE (Bottom) Versus Time.

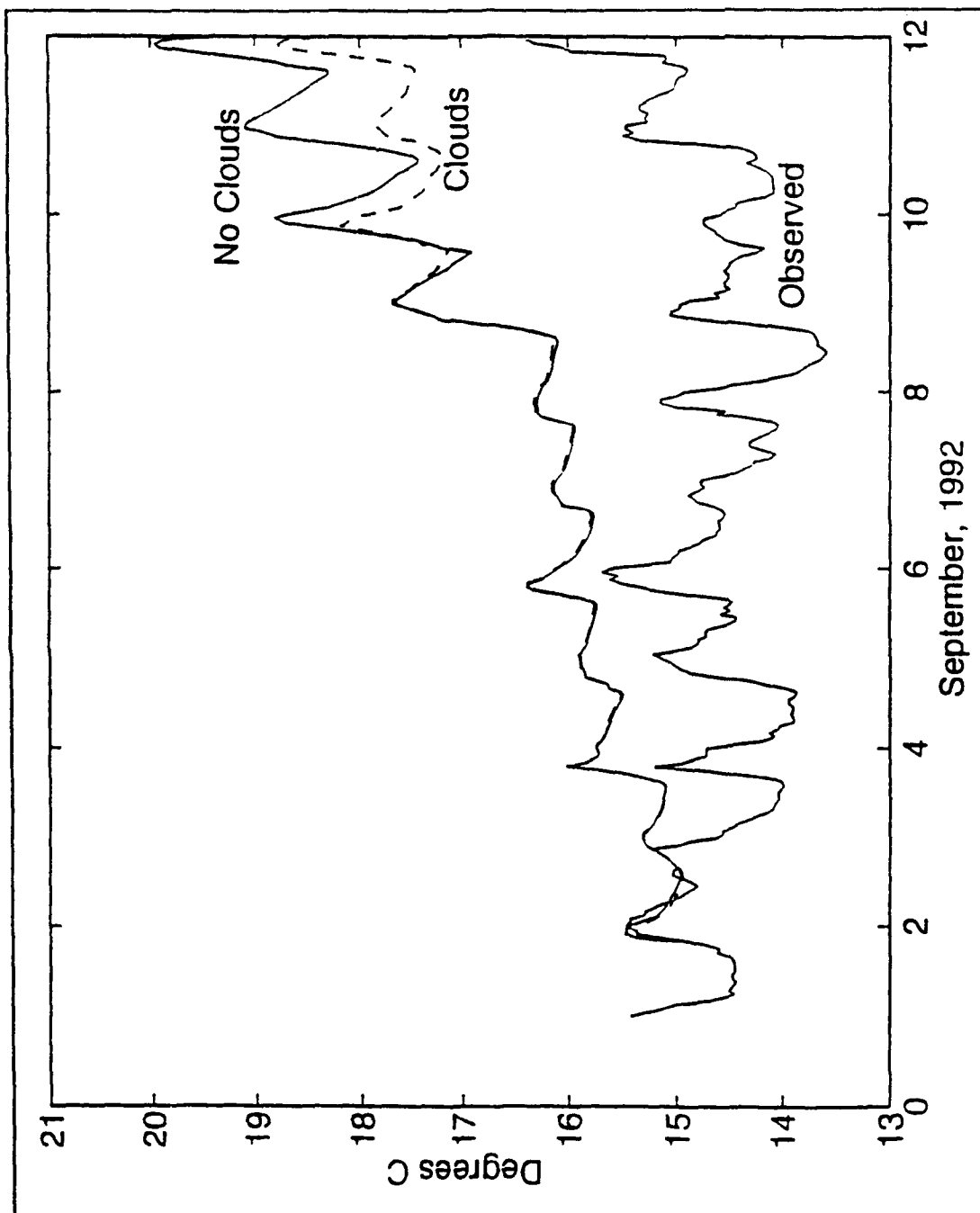


Figure 16a. Garwood Mixed Layer Temperatures Computed Using Zero Cloud Cover Assumption and Using Estimated Cloud Cover.

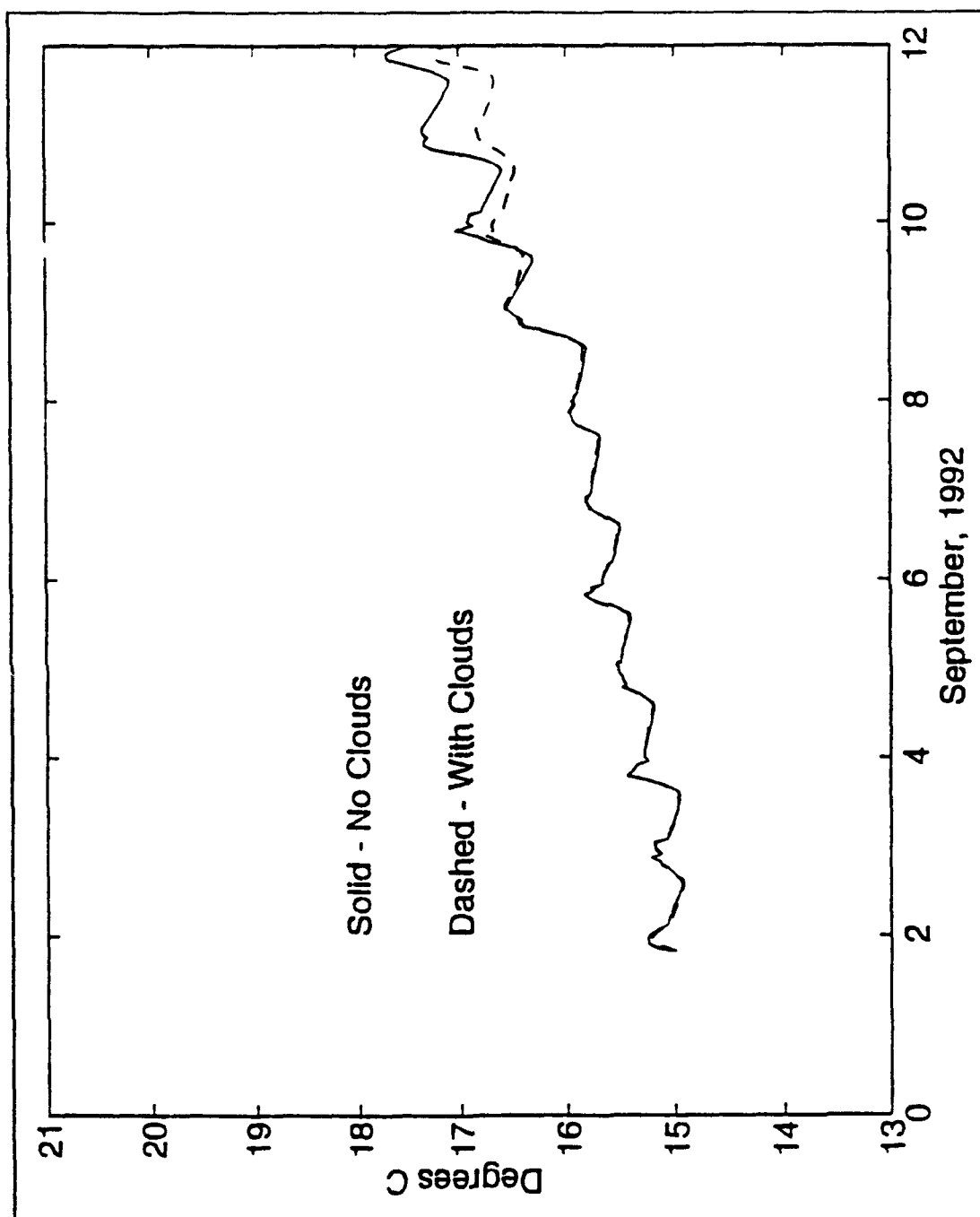


Figure 16b. PWP Mixed Layer Temperatures With and Without Clouds.

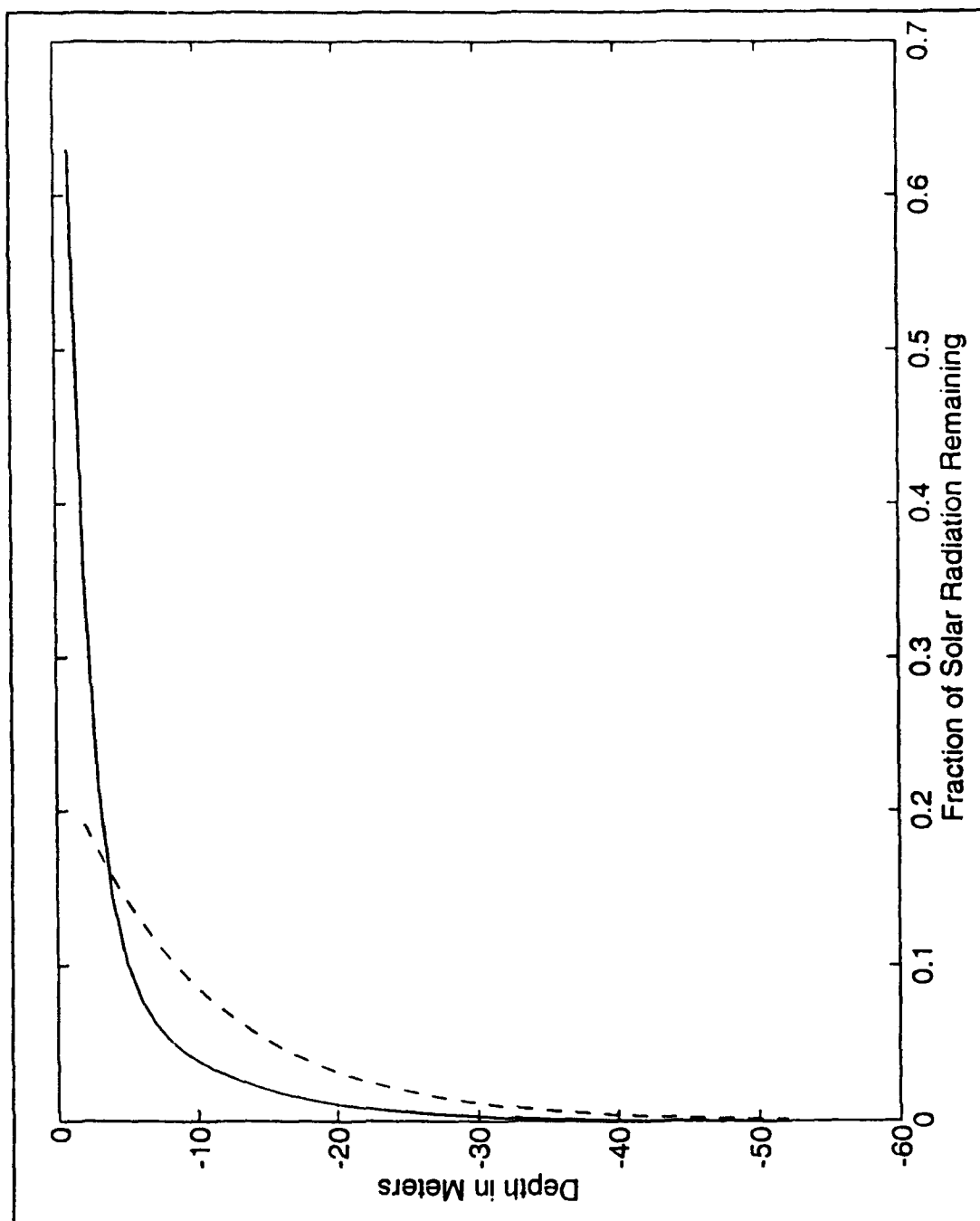


Figure 17. Total Absorption Profiles Computed by Both Models. Garwood Absorption is Dashed and PWP is Solid. Note that PWP Breaks the Absorption into Red and Blue Profiles in the Ratio 0.6 Red and 0.4 Blue.

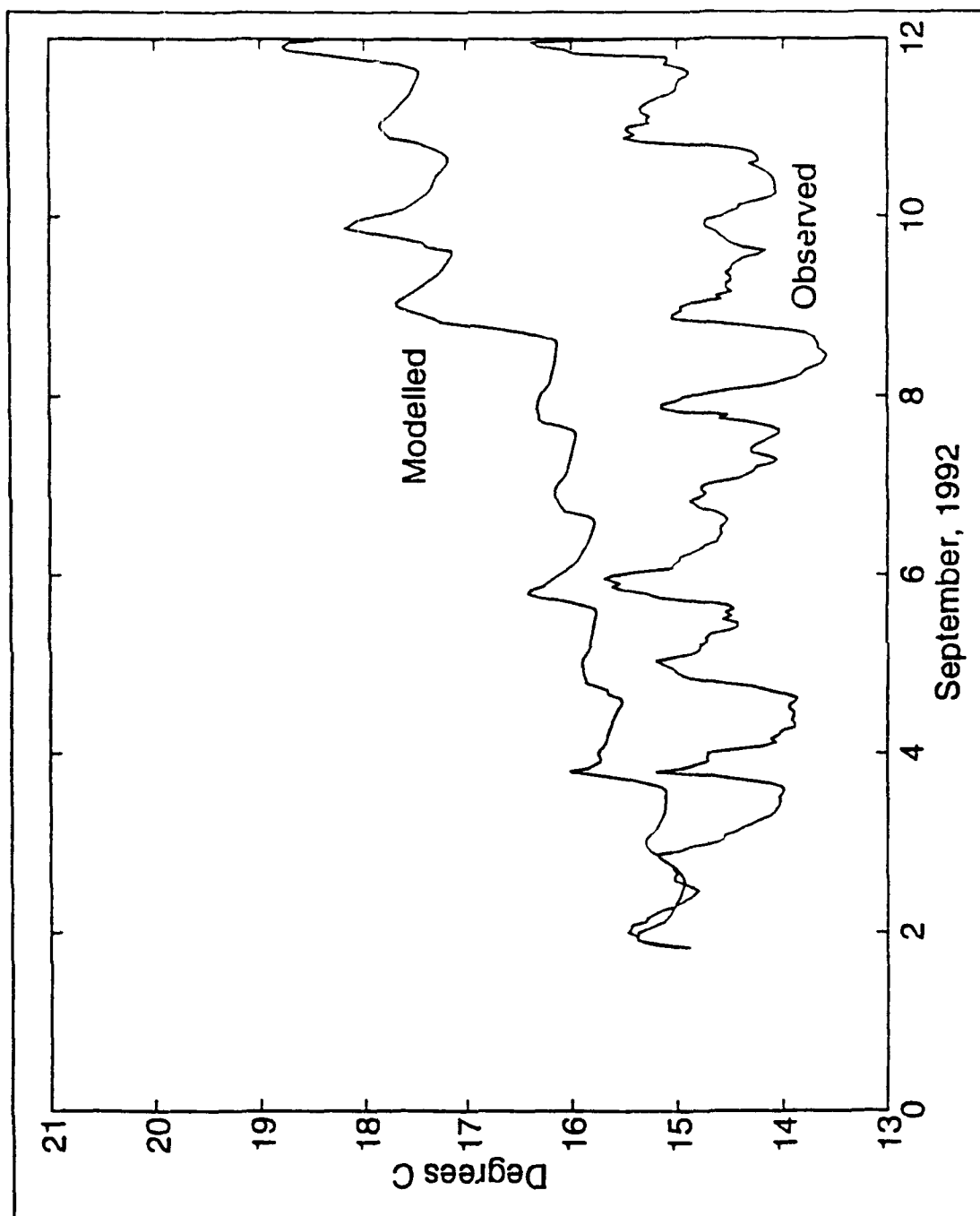


Figure 18a. Final Garwood Mixed Layer Temperatures Versus Observed Sea Surface Temperatures.

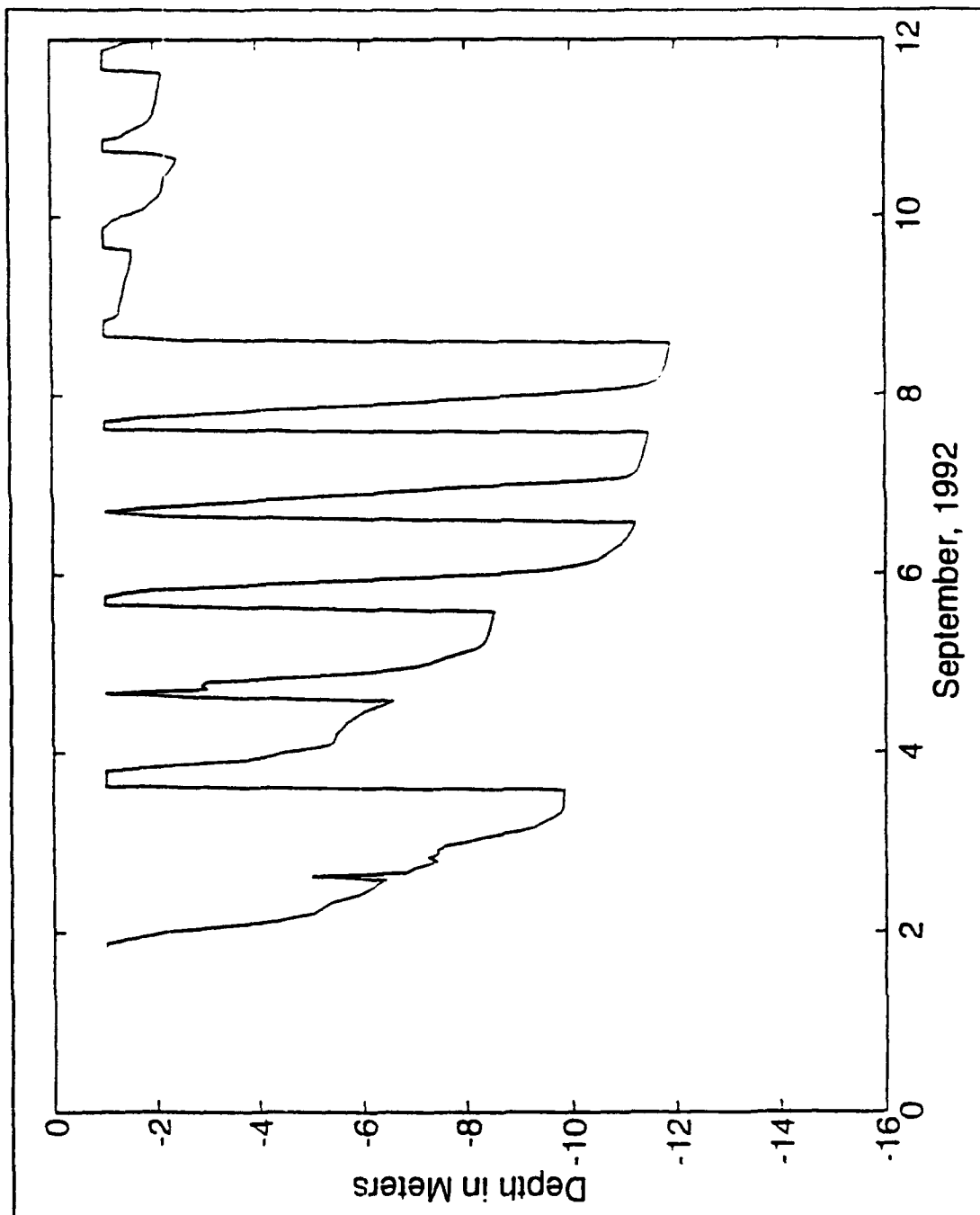


Figure 18b. Garwood Mixed Layer Depths.

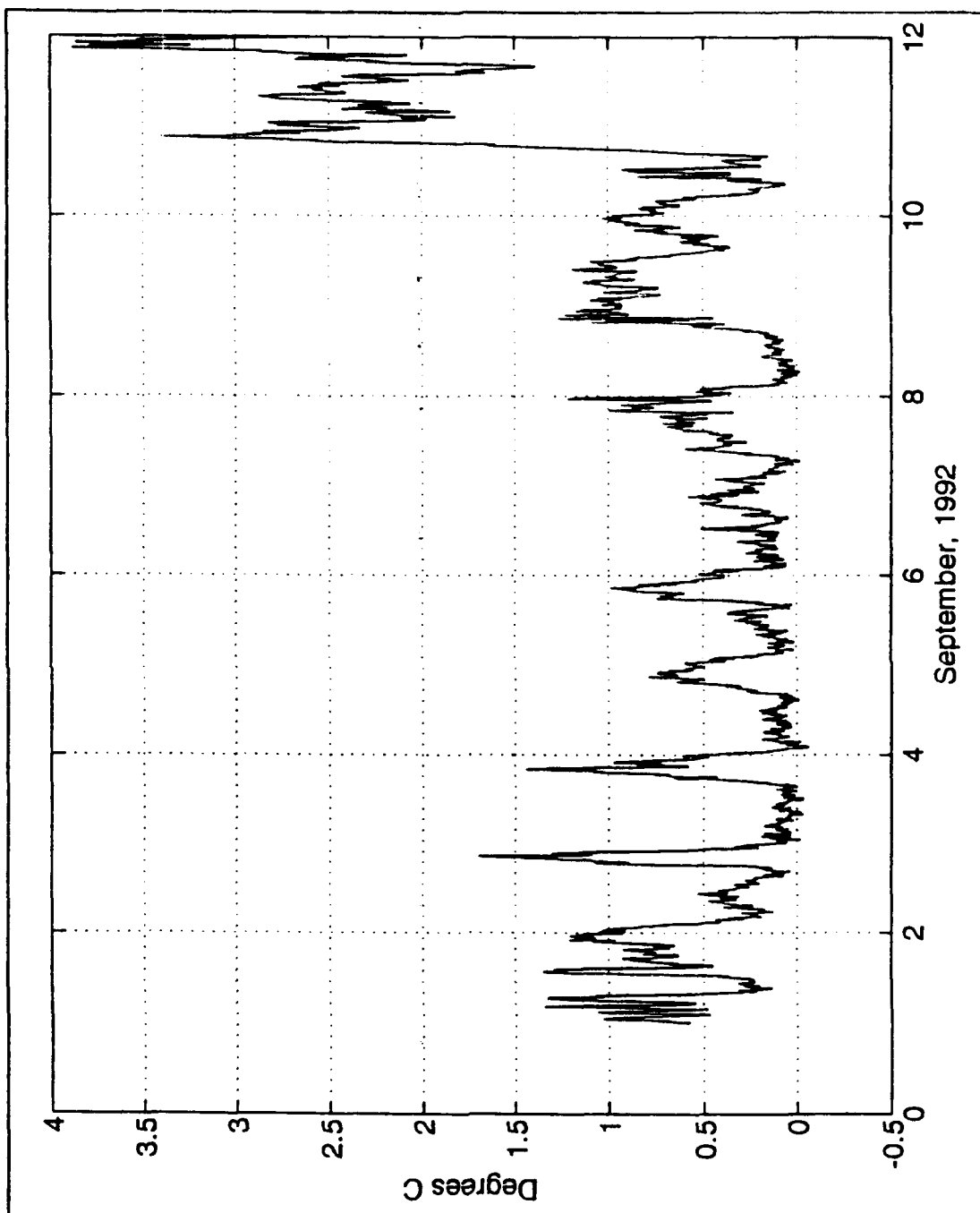


Figure 19. Observed Sea Surface Temperatures Minus 10 Meter Temperatures. Values Near Zero Indicate Periods of Deepening to Greater than 10 Meters.

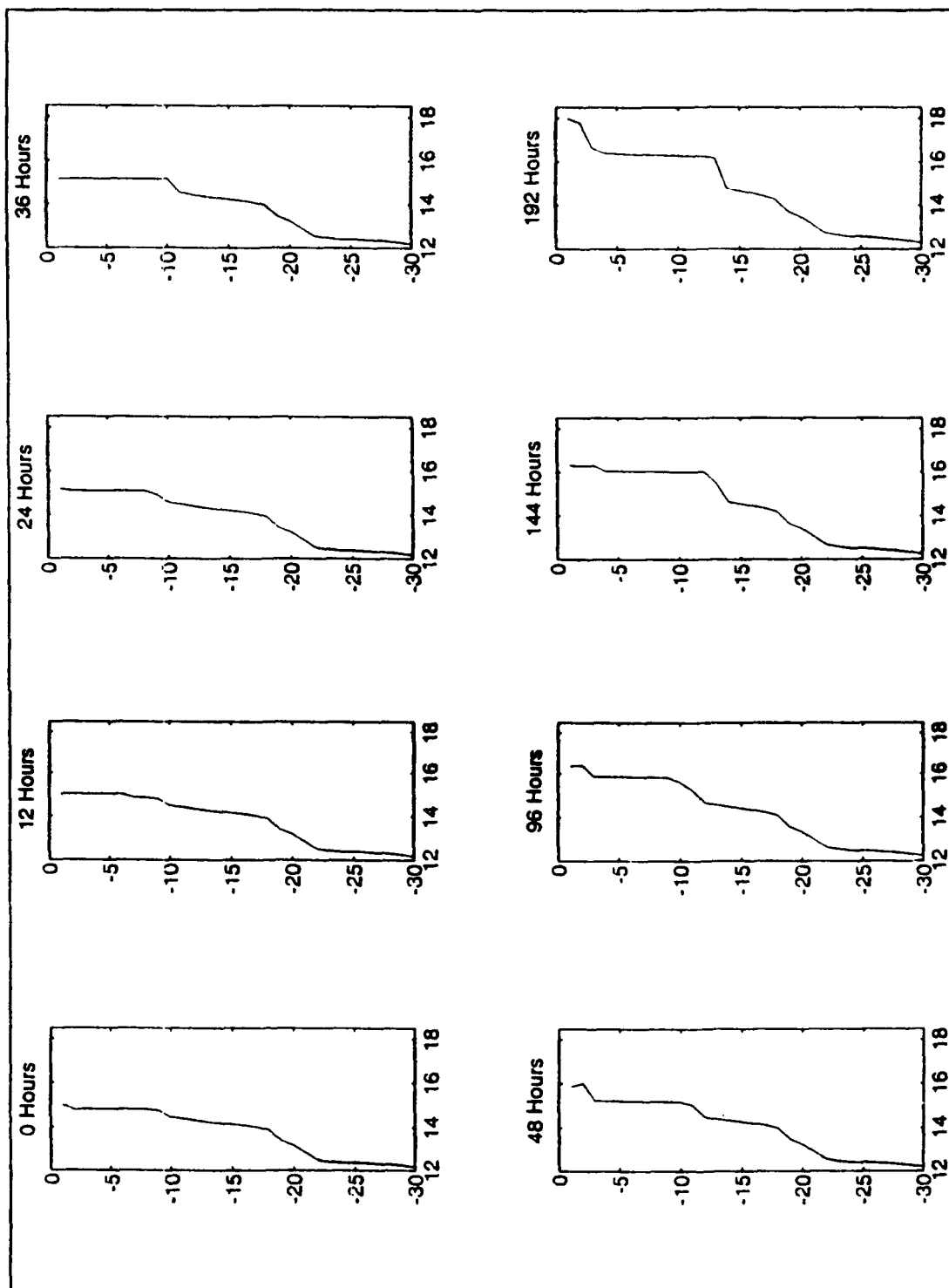


Figure 20. Sequence of Temperature Profiles From the Garwood Model. Time Since Model Initialization is Indicated at the Top of Each Profile.

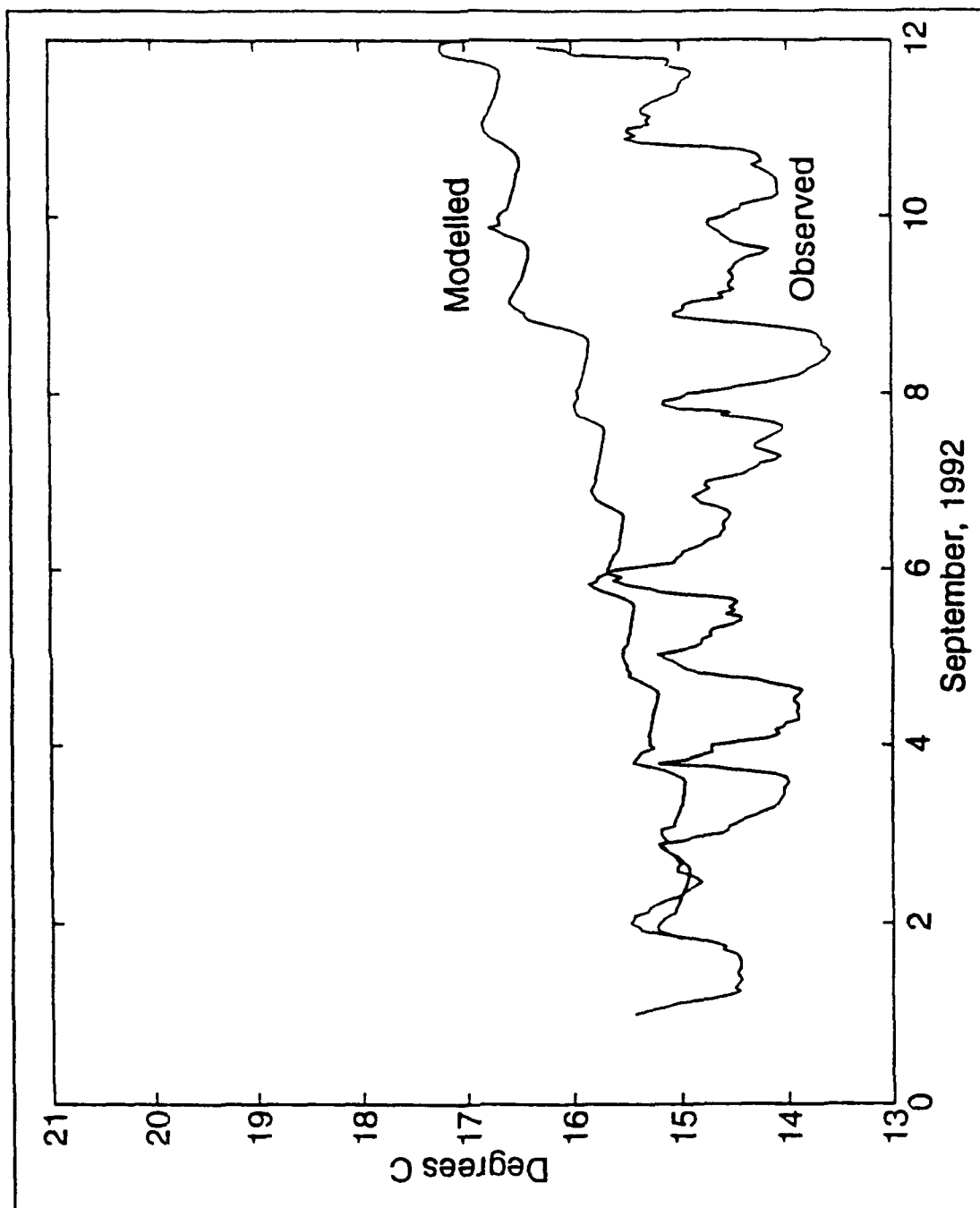


Figure 21a. Final PWP Mixed Layer Temperatures Versus Observed Sea Surface Temperatures.

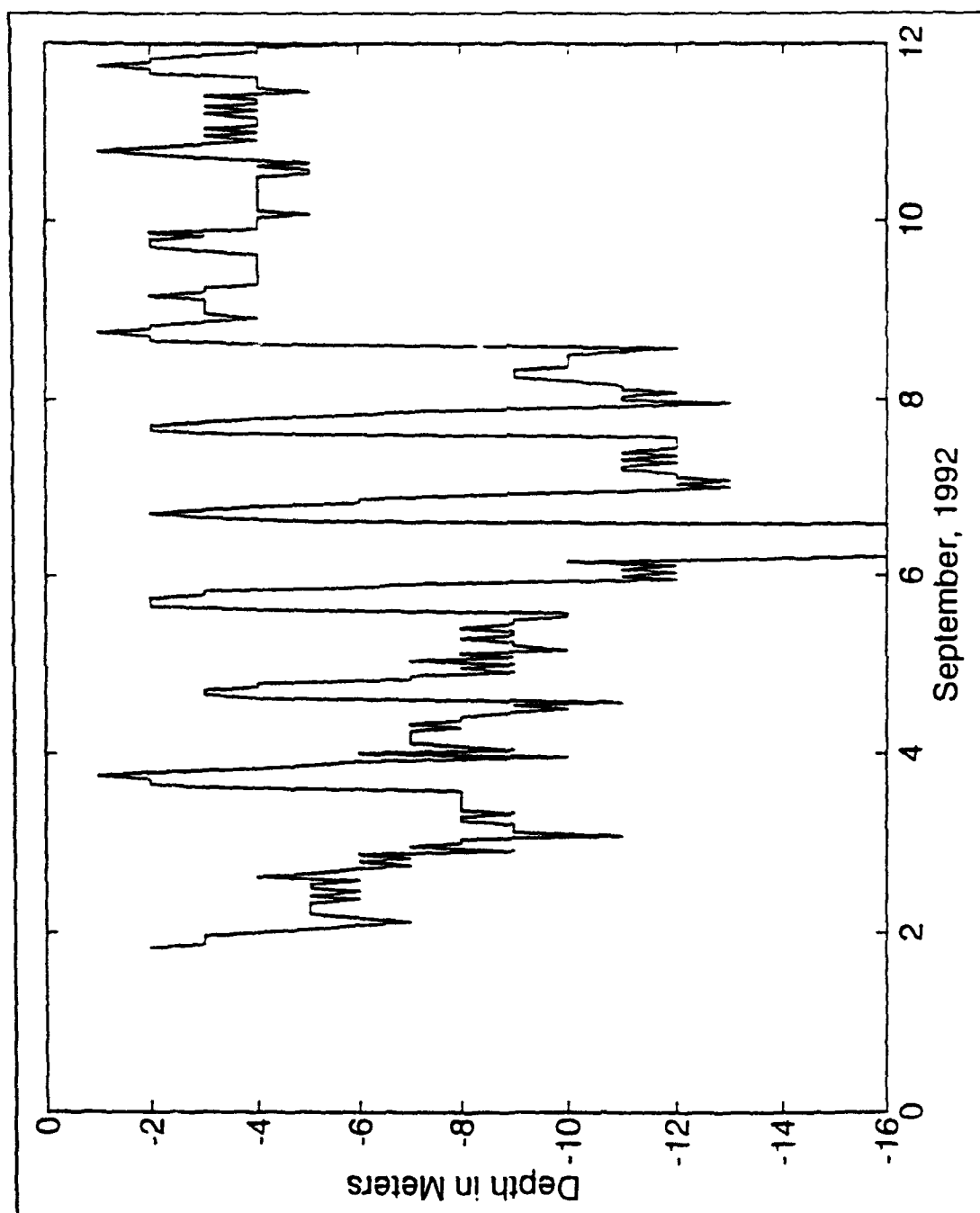


Figure 21b. PWP Mixed Layer Depths. Note That Depths are in Whole Numbers, Since They are Inferred from a Density Profile Which is Subject to the Model's Vertical Bin Spacing.

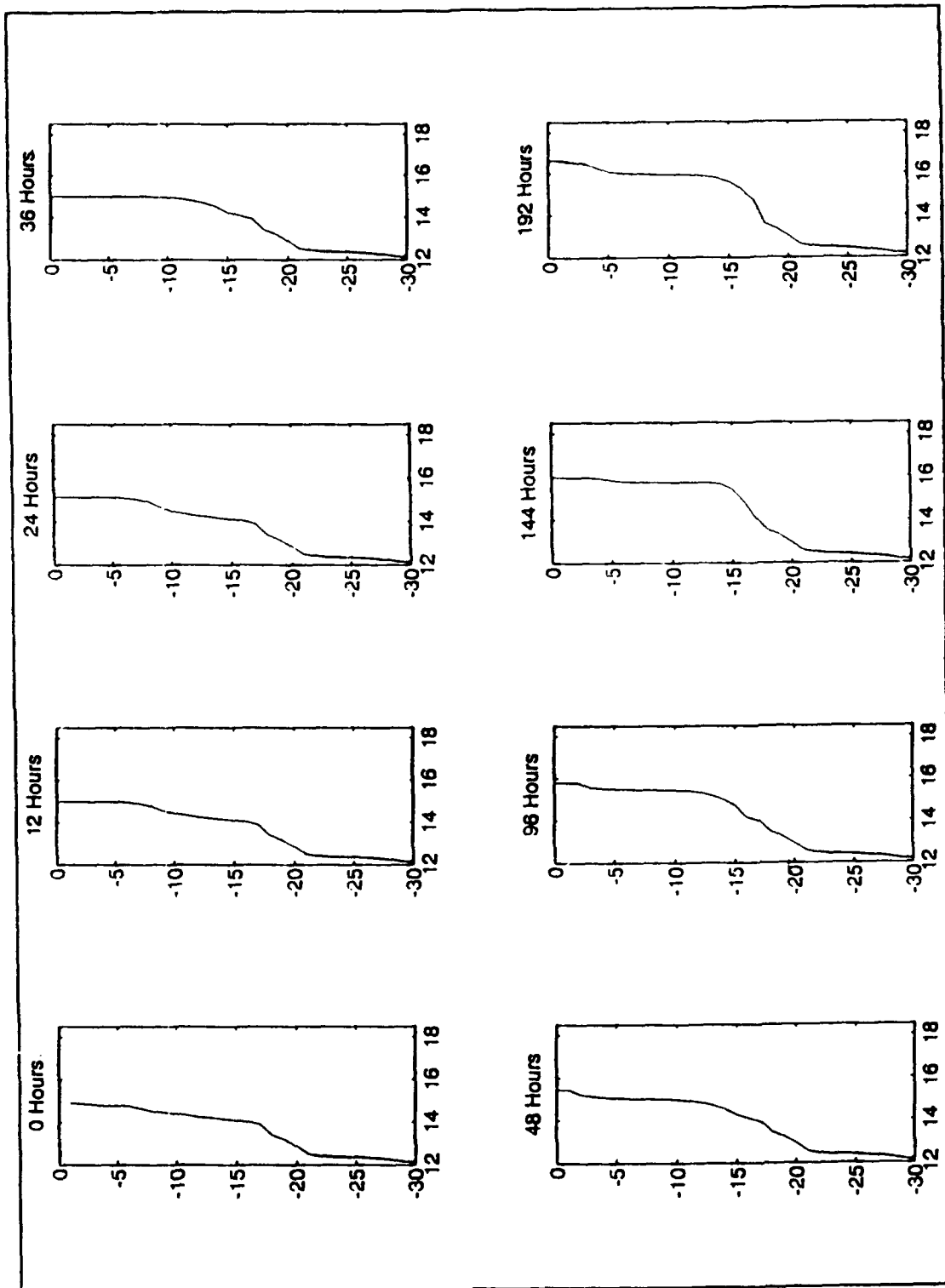


Figure 22. Sequence of Temperature Profiles from the PWP Model.

VI. DISCUSSION

A. RELATING MODEL TRENDS TO ADVECTION

As stated in the last chapter, both models exhibited an upward trend in mixed layer temperatures relative to the observations. These trends were 0.289 and 0.196°C per day for Garwood and PWP, as presented previously. The least squares fits used to compute these trends are shown in Figures 23a and b. If it is assumed that this trend is due entirely to the fact that no advective effects are included in the models and that any advection occurring is in the vertical, then an estimate of the magnitude of vertical advection can be made, according to the relationship

$$\frac{\partial T}{\partial t} = -w \frac{\partial T}{\partial z}. \quad (37)$$

Using a vertical temperature gradient from the initial profile of -2.4°C over the top 21 meters (the depth region with significant stratification), or -0.114°C/m, produces vertical velocities of 2.53 and 1.72 meters per day for Garwood and PWP, respectively. These values are within the range of upward velocities expected in an upwelling region (Huyer, 1983). Therefore, it is reasonable to suggest that the upward trend in both models' results could be entirely due to the

fact that no advection was included in the versions of the models used here.

Figure 24 shows the least squares fit lines of the raw data for surface, 10, 20, and 40 meter temperatures. A clear downward trend in the subsurface data suggests that colder water was being advected into the upper 40 meters, which could have contributed to maintaining fairly constant surface temperatures despite forcing that should produce a warming trend. This is another indication that vertical and/or horizontal advection was significant during the study period.

B. DIURNAL CYCLE

Apart from the trends seen in the models relative to the surface temperature data, the other major deviation of the models, as mentioned in the last chapter, is in the magnitude and characteristic shape of the diurnal cycle. This can be seen clearly if the aforementioned trends are removed from the model results, as done in Figures 25a and b. The models do produce a sharp increase in temperature each morning as the sun comes up, quite similar to that seen in the data, although the magnitude of this rise is in most cases much less than that seen in the data. After the models reach their peak sea surface temperature, which occurs at approximately 1506 PDT (one hour prior to the average time in the data), they begin a decline in temperature which is much more gradual than the observations. This is true in both models, although more so

in PWP. This reduced downward slope in mixed layer temperatures in the Garwood case results in nightly decreases of an average 0.54°C less than in the data. The shortfall in nocturnal cooling in PWP is even greater, at 0.76°C .

This discrepancy between the models and observations dictated further analysis of model behavior in response to varying forcing. In an effort to determine how the models were responding to heating and wind stress inputs independently, two additional test cases were run. The results of the model runs presented in the previous chapter and detrended in Figures 25a and b show how the models reproduced mixed layer temperature in response to the combined effects of varying wind stress and heat flux. In the first test case the wind stress is held constant, while the heat flux undergoes the usual diurnal variation. This is similar to what has been done in open ocean studies. Secondly, in an effort to measure the model response to diurnal variations of wind stress alone, winds were allowed to vary according to the observations while the total heat flux was held constant.

1. Constant Wind Forcing

The constant wind cases were run using constant eastward and northward winds of 3.672 and -1.038 m/s, respectively. These were the mean values observed over the 11 day period, corresponding to a mean wind toward 117°T , as mentioned in Chapter IV. Temperature results from both models

are presented in Figure 26a, while mixed layer depths are shown in Figure 26b. An extremely regular pattern of mixed layer temperatures is apparent, as would be expected from the relatively regular solar heating pattern. Mixed layer depths remain shallow in the absence of afternoon wind peaks. The Garwood model exhibits significantly more diurnal variability than PWP, warming an average 1.44°C each day as compared to only 0.67°C per day in PWP. Both models cool the mixed layer each night by an amount less than they warmed it during the day. In the case of the Garwood model, this cooling averages 0.91°C per day, implying a net gain of mixed layer temperature each day of 0.53°C . PWP cools by an average 0.18°C per day, resulting in a similar gain of 0.49°C . These substantial daily heat gains when the model is forced with constant winds of this magnitude produce the large upward trends seen in Figure 26a. This suggests that daily intensifying winds are an essential element in predicting the thermal structure in a sea breeze influenced region. Without the increased generation of turbulence from wind stress that occurs in the afternoons and early evenings, the large downward heat flux which is occurring at those times creates an unrealistically shallow mixed layer, and thus excessive mixed layer warming. Clearly, the timing of the peak in wind stress is critical. The fact that it occurs at a time when solar insolation is high allows the incoming heat to be distributed over a deeper layer than would otherwise be the case. If winds were light

in the afternoons and intensified at dusk, for example, much greater daily warming and nightly cooling would occur.

Of note in the constant wind case is the fact that temperature peaks occur at an average time of 0014Z and 0057Z (1714 and 1757 PDT) in Garwood and PWP, respectively. Recall that the observed surface temperatures peaked at an average time of 1603 PDT, while the model runs forced with varying wind stress and heat flux peaked at an average time of 1506 PDT. Thus, in the constant wind case, there is a lag with respect to the data, rather than the lead that was seen in the total forcing cases. Allowing the wind to vary, then, resulted in a phase shift of 2 to 3 hours, depending on the model, since increased afternoon mixing was able to begin cooling the layer sooner than when the winds were held constant.

2. Constant Heat Flux

For these cases, the wind stress computed from observed eastward and northward wind components as discussed previously was used, along with a constant downward surface heat flux of 157.7 W/m^2 , to force the models. Again, this was the mean value over the study period and is composed of a mean solar insolation of 231.3 W/m^2 (including nighttime periods) and a mean heat loss of 73.6 W/m^2 . Mixed layer temperature and depth results for these runs for the two models are presented in Figures 27a and b. These results for the Garwood

model very nearly duplicate those that resulted from the complete forcing case presented in the last chapter, with slight deviations occurring only over the last half of the period. PWP also produced a thermal pattern which more closely resembled that of the last chapter than did the constant wind stress case. However, in PWP, the diurnal variability is even more damped out than it was previously.

Particularly with respect to the Garwood model, these observations suggest that the details of the wind stress used to force the models is a greater determinant of the results than the heat flux. The fact that the total forcing case and the case with constant downward heat flux produced nearly identical mixed layer temperature patterns is quite surprising, and might suggest that the model does not respond to the diurnal heat flux cycle in a manner similar to the real ocean.

C. POSSIBLE REASONS FOR MODELS' UNDERESTIMATES OF NOCTURNAL COOLING

Mechanisms that might cause the models to underpredict the large, sharp temperature falls that are seen on most nights in the data are discussed next.

1. Penetrative Convection

After the sun sets, surface heat flux from the ocean to the atmosphere generates higher density water and thus convective instability. Both models deal with this by mixing

that water downward until static stability is returned throughout the water column. One suggestion to explain the reduced cooling in the PWP model relative to the observations each night is that the cool water at the surface actually descends in plumes which have associated vertical momentum. This causes them to overshoot the base of the mixed layer, entraining a larger quantity of dense water up into the layer. This would result in a cooler mixed layer by morning than would occur without this process, and would presumably cause the mixed layer to deepen more rapidly at the onset of upward buoyancy flux. PWP does not include this penetrative convection mechanism. Garwood does include such a mechanism and this could explain its increased nocturnal cooling relative to PWP. This mechanism is suggested by Large, et al. (1993).

2. Steady State TKE Assumption

Garwood's model assumes that the TKE is balanced at every time step. As discussed previously, an unsteady model (which handles only deepening of the mixed layer) was run with step function wind forcing. As seen in Figure 15, the TKE reaches a steady state in about an hour, but during that hour TKE exceeds the value to which it asymptotes. The presence of these short term transients in the ocean, which could be generated by constantly varying buoyancy forcing, as well as wind stress, could contribute to mixing that is not reproduced

by the steady-state model. This additional mixing, then, would result in cooler mixed layer temperatures.

3. Model Stratification

At initialization, it is known that a fairly accurate temperature profile is being used by the model. However, as the model mixed layer temperature increases, while the profile below the layer remains the same, there is a corresponding increase in the degree of stratification in the model as time progresses. This excess density contrast makes subsequent mixing more difficult. That is, a greater amount of turbulence is necessary for the same amount of entrainment. A visual representation of this temperature profile change was seen in Figures 20 and 22. The fact that on the first night of the period, before this effect could build, the models produced a temperature fall in line with the data lends support to this idea as a potential contributing factor.

4. Diurnal Advection

Another postulated mechanism for producing the large and sharp temperature decreases seen in the data at night is a diurnally varying advection. Although currents were not specifically studied here, Foster (1993) demonstrates from HF radar measurements of surface currents in Monterey Bay that the spectrum of surface currents is dominated by the diurnal period, presumably driven by the sea breeze. It is possible that, in response to the very regular variation of the surface

currents, there could be a similarly regular pattern of horizontal (or vertical) advection occurring within the bay. In order for horizontal advection to produce large temperature changes at M1, there must be a significant horizontal temperature gradient in the area, which is being forced across the mooring site on a diurnal time scale. Given the presence of upwelled waters in the region and the location of M1 near the mouth of the bay, it seems possible that such diurnally varying advective effects could be occurring. Without detailed surface temperature data at high temporal resolution in the area, it is not possible to test this hypothesis. Diurnal variations in vertical advection would require horizontal divergence/convergence of the diurnal surface currents. This hypothesis also requires additional data to test.

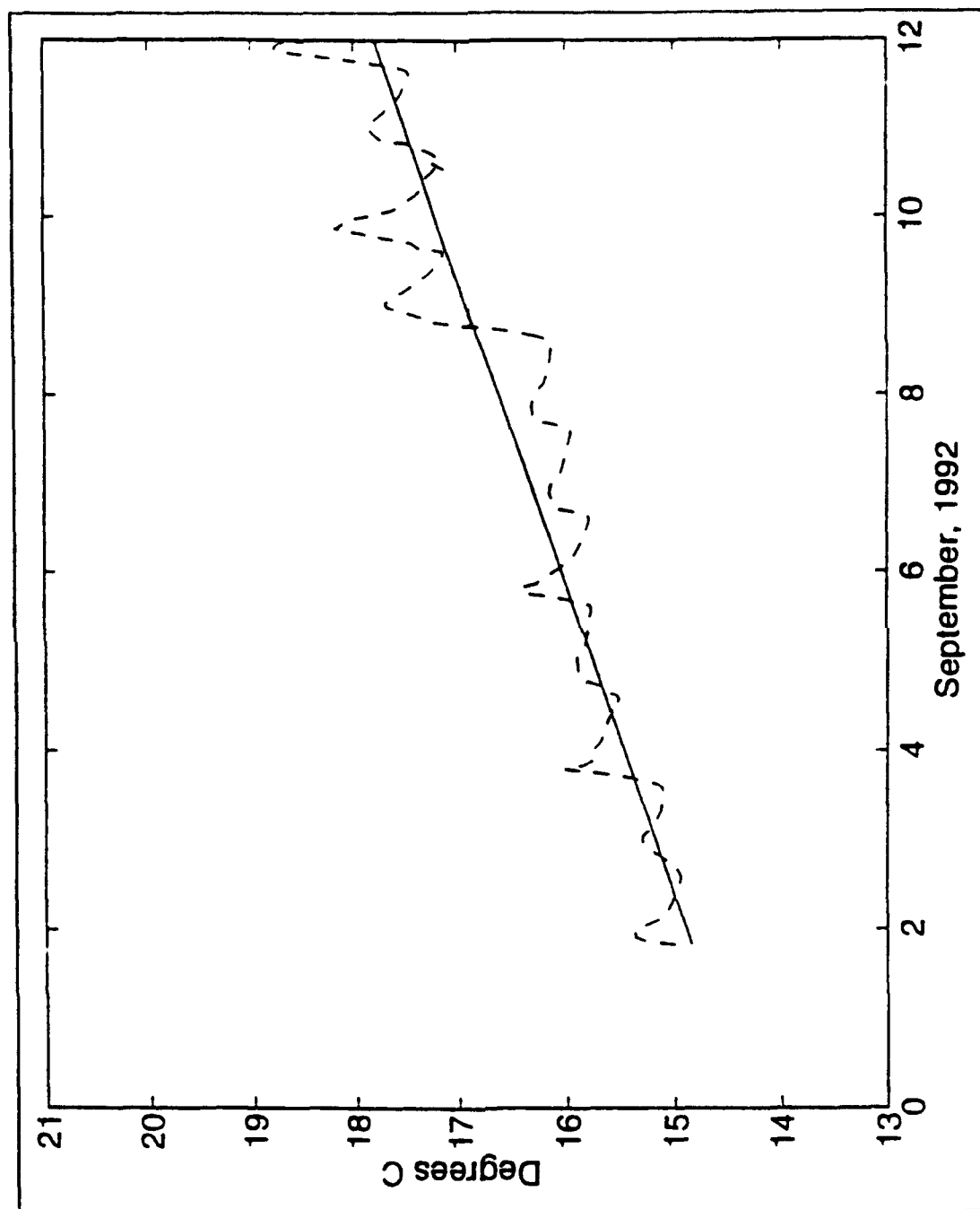


Figure 23a. Least Squares Fit to Garwood Temperatures.

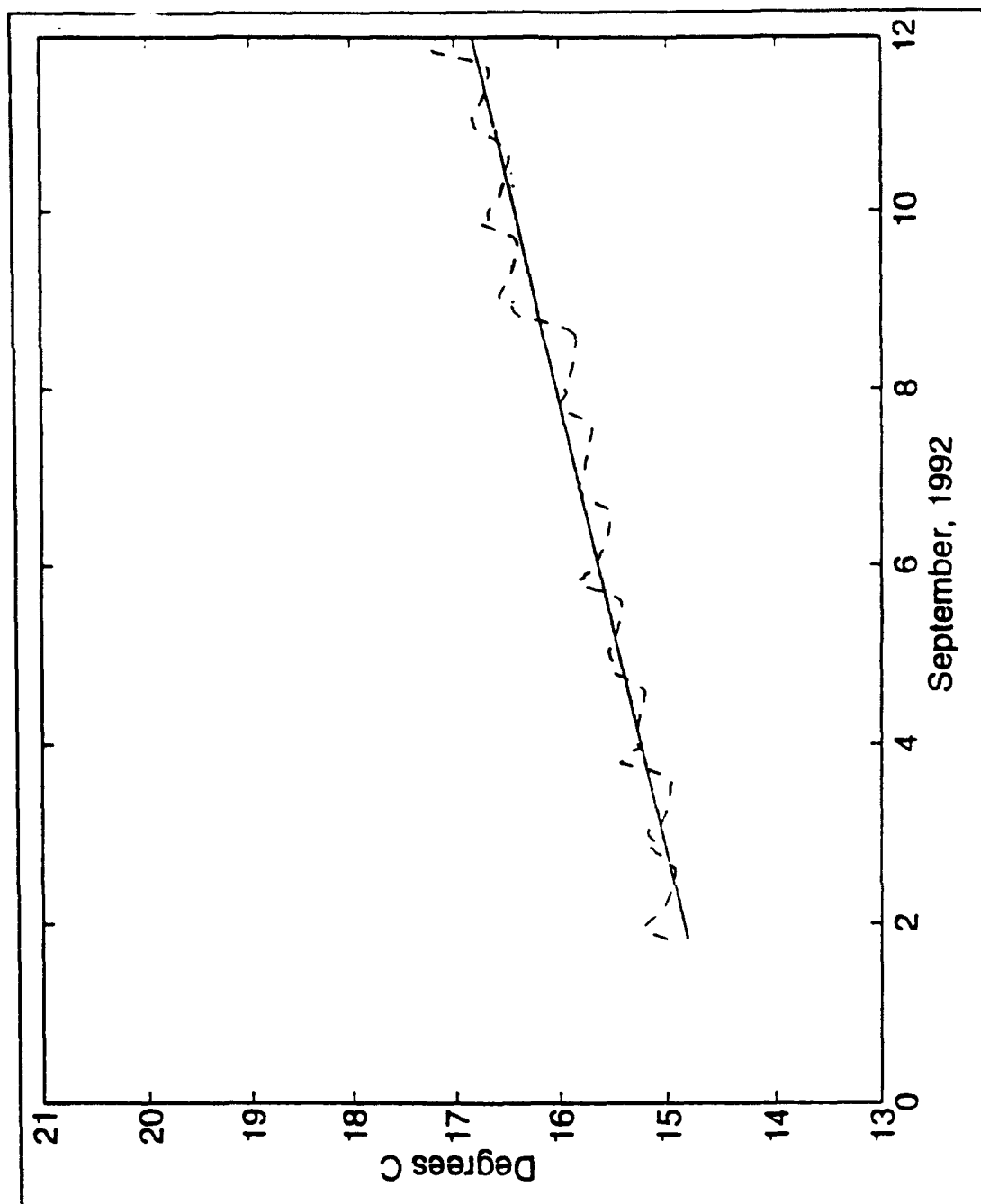


Figure 23b. Least Squares Fit to PWP Temperatures.

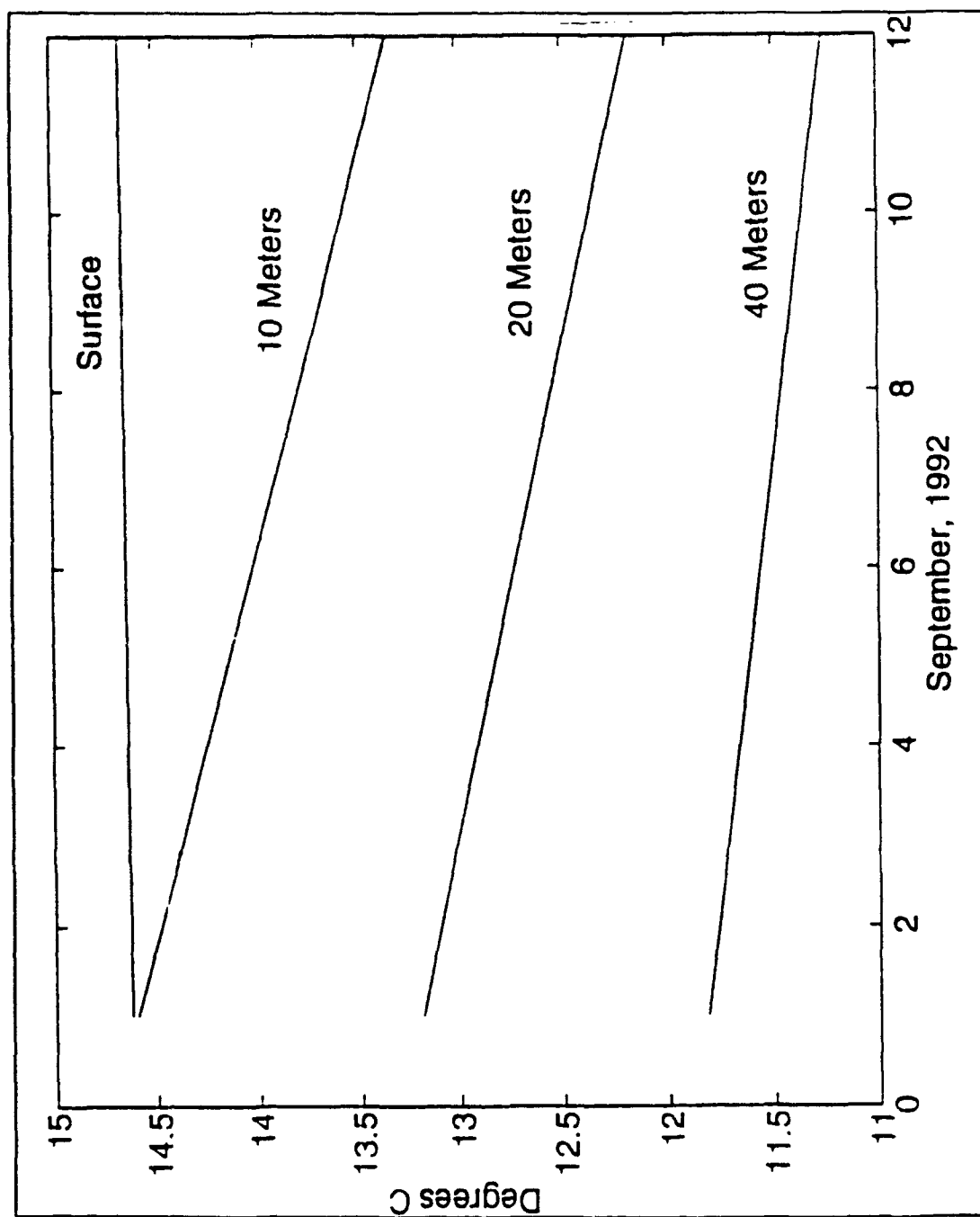


Figure 24. Least Squares Fits to Observed Temperatures.

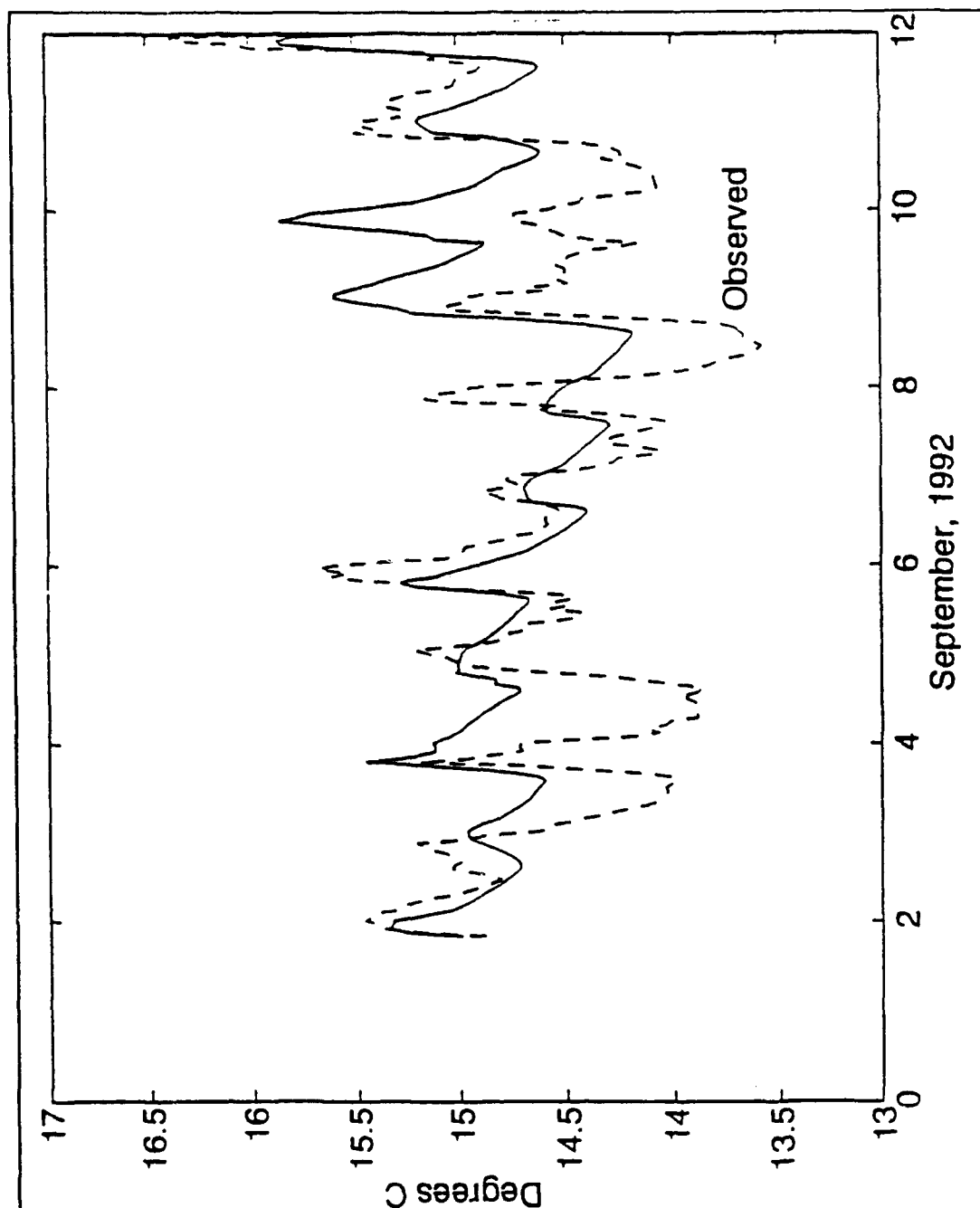


Figure 25a. Detrended Garwood Mixed Layer Temperatures (Solid) Versus Observed Sea Surface Temperature. Note Different Temperature Scale from Previous Plots.

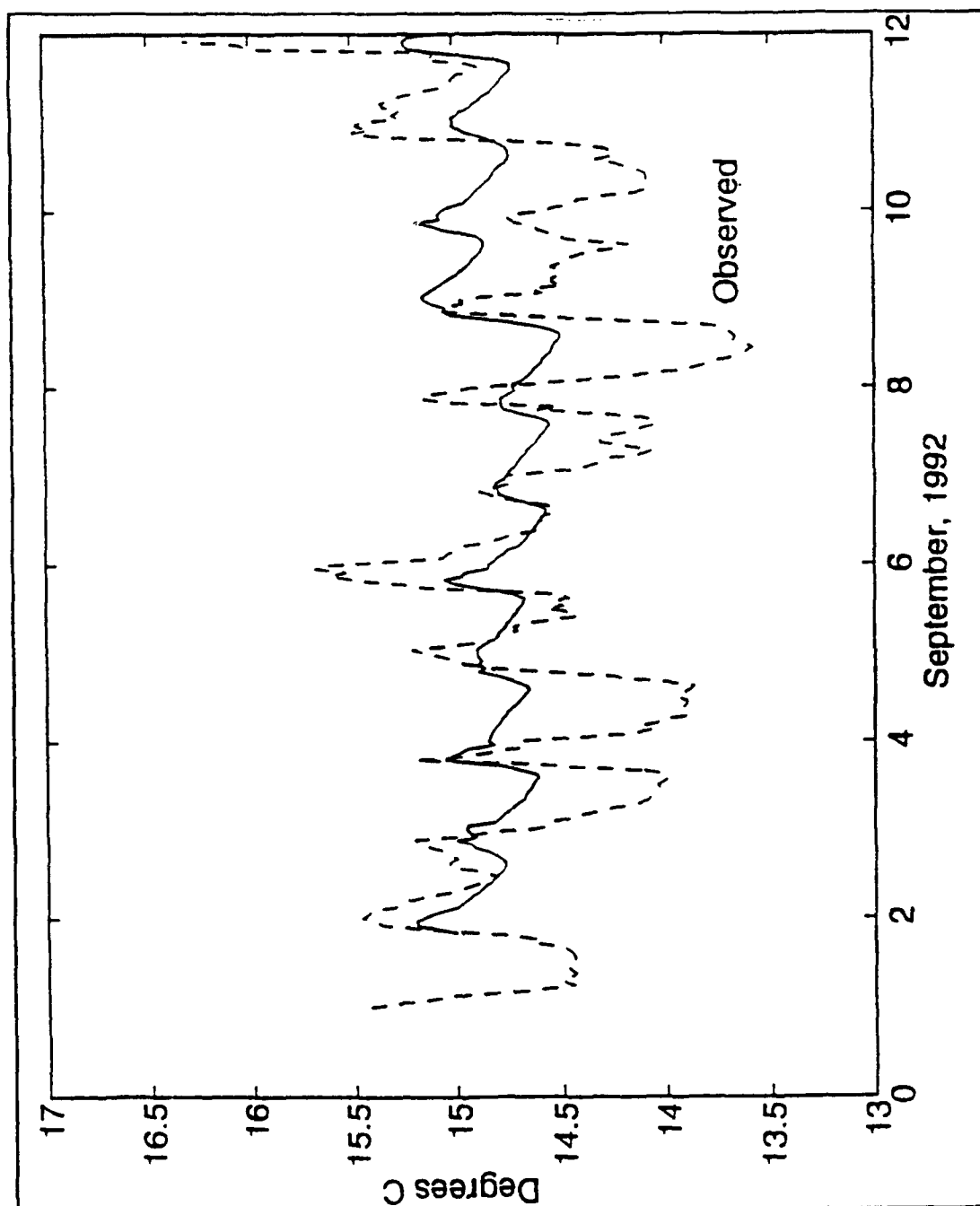


Figure 25b. Detrended PWP Mixed Layer Temperatures Versus Observed Sea Surface Temperatures.

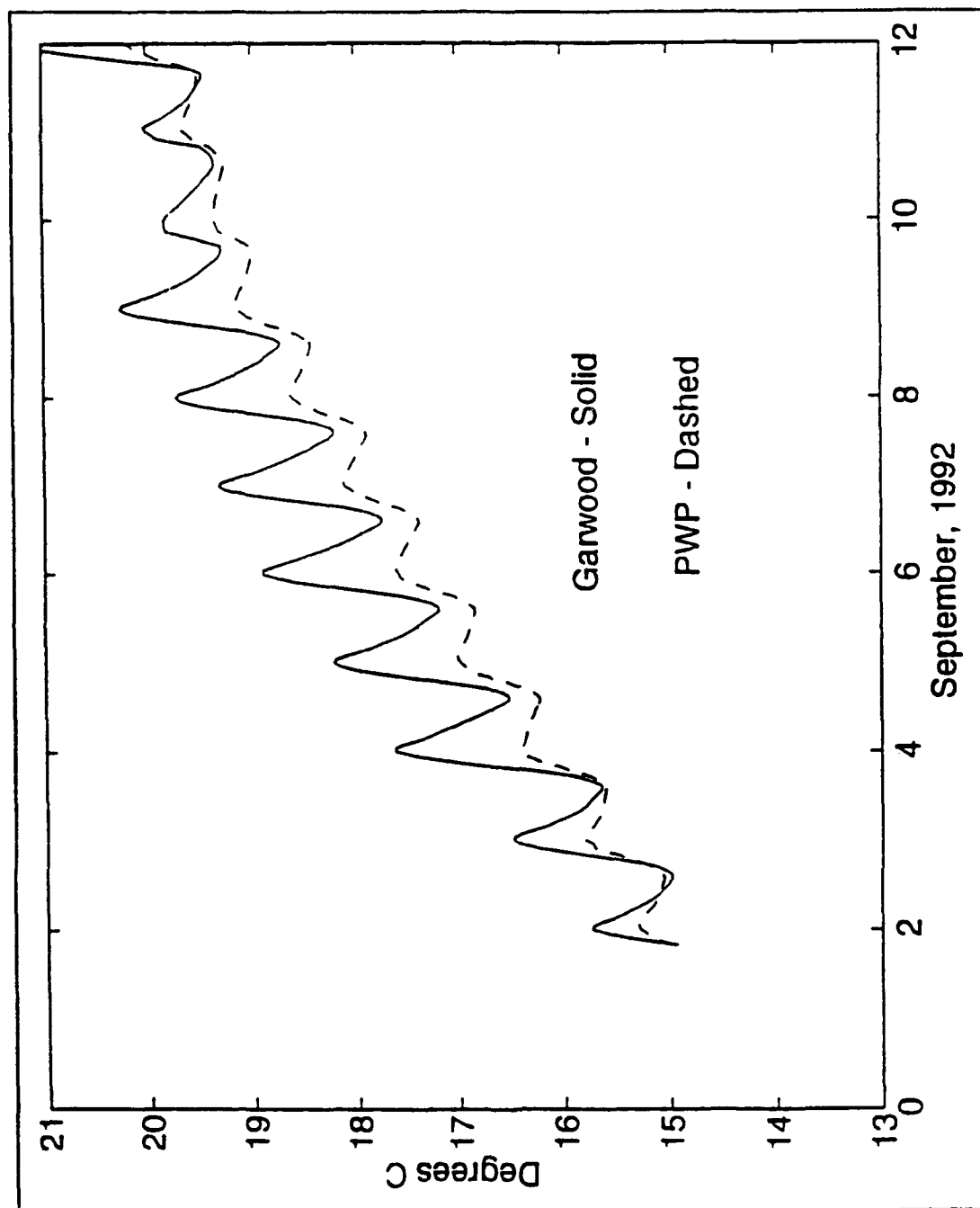


Figure 26a. Mixed Layer Temperatures with Constant Wind, Varying Heat Flux.

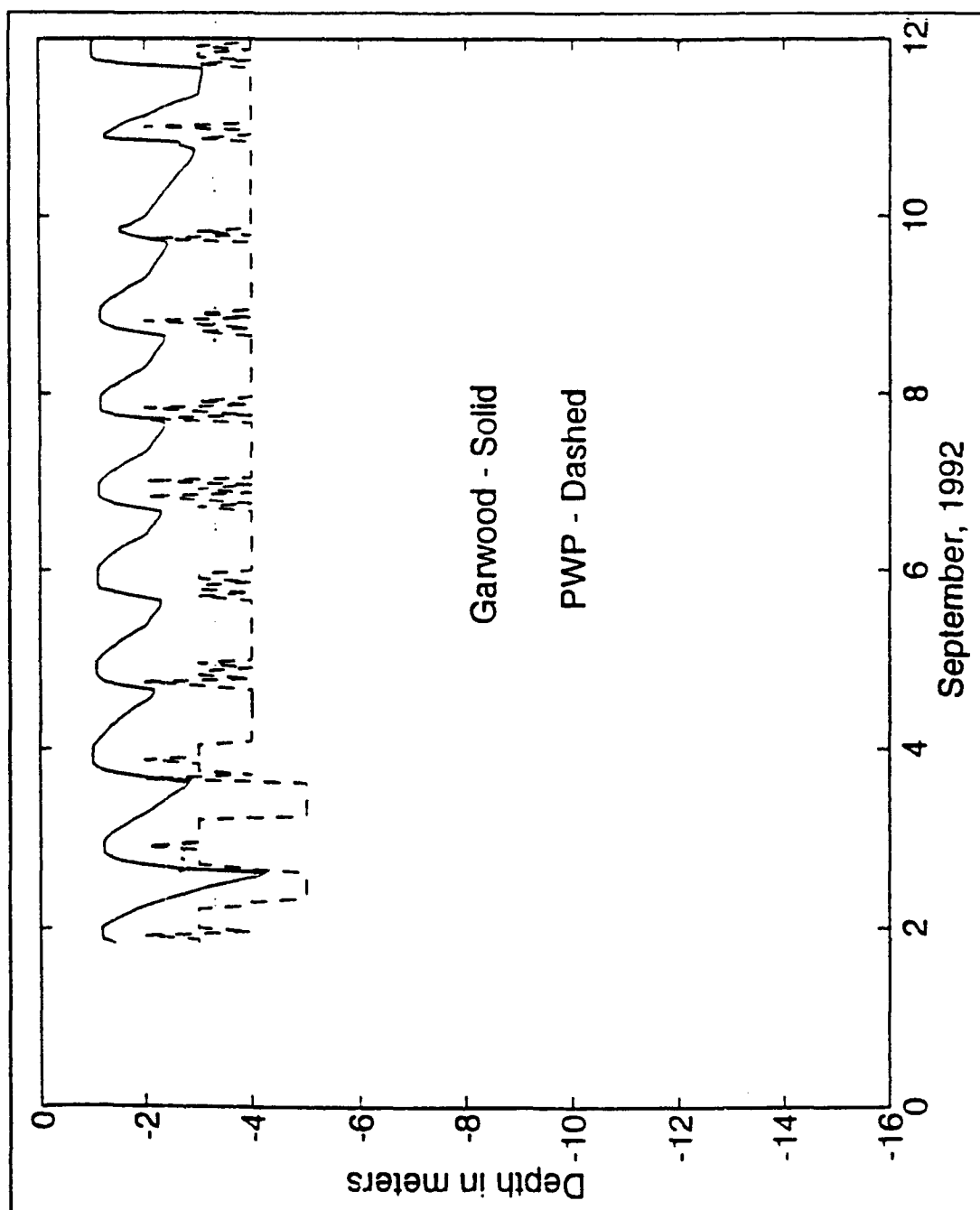


Figure 26b. Mixed Layer Depth with Constant Wind, Varying Heat Flux.

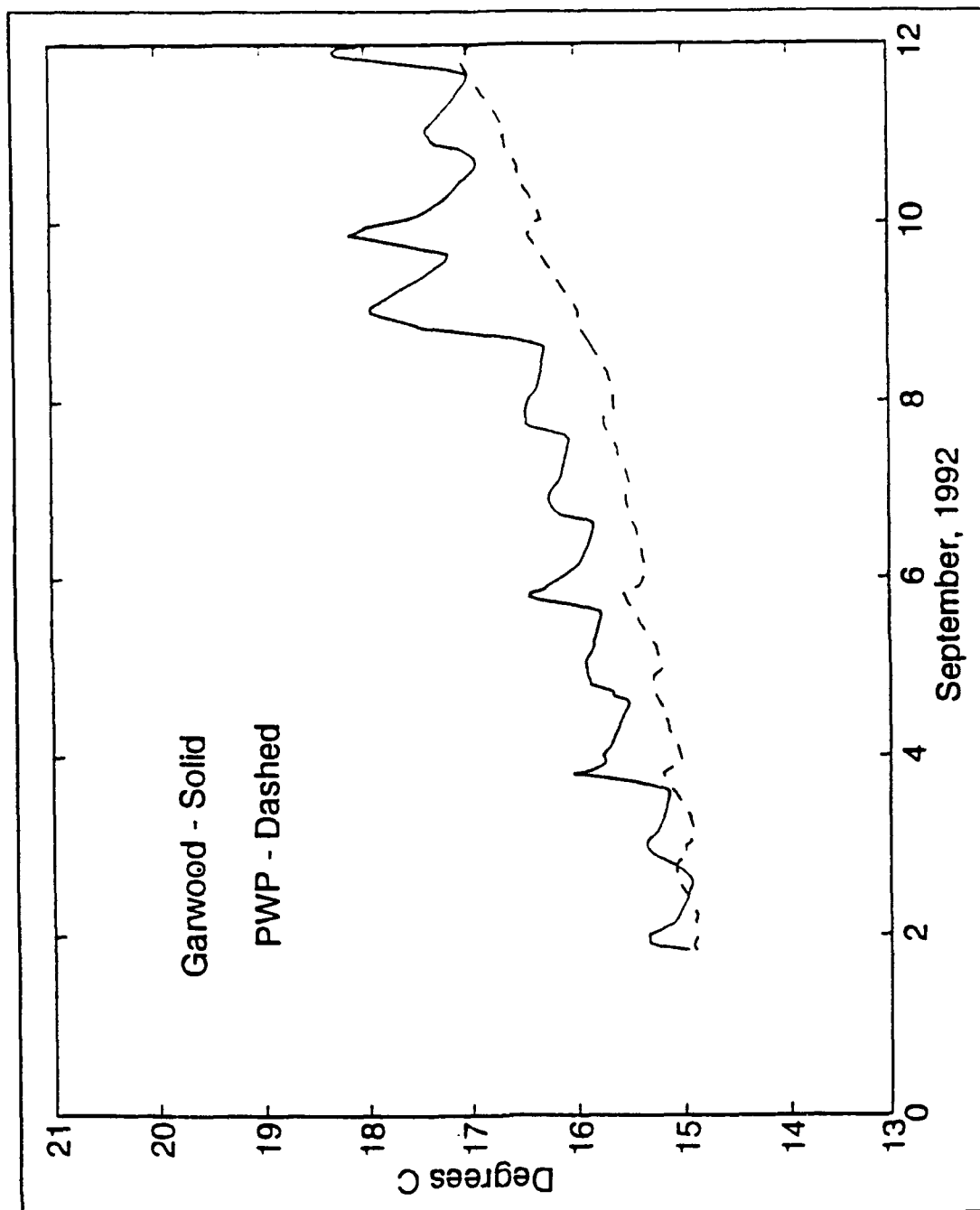


Figure 27a. Mixed Layer Temperatures with Constant Heat Flux, Varying Wind. Note Similarity of Garwood Pattern to Previous Result.

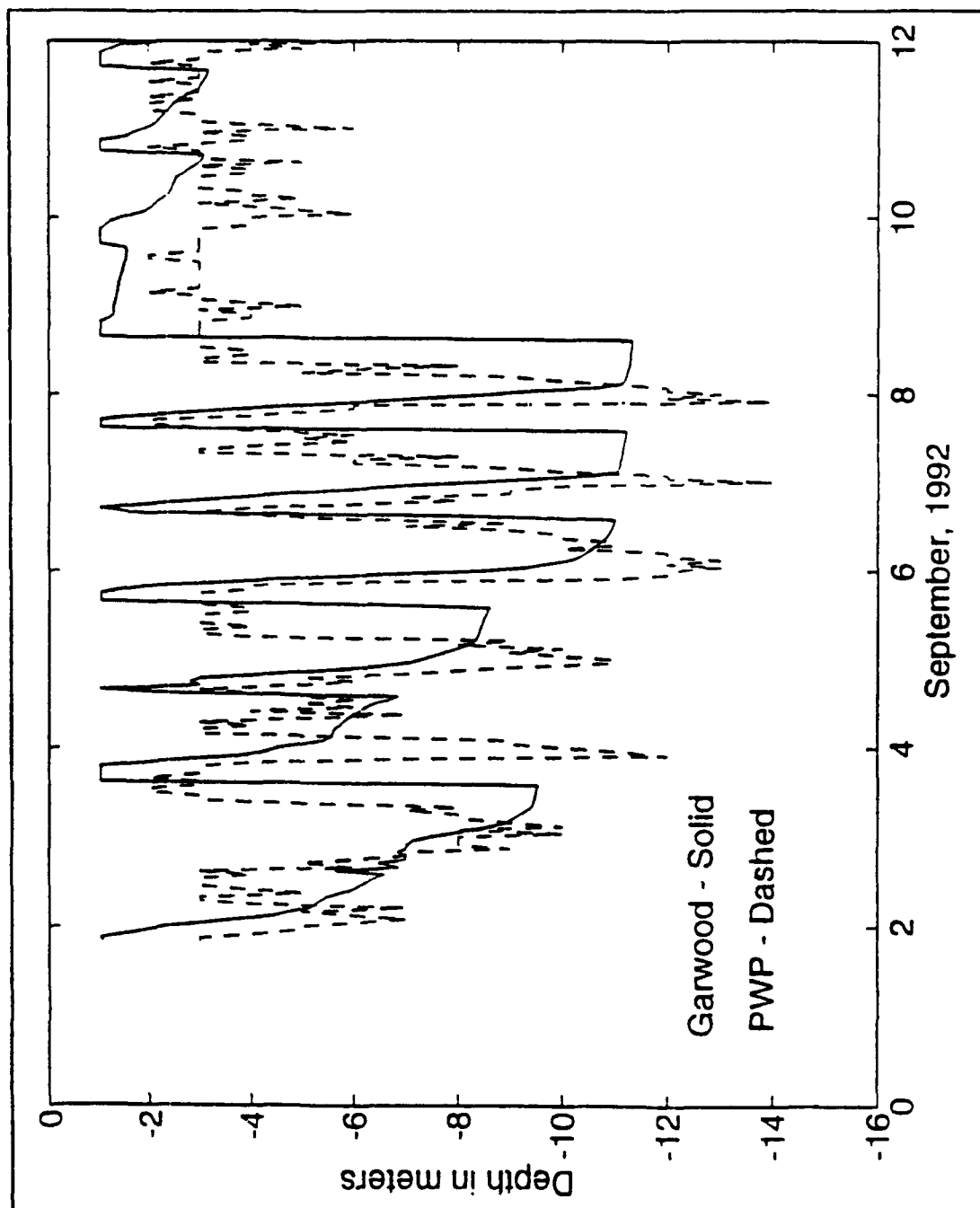


Figure 27b. Mixed Layer Depths with Constant Heat Flux, Varying Wind.

VII. CONCLUSIONS AND RECOMMENDATIONS

A. MIXED LAYER BEHAVIOR IN MONTEREY BAY

The behavior of the oceanic mixed layer in a region influenced by diurnally intensifying winds is studied. The study area is Monterey Bay, California, in which a sea breeze is clearly shown to be strongly influencing the temperature and depth of the mixed layer during September, 1992. This diurnal wind stress variability creates an interesting interaction with the diurnal heat flux present in other mixed layer studies. The wind stress reaches its peak at an average time of 1730 PDT. The downward heat flux peaks at about 1300 PDT. The sea surface temperature data presented in Chapter IV shows a pattern of large day to night temperature swings, with the peaks occurring at approximately 1600 PDT. In the evening, decreasing downward heat flux and large wind stress produce cooling, which is underpredicted by the models.

The models' mixed layer depth is also shown to undergo a diurnal variation influenced by the sea breeze. It is seen to deepen quickly in the evenings when winds are still quite strong and reach its greatest depth just prior to sunrise after a night of convective overturning. Shallowing in the morning occurs very suddenly in the presence of the light winds seen at those hours.

B. ONE-DIMENSIONAL MIXED LAYER MODELS IN SEA BREEZE REGIONS

The one-dimensional mixed layer models of Garwood (1977) and Price et al. (1986) are used to evaluate the capabilities of such models in this coastal environment. The models do a good job of predicting the phase of the mixed layer temperature pattern seen in the data. Compared to observations, a lead of about one hour is seen in the model temperature peaks, with a lag of less than an hour in the minima. The daily increases in mixed layer temperature are very similar in slope, although frequently with reduced magnitude, in the models to what is observed in the data.

Both models exhibit two major differences from what is seen in the observations over this period. The first of these is the upward trend in mixed layer temperatures relative to the data (0.29°C per day in Garwood and 0.20°C per day in PWP). This is postulated to be primarily the result of the fact that no advection is included in either model. Reasonable values of vertical advection are obtained using the assumption that all of the missing advection is in the vertical. The other characteristic of the model results that differs from the data is the fact that the cooling at night is reduced in both magnitude and rate. This is true in both models, although the Garwood model produces a better diurnal cycle than does PWP. This lack of cooling is seen to be true to the same degree when the Garwood model is forced with a constant downward heat flux. These results suggest that, at

least in the presence of diurnal wind stress variation, the upward heat flux phase of the daily buoyancy forcing cycle has little influence on the model. Two mechanisms which could produce the large, sharp temperature drops observed each night in the data are penetrative convection and diurnally varying advection. The former is not present in PWP and the latter is not included in either model. Transients in the turbulent kinetic energy produced by the constantly varying forcing are not included in the Garwood model, which assumes steady state TKE at each time step. This and the increasing stratification in the models as time progresses would reduce the amount of mixing and cooling that occur in the models relative to that in the ocean.

Overall, it is concluded that the turbulence budget type of model reflects the real ocean in this environment to a greater degree than does the Richardson number instability type, based on the models studied here. However, both types apparently suffer from their one-dimensionality in a coastal region where vertical and horizontal advective effects are apparently present.

C. RECOMMENDATIONS

Since it is possible to add vertical advection to a one-dimensional model, it is recommended that this be done in an area such as this where these effects are clearly not negligible. By adding the advection at each model time step,

the stratification would not build as much as was seen in this study and a more realistic trend would result. Also, it is possible that this would also allow a more realistic prediction of nocturnal cooling, particularly later in the model run.

In order to investigate the possibility of additional mixing due to transients of TKE, it would be beneficial to run a non-steady state model at a shorter time step (say, 10 minutes) for the entire period. It would be necessary to use a model which allows both deepening and shoaling of the mixed layer.

This study brings up a variety of possible future efforts related to coastal mixed layer physics. Conducting a similar study with this data during another time of year (January, for example) when the sea breeze is not well established would provide an interesting comparison. Since upwelling is reduced or absent along the coast during this time, and the temperature field is more uniform in the horizontal, it is possible that advective effects would also be reduced, and the models would more accurately reflect the data.

Use of the surface current data from high frequency radar, such as that used by Foster (1993), would allow convergence at M1 to be computed, thus making possible a determination of the vertical velocity near the surface. This, together with the vertical temperature gradient, can be used to calculate vertical advection. To determine the variability of

horizontal advection, it would be useful to obtain an improved picture of sea surface temperatures within the bay. This could be done through a combination of extensive in situ measurements and the use of satellite derived sea surface temperatures. Combining this information with velocity results produced by the models may provide further insights into the three-dimensional forcing occurring at M1 and other coastal locations.

Finally, a more complete picture of mixed layer behavior should be obtained through a series of upper ocean CTD or bathythermograph casts collocated with continuous meteorological observations. These casts should be of sufficient frequency to allow resolution of changes on an hourly or smaller time scale. This would eliminate the problem encountered in this study in which temperature data was available from only the surface, 10 and 20 meters. This would also allow a more accurate description of density variations, since salinity would be included.

LIST OF REFERENCES

- Adamec, D., R.L. Elsberry, R.W. Garwood, Jr., and R.L. Haney, An embedded mixed-layer-ocean circulation model, *Dynamics of the Atmosphere and Oceans*, 6, 69-96, 1981.
- Ball, F.K., Control of inversion height by surface heating, *Quarterly Journal of the Royal Meteorological Society*, 86, 483-494, 1960.
- Beardsley, R.C., and C.E. Dorman, C.A. Friehe, L.K. Rosenfeld, and C.D. Winant, Local atmospheric forcing during the Coastal Ocean Dynamics Experiment 1. A description of the marine boundary layer and atmospheric conditions over a northern California upwelling region, *Journal of Geophysical Research*, 92, 1467-1488, 1987.
- Benjamin, T.B., The threefold classification of unstable disturbances in flexible surfaces bounding inviscid flows, *Journal of Fluid Mechanics*, 16, 435-450, 1963.
- Burt, W.B., D.B. Enfield, R.L. Smith, and H. Crew, The surface wind over an upwelling area near Pisco Peru, *Boundary Layer Meteorology*, 3, 385-391, 1973.
- Burt, W.B., H. Crew, W. Plutchak, and J. Dumon, Diurnal variation of winds over an upwelling region off Oregon, *Boundary Layer Meteorology*, 6, 35-45, 1974.
- Chavez, F.P., and others, The MBARI program for obtaining real-time measurements in Monterey Bay, *Oceans '91 Proceedings*, 1991.
- Cushman-Roisin, B., Deepening of the wind-mixed layer: A model of the vertical structure, *Tellus*, 33, 564-582, 1981.
- Deardorff, J.W., A three-dimensional numerical investigation of the idealized planetary boundary layer, *Geophysical Fluid Dynamics*, 1, 377-410, 1970.
- Denman, K.L., A time-dependent model of the upper ocean, *Journal of Physical Oceanography*, 3, 173-184, 1973.
- Elsberry, R.L., T.S. Fraim and R.N. Trapnell, A mixed layer model of the oceanic thermal response to hurricanes, *Journal of Geophysical Research*, 81, 1153-1162, 1976.

Eppley Laboratory, Inc., Instrumentation for the Measurement of Components of Solar and Terrestrial Radiation, unpublished document, Newport, RI, 31 pp., 1971.

Foster, M., Evolution of diurnal surface winds and surface currents for Monterey Bay, Master's Thesis, Naval Postgraduate School, Monterey, California, December 1993.

Garwood, R.W., An oceanic mixed layer model capable of simulating cyclic states, *Journal of Physical Oceanography*, 7, 455-469, 1977.

Geisler, J.E., and E.B. Kraus, The well-mixed Ekman boundary layer, *Deep Sea Research*, 16, Supplement, 73-84, 1969.

Halpern, D., Summertime surface diurnal period winds measured over an upwelling region near the Oregon coast, *Journal of Geophysical Research*, 79, 2223-2230, 1974.

Halpern, D., Description of wind and upper ocean current and temperature variations on the continental shelf off northwest Africa during March and April, 1974, *Journal of Physical Oceanography*, 7, 422-430, 1977.

Husby, David M. and Gunter R. Seckel, Large-scale air-sea interactions at Ocean Weather Station V, 1951-71, NOAA Technical Report NMFS SSRF-696, 44 pp., 1975.

Huyer, A., Coastal upwelling in the California Current system, *Progress in Oceanography*, 12, 259-284, 1983.

Jerlov, N.G., Marine Optics, Elsevier, New York, 231 pp., 1976.

Johnson, A., and J.J. O'Brien, A study of an Oregon sea breeze event, *Journal of Applied Meteorology*, 12, 1267-1283, 1975.

Kent, R.E., and D.W. Pritchard, A test of mixing length theories in a coastal plain estuary, *Journal of Marine Research*, 18, 62-72, 1959.

Kim, J., A generalized bulk model of the oceanic mixed layer, *Journal of Physical Oceanography*, 6, 686-695, 1976.

Kraus, E.B., and J.S. Turner, A one-dimensional model of the seasonal thermocline, part II, *Tellus*, 19, 98-105, 1967.

- Kundu, P.K., A numerical investigation of mixed layer dynamics, *Journal of Physical Oceanography*, 10, 220-236, 1980.
- Large, W.G., and S. Pond, Open ocean momentum flux measurements in moderate to strong winds, *Journal of Physical Oceanography*, 11, 324-336, 1981.
- Large, W.G., J.C. McWilliams, and S.C. Doney, An oceanic vertical mixing scheme with a K-profile boundary layer parameterization, submitted to *Reviews of Geophysics*, September, 1993.
- Luan, S., Long-term momentum and heat balances and turbulent mixing in the upper equatorial Pacific Ocean, Ph.D. dissertation, Oregon State University, June 1993.
- Martin, P.J., Simulation of the mixed layer at OWS November and Papa with several models, *Journal of Geophysical Research*, 90, 903-916, 1985.
- McCormick, M.J., and D. Scavia, Calculation of vertical profiles of lake-averaged temperature and diffusivity, in lakes Ontario and Washington, *Water Resources Research*, 17, 305-310, 1981.
- McCormick, M.J., and G.A. Meadows, An intercomparison of four mixed layer models in a shallow inland sea, *Journal of Geophysical Research*, 93, 6774-6788, 1988.
- Mellor, G.L., and T. Yamada, A hierarchy of turbulence closure models for planetary boundary layers, *Journal of Atmospheric Science*, 31, 1791-1806, 1974.
- Mellor, G.L., and T. Yamada, Development of a turbulence closure model for geophysical fluid problems, *Reviews of Geophysics*, 20, 851-875, 1982.
- Milburn, H.B., and P.D. McClain, ATLAS - A low cost satellite data telemetry mooring developed for NOAA's climate research mission, *Proceedings of Marine Data Systems International Symposium '86*, April 20 - May 2, 1986, New Orleans, LA, 393-396, 1986.
- Miropol'skiy, Y.A., Nonstationary model of the wind-convection mixing layer in the ocean, *Izv. Atmospheric and Oceanic Physics*, 6, 1284-1294, 1970.
- Muller, P., R.W. Garwood, Jr., and J.P. Garner, Effect of vertical advection on the dynamics of the ocean surface mixed layer, *Annals of Geophysics*, 2, 387-398, 1984.

- Munk, W.H., and E.R. Anderson, Notes on a theory of the thermocline, *Journal of Marine Research*, 7, 276-295, 1948.
- Niiler, P.P., Deepening of the wind-mixed layer, *Journal of Marine Research*, 33, 405-422, 1975.
- Niiler, P.P., and E.B. Kraus, One-dimensional models of the upper ocean, in Modeling and Prediction of the Upper Layers of the Ocean, edited by E.B. Kraus, pp.143-172, Pergamon Press, 1977.
- Pacanowski, R.C., and S.G.H. Philander, Parameterization of vertical mixing in numerical models of tropical oceans, *Journal of Physical Oceanography*, 11, 1443-1451, 1981.
- Petruncio, E.T., *Characterization of Monterey Bay tidal currents by remote and in-situ measurements*, Master's Thesis, Naval Postgraduate School, Monterey, California, December 1993.
- Pollard, R.T., P.B. Rhines, and R.O.R.Y. Thompson, The deepening of the wind-mixed layer, *Geophysical Fluid Dynamics*, 4, 381-404, 1973.
- Price, J.F., C.N.K. Mooers, and J.C. Van Leer, Observation and simulation of storm-induced mixed-layer deepening, *Journal of Physical Oceanography*, 8, 582-599, 1978.
- Price, J.F., R.A. Weller, and R. Pinkel, Diurnal cycling: Observations and models of the upper ocean response to diurnal heating, cooling, and wind mixing, *Journal of Geophysical Research*, 91, 8411-8427, 1986.
- Resnyanskiy, Y.D., Parameterization of the integral turbulent energy dissipation in the upper quasihomogeneous layer of the ocean, *Izv. Atmospheric and Oceanic Physics*, 11, 726-733, 1975.
- Rosenfeld, L.K., Diurnal period wind stress and current fluctuations over the continental shelf off northern California, *Journal of Geophysical Research*, 93, 2257-2276, 1988.
- Rosenfeld, L.K., F.B. Schwing, N. Garfield, and D.E. Tracy, Bifurcated Flow From an Upwelling Center: A Cold Water Source for Monterey Bay, *Continental Shelf Research*, in press, 1993.

INITIAL DISTRIBUTION LIST

	No. Copies
1. Defense Technical Information Center Cameron Station Alexandria VA 22304-6145	2
2. Library, Code 052 Naval Postgraduate School Monterey CA 93943-5002	2
3. Oceanography Department Code OC/CO Naval Postgraduate School 833 Dyer Rd. Rm. 331 Monterey, CA 93943-5122	1
4. Meteorology Department Code MR/HY Naval Postgraduate School 589 Dyer Rd. Rm. 252 Monterey, CA 93943-5114	1
5. Professor Carlyle H. Wash Meteorology Department, Code 63WX Naval Postgraduate School Monterey, CA 93943-5114	1
6. Dr. Leslie K. Rosenfeld Monterey Bay Aquarium Research Institute 160 Central Ave. Pacific Grove, CA 93950	1
7. Professor Roland W. Garwood Oceanography Department, Code OC/GD Naval Postgraduate School Monterey, CA 93943-5122	1
8. LT Patrick S. Cross, USN NOCD Fallon NAS Fallon, NV 89496-5000	1
9. Director Naval Oceanography Division Naval Observatory 34th and Massachusetts Ave. NW Washington, DC 20390	1

- | | |
|--|---|
| 10. Commander | 1 |
| Naval Meteorology and Oceanography Command | |
| Stennis Space Center, MS 39529-5000 | |
| 11. Dr. Francisco Chavez | 1 |
| Monterey Bay Aquarium Research Institute | |
| 160 Central Ave. | |
| Pacific Grove, CA 93950 | |
| 12. Dr. James F. Price | 1 |
| Woods Hole Oceanographic Institution | |
| Department of Physical Oceanography | |
| Woods Hole, MA 02543 | |
| 13. Dr. Clayton Paulson | 1 |
| College of Oceanography | |
| Oregon State University | |
| Corvallis, OR 97331 | |